

CHAPTER I

INTRODUCTION

1.1 General Introduction

1.1.1 Methanol as a feedstock

Methanol (CH_3OH) is an industrially important base chemical, which is widely used for the production of formaldehyde, methyl-*tert*-butyl-ether and acetic acid. With an annual production of 32.1 MT (2004) [1] it is one of the most produced chemicals along with ammonia and sulfuric acid. Especially today, in times of diminishing oil and gas reserves and an increasing demand for energy, methanol has attracted attention as perspective alternative fuel. Methanol has the highest H:C ratio with a value of 4, making it a practically convenient hydrogen storage chemical. Furthermore, methanol can be directly used in fuel cells for energy productions (direct methanol fuel cell, DMFC). Due to the liquid state of methanol, the existing infrastructure for storage and transportation of fuels might still be used, if methanol was commonly used as fuel. As methanol can be formed from CO_2 , the synthesis of methanol might become in future an efficient way for CO_2 recycling [2]. These perspectives may lead to a strongly increasing demand for methanol in future.

The industrial importance of the methanol synthesis reaction is derived from methanol's many uses as a feedstock for fuels and precursors [3]. Researchers at Mobil have found that methanol can be converted into high octane gasoline making use of ZSM-5 zeolite catalyst [4]. As a fuel, it burns environmentally friendly, with no NO_x emission and at lower temperatures. Lastly, methanol is used in the manufacture of biodiesel employing an etherification process [5].

1.1.2 Historical Development of ZnO based catalyst

The industrial production of methanol started in 1923 with the BASF high-pressure methanol synthesis process. A ZnO/Cr₂O₃ catalyst was used for the production of methanol from synthesis gas. To obtain high yields, the catalyst required high pressures between 250 and 350 bar and high temperatures between 573 and 673 K [2]. The catalyst was very stable against sulfur or halogen impurities in the synthesis gas [3]. Since 1966, the ternary Cu/ZnO/Al₂O₃ catalyst has widely been used for methanol synthesis in the ICI low-pressure methanol synthesis process, operating at significantly milder conditions with pressures in the range from 50 to 100 bar and temperatures between 513 and 533 K [4]. Due to the high sensitivity of the Cu/ZnO/Al₂O₃ system towards catalyst poisons, the substitution of the old systems by the new ones took place, when a cleaner synthesis gas, containing less sulfur and halogens, was available [1]. This happened due to the use of natural gas instead of coal as source for synthesis gas and the availability of better gas purification technologies.

The properties of the different catalyst systems are diverse, all of them show their own specific behaviour under catalytic conditions and fundamental differences between the catalyst systems were reported. All the above mentioned catalyst systems have three features in common: firstly, all three systems contain ZnO. This was the main active component of the ZnO/Cr₂O₃ system [2], but its role in the other systems is still debated. In fact, pure ZnO is also an active catalyst for methanol synthesis [2, 7-10]. Secondly, all above mentioned systems can produce methanol in high yield and with high selectivity, yet from different synthesis gases [2-6]. Methanol can in principle be produced from either CO or CO₂, according to the reaction equations 1.1 and 1.2



While pure ZnO and the ZnO/Cr₂O₃ catalyst produced methanol in high yields from CO and H₂, basic agreement has been achieved, that on the Cu catalysts CO₂ is the main carbon source for methanol synthesis [11-13]. On the Au/ZnO catalysts, so far, both carbon oxides seem to act as carbon source, but selectivity was higher in methanol synthesis from CO [5, 6]. One reason for the high selectivity of the Cu catalysts might be that they cannot dissociate the CO molecule, which excludes methane formation [14]. Thirdly, in spite of the fact that all systems are believed to behave differently in the catalysis of methanol synthesis, they are all able to catalyse not only methanol synthesis, but also undergo water-gas shift reaction [2, 3, 5, 6, 13, 14]:



This already point to the complications in evaluating the reaction pathway: due to water gas shift, a fast interconversion of the carbon oxides occurs. Consequently, it is already difficult to define the starting point of the mechanism, which of the carbon oxides is used as carbon source for methanol formation.

1.2 Methanol production volume estimates

1.2.1 Methanol Production Statistics

In 2000, worldwide methanol production capacity stands at 12.5 billion gallons (37.5 million tons) per year, with a utilization rate of just fewer than 80 percent. The world methanol industry has a significant impact on the global economy, generating over USD 12 billion in annual economic activity while creating over 100,000 direct and indirect jobs [22].

1.2.2 Methanol Global Demand

On a global basis, methanol consumption in 2008 was approximately 45 million metric tons or nearly 15 billion gallons. This is roughly equivalent to global fuel ethanol demand. By 2012, methanol demand is expected to reach over 50 million metric tons or 17 billion gallons. At the same time, global production capacity is growing at an even faster rate, and is likely to reach 85 million metric tons (28 billion gallons) by 2012. Based on these forecasts, there will be 34 million tons of excess production capacity around the world, enough to produce 11 billion gallons of methanol per year. Additional billions of gallons of production capacity also is available today in “mothballed” plants in North America and Europe, that have been shut down due to high natural gas prices. China is now the world’s largest methanol producer and consumer, and by some estimates Chinese methanol production alone could exceed 60 million metric tons in the next few years.

1.2.3 Methanol Domestic Demand

In Malaysia, methanol has been largely produced by Petronas Methanol Labuan, PMLSB since 1992 and currently has a methanol output capacity of 1800 t/d and accounts for 35.3% of the total methanol production in South East Asia [24]. It however is on its way to becoming the first Mega-Methanol plant in the region with its expansion project to produce an output of greater than 2500 t/d.

For year 2000 starting from the month of January till August 2000, Malaysia is the supplier with the highest price to Sri Lanka but in small amounts. However, Malaysia offers the lowest price to Korea around RM 0.37/kg. Indonesia remains the top importer of Malaysian methanol and it’s followed by Japan [25].

1.3 Role of Carbon Nanotubes in Catalytic Reactions

Carbon nanotubes (CNTs) that are featuring uniform pore size distribution, meso and macro pore structure, inert surface properties, and resistance to acid and base environment can play an important role in a number of catalytic reactions [20]. CNTs are essentially composed of graphite layers with a tubular morphology [17-18]. Structural parameters of CNT such as inner and outer diameter and length of nanotubes can be controlled using different synthesis processes and operating conditions. It has been shown that CNTs offer improved performance for conversion reactions [16-19, 21].

These properties of CNTs have created interest in methanol synthesis production.

1.4 Problem statement

Presently Industry plant in Malaysia encounters serious technological problems in course of methanol production, these problems include:

- Daily output of methanol progressively decreases reaching the decrement up to 100t/d by the end of the 3rd year of service.
- Catalyst is sintering and jamming in the reactor's tubes in course of its relatively short 3-years operational life span, hence tedious manual methods are to be applied to clear off the tubes from the stuck catalyst. This phenomenon is caused by sintering of catalyst's pellets and with the reduction of surface area of catalyst at high temperatures [23].
- Carbonlike substance on the surface of spent catalyst as well as some sulfurization on the spent catalyst surface has been a cause of carbonization [26]. The effect of sulfur poisoning is associated with formation of strong Cu-S bonds. This effect hinders chemisorptions and lateral diffusion of CO molecules on the Cu surface. This results in turn inhibition of the surface reaction.

1.5 Research Objectives

Research Objectives are as below shown:

- Synthesis and investigation of Cu/ZnO/Al₂O₃ catalyst supported with Carbon Nanotubes, in-house made Cu/ZnO/Al₂O₃ catalyst and commercial pre-catalyst.
- Microreactor-GC study of the activity of each catalyst in process of Hydrogenation of Carbon Monoxide.

1.6 Scope of the Study

The spent industrial samples (SICat) obtained from the plant reactor were subjected to detailed laboratory examination using advanced instruments such as FESEM (Field Emission Scanning Electron Microscope), EFTEM (Energy Filter Transmission Electron Microscope), Catalytic Microreactor coupled with GC (Gas Chromatography), TPDRO (Thermo Programmed Desorption Reduction/ Oxidation), XRD (X-Ray Diffraction), XPS (X-Ray Photoelectron Spectroscopy), and LEIS (Low Energy Ion Scattering Spectroscopy) and comparative measurement of various fresh and aged catalyst adsorptive properties. Concurrently the kinetics of methanol synthesis over in-house made catalyst (intact and supported with CNT) and commercial pre-catalysts (CPCat) was investigated at laboratory scale Catalytic Microreactor coupled with GC. The changes of the surface morphology and composition were investigated by the above said methods. The experimental data have been analyzed and eventually the kinetics and mechanisms of the catalysis revealed.

CHAPTER II

LITERATURE REVIEW

2.1 Manufacture of Methanol

Methanol production economics highly depended on the feedstock selection and prices. Methanol can be manufactured from any hydrocarbon source; naphtha, oil, coal, wood, bio-mass, etc. The naphtha, fraction of crude oil distillation, is used as a raw material in many older facilities for the manufacture of methanol. When naphtha is reacted with a high steam ratio, under pressure and at high temperature, synthesis gas of low methane content is obtained. Most of the carbon from the naphtha is converted to carbon monoxide and carbon dioxide (Equations 2.1 to 2.2):



The mixture of hydrogen and carbon oxides is compressed and is passed over a catalyst under high pressure and at high temperature, methanol is formed (2.3 and 2.4).



The mixture of methanol, water, and other impurities is distilled to produce methanol of 99.95 mole percent purity.

Methanol can be produced from a variety of sources, such as natural gas, coal, biomass, and petroleum. Table 2.1 summarizes the various processes, feedstocks, and catalysts for the production of methanol and its precursor, syngas.

Methanol is synthesized industrially via syngas. Alternative processes considered but not commercialized include synthesis from syngas in two steps via methyl format [27], direct oxidation of methane over a heterogeneous catalyst, and bioprocess [28].

Table 2.1 Feedstock, Processes, and Catalysts for Production of Syngas and Methanol.

Feedstock	Processes and main reaction	Catalysts
Syngas Manufacture		
Natural gas	Steam reforming: $\text{CH}_4 + \text{H}_2\text{O} \longrightarrow \text{CO} + 3\text{H}_2$	Ni on Al_2O_3
Natural gas	Auto thermal reforming $\text{CH}_4 + 2\text{O}_2 \longrightarrow \text{CO}_2 + 2\text{H}_2\text{O}$, Then $\text{CH}_4 + \text{H}_2\text{O} \longrightarrow \text{CO} + 3\text{H}_2$ $\text{CO}_2 + 1/2\text{O}_2 \longrightarrow \text{CO} + \text{H}_2\text{O}$	-- Ni on refractory supports
Natural gas	Partial oxidation $\text{CH}_4 + 1/2\text{O}_2 \longrightarrow \text{CO} + 2\text{H}_2$	Noncatalytic or lanthanide/Ru, supported Ru, Ni, Pd
Coal	Gasification (in presence of $\text{H}_2\text{O}/\text{O}_2$)	--
Biomass	Gasification	--
Others (e.g., liquefied petroleum gas, naphta, hevy fuel oil)	Steam reforming (light hydrocarbons)	Alkalized Ni on Al_2O_3 or on $\text{Ca}/\text{Al}_2\text{O}_3$
Methanol manufacture		
Syngas	Methanol synthesis: $\text{CO} + 2\text{H}_2 \longrightarrow \text{CH}_3\text{OH}$, $\text{CO}_2 + 3\text{H}_2 \longrightarrow \text{CH}_3\text{OH} + \text{H}_2\text{O}$	$\text{Cu}/\text{ZnO}/\text{Al}_2\text{O}_3$ $\text{Cu}/\text{ZnO}/\text{Cr}_2\text{O}_3$, or Zn/Cr
Syngas	Two-step methanol synthesis; $\text{CH}_3\text{OH} + \text{CO} \longrightarrow \text{HCOOCH}_3$, then $\text{HCOOCH}_3 + \text{CO} \longrightarrow 2\text{CH}_3\text{OH}$	Potassium methoxide, Cu chromite
Methane	Direct oxidation $\text{CH}_4 + 1/2\text{O}_2$ (or N_2O) $\rightarrow \text{CH}_3\text{OH}$	Metal oxides (e.g., MoO_3 based)

2.1.1 Indirect Route via Syngas to Methanol

The conversion of natural gas to methanol via syngas is a widely used industrial process. A typical conventional process includes desulfurization of natural gas, steam reforming, methanol synthesis and purification by distillation. Steam reforming of natural gas is an endothermic reaction and operates at high temperatures (reformed gas effluent at about 800-880°C). Methanol synthesis from syngas is an exothermic reaction and operates at 200-300°C.

Production of syngas is traditionally performed in one step by steam reforming. Many of the modern processes adopt two-step reforming: primary steam reforming followed by autothermal reforming. The primary reformer is simplified and reduced in size and can be operated at a reduced temperature. Oxygen is blown to the autothermal reformer first to produce CO and H₂O with heat generation. The secondary reforming operates at higher temperatures to ensure low leakage of methane. The combined process is integrated to produce stoichiometric syngas for methanol synthesis. The process reduces energy consumption and investment and is particularly suitable for larger capacities. The two-step reforming process has been used by Topsoe, Lurgi, Mitsubishi, and others.

Syngas can also be produced by partial oxidation of methane. It is a mildly exothermic and selective process. It yields an H₂/CO ratio lower than that by steam reforming. Traditionally, it operates at very high temperatures. Catalytic partial oxidation holds promise to reduce the operation temperature drastically. This could be an ideal process for the production of methanol syngas. Petronas Methanol Labuan Sdn. Bhd. (PMLSB) employs Lurgi technology that features high throughput and cost saving process via energy utilization of the exothermic catalytic reaction occurring in the multi tubular fixed bed reactor.

Methanol synthesis is another important step in the integrated process. Current low-pressure processes operate at 5-10 MPa (50-100 atm) in vapor phase using quench (ICI), tubular (Lurgi), or double-tube heat exchanger (Mitsubishi) reactors. Single-pass conversion of syngas is low and is limited by equilibrium conversion. A high rate of gas recycling is needed [29-31].

2.1.2 Direct Oxidation of Methane to Methanol

In the past few years, there have been many active research programs around the world on the direct conversion of methane to methanol and/or formaldehyde, C₂ hydrocarbons, and others. Methanol and formaldehyde can be produced by partial oxidation of methane under controlled conditions in a homogeneous or catalytic reaction process. Many catalysts, such as Mo-based oxides, aluminosilicates, promoted superacids, and silicoferrate, have been used for the reaction. Since the activation energy for the subsequent oxidation of methanol and formaldehyde to carbon oxides is usually smaller than that for partial oxidation, high selectivities for methanol and formaldehyde have been demonstrated only at low methane conversions. Reaction conditions (e.g., O₂ or N₂O to CH₄ ratio, temperature, and residence time) and surface area of supports play important roles in methanol and formaldehyde yield. In general, low pressure favors the formation of formaldehyde. High pressure and low O₂/CH₄ ratios favor the formation of methanol. The low yields achieved to date are a major obstacle to economical commercialization of this route.

2.2 Applications of Methanol

Methanol has been used in a variety of applications, which can be divided into three categories: feedstock for other chemicals, fuel use, and other direct uses as a solvent, antifreeze, inhibitor, or substrate. Primary and secondary derivatives or applications of methanol are summarized in Table 2.2. Chemical feedstock accounted for 62% of the total U.S. methanol consumption of 5.16 million t in 1990, fuel use for 27%, and other direct uses for 11% [1]. Growth in methanol consumption in the next few years will come largely from fuel use, especially MTBE [17, 18]. The demand pattern will change. SRI (Stanford Research Institute) International forecasted that the fuel industry will become the largest sector for U.S. methanol consumption in 1995. It will account for 54% of about 8.6 million ton methanol demand, followed by 39% as a chemical feedstock and 7% in other uses [1].

2.2.1 Feedstock for chemicals

Methanol is the simplest aliphatic alcohol. It contains only one carbon atom. Unlike higher alcohols, it cannot form an olefin through dehydration. However, it can undergo other typical reactions of aliphatic alcohols involving cleavage of a C-H bond or O-H bond and displacement of the -OH group [19].

Table 2.2 Overview of Methanol Applications

Direct derivatives or uses	Secondary derivatives or uses
<p>Fuel or fuel additives</p> <p>Neat methanol fuel</p> <p>Methanol blended with gasoline</p> <p>MTBE</p> <p>TAME</p> <p>Methanol to gasoline</p>	<p>Oxygenate in gasoline</p> <p>Oxygenate in gasoline</p>
<p>Chemicals</p> <p>Formaldehyde</p> <p>Acetic acid</p>	<p>Urea-formaldehyde resins</p> <p>Phenolic resins</p> <p>Acetylenic chemicals</p> <p>Polyacetal resins</p> <p>Vinyl acetate</p> <p>Acetic anhydride</p> <p>Ethyl acetate</p> <p>Solvent for terephthalic acid</p>
<p>Chloromethanes</p> <p>Methyl chloride</p> <p>Methylene chloride</p> <p>Chloroform</p>	<p>Organic paint-removal solvent</p> <p>Solvent and cleaning application</p> <p>Auxiliary blowing agent</p> <p>HCFC-22 as a refrigerant</p>
<p>Methyl methacrylate</p>	<p>Acrylic sheet</p> <p>Molding and extruding compounds</p> <p>Coating resins</p>
<p>Dimethyl terephthalate</p>	<p>Polyester</p>
<p>Methylamines</p> <p>Monomethylamine</p> <p>Dimethylamine</p> <p>Trimethylamine</p>	<p><i>n</i>-Methyl-2-pyrrolidone, water-gel explosives</p> <p>dimethylformamide, dimethylacetamide</p> <p>chlorine chloride</p>

MTBE is produced by reacting methanol with isobutene. Isobutene is contained in the C₄ stream from steam crackers, and from fluid catalytic cracking in the crude oil-refining process. However, isobutene has been in short supply in many locations. The use of raw materials other than isobutene for MTBE production has been actively sought. Figure 1 describes the reaction network for MTBE production.

Isobutene can be made by dehydration of *t*-butyl alcohol, isomerization of *n*-butenes [53], and isomerization and dehydrogenation of *n*-butane [54,55]. *t*-butanol can also react with methanol to form MTBE over acid alumina, silica, clay, or zeolite in one step [56,57]. *t*-butanol is readily available by oxidation of isobutane or, in the future, from syngas. The C₄ fraction from the methanol-to-olefins process may be used for MTBE production, and the C₅ fraction may be used to make TAME. It is also conceivable that these ethers could be based on nonpetroleum sources. These present vast research opportunities for developing efficient catalysts and integrated processes depend on the availability of feedstock. Reactive distillation, in which the reaction of isobutene and methanol and the distillation to remove MTBE occur in the same tower, is another active research area. Development of efficient processes to separate and recover unreacted methanol from C₄ at a low cost is being sought. Potential processes include using a light hydrocarbons stripping gas [58], silica as an absorbent [59], and pervaporation [60].

2.2.2 Methanol in Transportation Fuel

Some applications of dissociated methanol are emerging:

1. Alternative automobile fuel
2. Supplemental gas turbine fuel at peak demand of electricity
3. Supplying H₂ for fuel cells
4. Fuel and cooling system for hypersonic jets
5. Source of CO and H₂ for chemical processes and material processing

- 1 Methanol can act as an alternative automobile fuel, because of limited space in the engine compartment and limited temperatures during cold start, on-board methanol dissociation would need catalysts that are active at low temperatures. The activity and stability are two key points for these catalysts. Coke formation has been a problem that results in catalyst deactivation [61]. Methanol dissociation on board a vehicle also requires a compact and efficient heat-exchange reactor to make use of engine waste heat. The reactor should also be resistant to the maximum anticipated exhaust temperature, thermal cycling fatigue, hydrogen embrittlement, and methanol corrosion. Although a number of catalysts and dissociators have been devised, there are still many opportunities to improvement [44-52].
- 2 Methanol dissociation on board a passenger vehicle operates near atmospheric pressure, a condition that thermodynamically strongly favors the dissociation reaction. However, applying the dissociation to a diesel engine would require operation at such high pressure as 10-20 MPa (100-200 atm). Exhaust gas temperatures from a diesel engine could vary in a wide range from as low as 150°C to well over 500°C. Development of an active and stable catalyst and technology to accommodate these harsh conditions is a challenge for use of dissociated methanol in a diesel engine.
- 3 Methanol dissociation can also be driven by heat from gas turbine exhaust gas. This would increase the heating value and make dissociated methanol an attractive peaking fuel for power plants. For this application, methanol dissociation must be conducted at about 1.5-2 MPa (15-20 atm).
- 4 The dissociation of methanol could provide a convenient, economical, and clean source of CO and H₂ for applications in fuel cells, chemical processes (e.g., carbonylation, hydrogenation, and hydroformylation), and materials processing. As an on-site source of CO and H₂, it can be operated under mild conditions and produces no sulfur or soot, as opposed to high-temperature reforming or partial oxidation using other hydrocarbons.

- 5 Because of its endothermic nature, methanol dissociation could provide not only an efficient fuel but also an efficient method for cooling. For example, engine cooling is a critical issue for hypersonic jets being developed by the U.S Air Force. Methanol dissociation is promising for both the cooling and fuel systems [62].

2.2.3 Other Direct Uses of Methanol

As A Solvent: Methanol is used as a solvent in automobile windshield washer fluid and as a cosolvent in various formulations for paint and varnish removers. It is also used as a process solvent in chemical processes for extraction, washing, crystallization, and precipitation. For example, methanol is used as an “antisolvent” for precipitation of polyphenylene oxide after its polymerizations. It should be pointed out here that there have been active studies in using the extracts of agricultural plants in medicine. Methanol is often used for these extractions. Methanol extract of some plants show antibacterial activities [40,41]. This provides a potential use of methanol in traditional medicine.

As An Antifreeze: Methanol has high freezing point depression ability. It depresses the freezing point of water by 54.5°C for a 50-50 wt% methanol-water mixture [42]. The largest antifreeze use of methanol is in the cooling system for internal combustion engines [43]. However, the antifreeze market for methanol has been saturated. Its market share has been lost to ethylene glycol since 1960 because of the superior performance of the glycol.

As An Inhibitor: Methanol finds little use as an inhibitor. It inhibits formaldehyde polymerization and is present in the formaldehyde solution and paraformaldehyde. Methanol can also serve as a hydrate inhibitor for natural gas processing.

2.3 Properties of Methanol

2.3.1 Physical Properties

Methanol is a colorless liquid, completely miscible with water and organic solvents and is very hygroscopic. It boils at 64.96° C (148.93° F) and solidifies at -93.9° C (-137° F). It forms explosive mixtures with air and burns with a nonluminous flame. It is a violent poison; drinking mixtures containing methanol has caused many cases of blindness or death. Methanol has a settled odor. Methanol is a potent nerve poison. Key physical properties are:

- Formula: CH₃OH
- Melting Point : -97.7⁰C
- Boiling Point : 65⁰C
- Relative Density : 0.79
- Molecular weight: 32.042 kg/kmol
- Heat of Formation -201.3 MJ/kmol

Liquid Properties:

- Density at 20⁰C 791 kg/m³ at 20 °C
- Heat of Vaporization 35278 kJ/kmol

2.3.2 Chemical Properties

Methanol is a clear, colorless, and volatile liquid, giving off a mild alcoholic odor at room temperature. It is polar, acid base neutral and generally considered non-corrosive. It is miscible with water and in most organic solvents it is capable of dissolving many inorganic salts. Anhydrous methanol is hygroscopic. Methanol is toxic to human beings but is not considered particularly harmful to the environment.

Methanol is the simplest aliphatic alcohol. It contains only one carbon atom. Unlike higher alcohols, it cannot form an olefin through dehydration. However, it can undergo other typical reactions of aliphatic alcohols involving cleavage of a C-H bond

or O-H bond and displacement of the –OH group [39]. Table 2.3 summarizes the reactions of methanol, which are classified in terms of their mechanisms. Examples of the reaction and products are given.

Hemolytic dissociation energies of the C-O and O-H bonds in methanol are relatively high. Catalysts are often used to activate the bonds and to increase the selectivity to desired products.

Table 2.3 Reactivities of Methanol

Mechanisms	Reactions	Other reactants	Product
O-H bond cleavage	Esterification	Acetic acid	Methyl acetate
	Addition	Phosgene	Dimethyl carbonate
Terephthalic acid		Dimethyl terephthalate	
Acetone		Ketal	
Isobutene		Methyl t-butyl ether	
Hydroxyl group displacement	Halogenation	HCl	Methyl chloride
	Carbonylation	CO	Acetic acid
	Dehydration	--	Dimethyl ether
	Ammonolysis	NH ₃	Methylamines
C-H bond and O-H bond cleavage	Oxidative dehydrogenation		Formaldehyde
	Dissociation	--	CO and H ₂

2.4 Historical Catalyst Development

Cu/ZnO based catalysts are industrial low-pressure methanol synthesis catalysts. In general, the selectivity of the catalysts decreases when operating at high pressure, high temperatures, high CO/H₂ or CO/CO₂ ratios, and low space velocities [29]. Improved catalyst activity would allow a change in operation conditions in favor of high selectivity. Fundamental studies on reaction mechanisms and kinetics, active sites, and effect of process conditions have been the subject of many research programs and have been discussed in several review papers [30-32]. New types of effective catalysts and reactors are receiving significant attention.

Recent advancement in catalyst development have led to some promising catalysts not based Cu/ZnO. These may be classified into five types: intermetallic Cu/Th, Cu/lanthanides, Pt group on silica, Raney Cu, and homogeneous catalyst. It should be pointed out here that some of these potential catalysts are active at 100⁰C or lower. This would permit high conversions of syngas in a single pass and therefore reduce or eliminate costly gas recycling. For example on ICI group has shown that Cu/lanthanides catalysts, when properly treated, can be active at temperatures as low as 70⁰C [33]. Brookhaven National Laboratory has developed a liquid-phase system that would permit the reaction to proceed at fully isothermal conditions around 100⁰C [34].

Even the industrial Cu/ZnO/Al₂O₃-based catalysts have been modified to achieve higher productivity or longer catalyst life. ICI recently announced its third-generation Cu/ZnO/Al₂O₃ catalyst, described as a “step change” over the previous catalysts [35, 36]. This development was made through optimized formulation and particle and pellet size. Researchers at the University of New South Wales, Australia claimed another new breakthrough on this type of the catalyst [35]. A 100% improvement in performance over the previous catalysts was claimed.

2.5 Economics

Conversion of remote natural gas to methanol even by conventional methanol technology is economically competitive compared with shipping LNG. Delivered fuel cost based on 323 billion Btu/day project and 6800 mile shipping distance was estimated to be about \$4.6/million Btu (calculation of capital was based on U.S Gulf Coast, 1986) using conventional methanol technologies about \$4.8/million Btu for LNG [34]. Advanced and potential methanol technologies would make the methanol route even more attractive. Delivered fuel cost based on Brookhaven’s low-temperature methanol process was claimed to be only \$3.6/million Btu under the same conditions [34]. The capital cost for production facilities, shipping tankers, and receiving terminals would be about 50% lower than the LNG investment.

Economics of the methanol technologies for remote natural gas has also been studied by Catalytica [37]. They described improved methanol technologies, such as advanced syngas generation using oxygen followed by improved ICI technology or including, CO₂/H₂O removal in the syngas production step, followed by low-temperature methanol synthesis. These improved technologies have a \$0.06-0.08/gal advantage over conventional methanol technology. Additional several cents/gal savings can be realized if a high-yield process of direct oxidation of methane to methanol can be successfully developed.

Methanol synthesis is the most profitable way to add values to natural gas [38]. Methanol production is shifting from developed countries to developing countries. New plants will be located in increasingly varied and remote locations to utilize abundant remote natural gas.

2.6 Lurgi Methanol production

Lurgi's Methanol synthesis process is an advanced technology for converting natural gas to methanol at low cost in large quantities. It permits the construction of highly efficient single-train plants of at least double the capacity of those built to date.

This paves the way for new downstream industries like Lurgi's MPT process which can use methanol as a competitive feedstock.

2.6.1 The Concept of Lurgi Technology for Methanol Production

The Lurgi Methanol technology has been developed for world-scale methanol plants with capacities greater than one million metric tons per year. To achieve such a capacity, a special process design is needed, incorporating advanced but proven and reliable technology, cost-optimized energy efficiency, low environmental impact and low investment cost.

The main process features to achieve these targets module:

- Oxygen-blown natural gas reforming, either in combination with steam reforming, or as pure auto thermal reforming.
- Two-step methanol synthesis in water-and gas-cooled reactors operating along the optimum reaction route.
- Adjustment of syngas composition by hydrogen recycle.
- Methanol Purification.

2.6.2 Synthesis Gas Production

The synthesis gas production section accounts for more than 50% of the capital cost of a methanol plant. Thus, optimization of this section yields a significant cost benefit.

Conventional steam reforming is economically applied in small and medium-sized methanol plants, with the maximum single-train capacity being limited to about 3000 mtpd. Oxygen-blown natural gas reforming, either in combination with steam reforming or as pure auto thermal reforming, is today considered to be the best suited technology for large syngas plants.

The configuration of the reforming process mainly depends on the feedstock composition which may vary from light natural gas (nearly 100% methane content) to oil-associated gases.

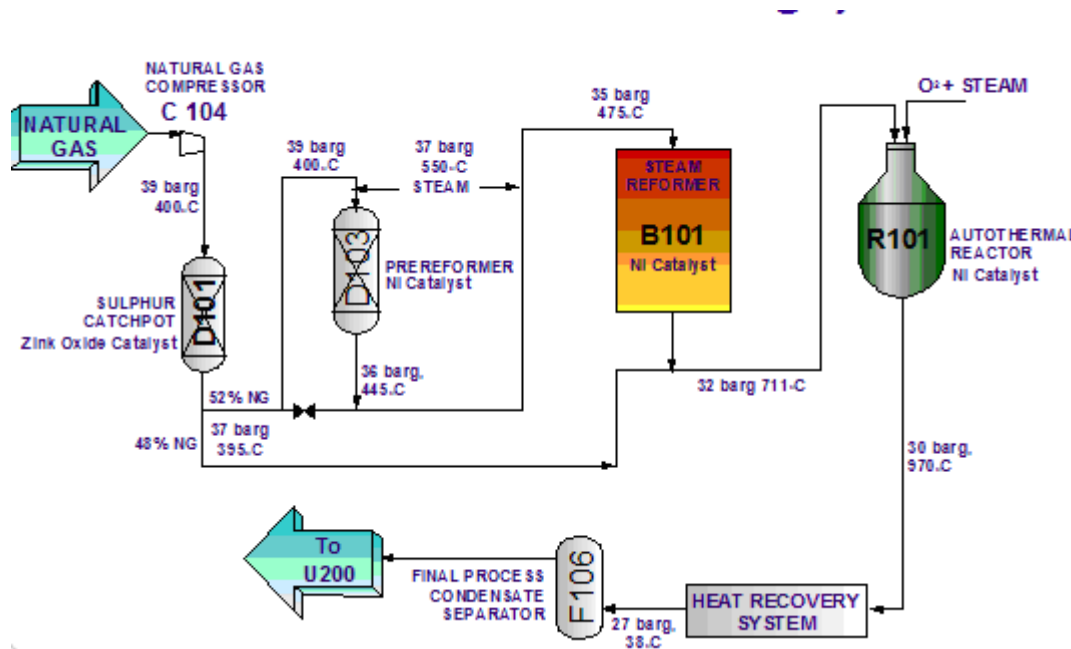


Figure 2.1 Typical Natural Gas Reforming System

Pure Autothermal reforming can be applied for syngas production whenever light natural gas is available as feedstock to the process (Figure 2.1).

The desulfurized and optionally pre-reformed feedstock is reformed with steam to synthesis gas at about 40 bar and higher using oxygen as reforming agent. The process generates a carbon-free synthesis gas and offers great operating flexibility over a wide range to meet specific requirements. Reformer outlet temperatures are typically in the range of 950 C-1050° C. The synthesis gas is compressed in a single-casing synthesis gas compressor with integrated recycle stage to the pressure required for methanol synthesis.

Even when using pure methane as feedstock for autothermal reforming, it is necessary to condition the synthesis gas, as its stoichiometric number below 2.0. The most economic way to achieve the required gas composition is to add hydrogen, withdrawn from the methanol synthesis purge stream by a membrane unit or a pressure swing adsorption unit.

Compared to its competitors, Lurgi has the most references and experience for this reforming technology. This process has been implemented in Lurgi plants since the 1950s. Significant progress in optimizing design and assuring plant availability was achieved at the end of the 1980s when reliable simulation tools became available.

For heavy natural gases and oil-associated gases, the required stoichiometric number cannot be obtained by pure autothermal reforming, even if all hydrogen available is recycled. For these applications, the Lurgi Methanol production process concept combines autothermal and steam reforming as the most economic way to generate synthesis gas for methanol plants. After desulfurisation, a feed gas branch stream is decomposed in a steam reformer at high pressure (35-40 bar) and relatively low temperature (700-800°C). The reformed gas is then mixed with the remainder of the feedgas and reformed to syngas at high pressure in the autothermal reactor. This concept has become known as the Lurgi Combined Reforming Process. The main advantage of the combined reforming process over similar process alternatives is the patented feedgas bypass of the steam reformer. For most natural gases, less than half of the feedgas is routed through the steam reformer, the overall process steam requirements also being roughly halved compared with other processes, which use an autothermal reformer downstream of the steam reformer without such a bypass. The lower process steam consumption translates into reduced energy requirements and lower investment.

The Lurgi Combined Reforming Process is also ideal to generate synthesis gas for the Fischer-Tropsch synthesis. The world's largest plant of this type was built by Lurgi in South Africa. The synthesis gas capacity of this plant would be sufficient to produce about 9,000 mtpd methanol.

2.6.3 Lurgi MegaMethanol Process

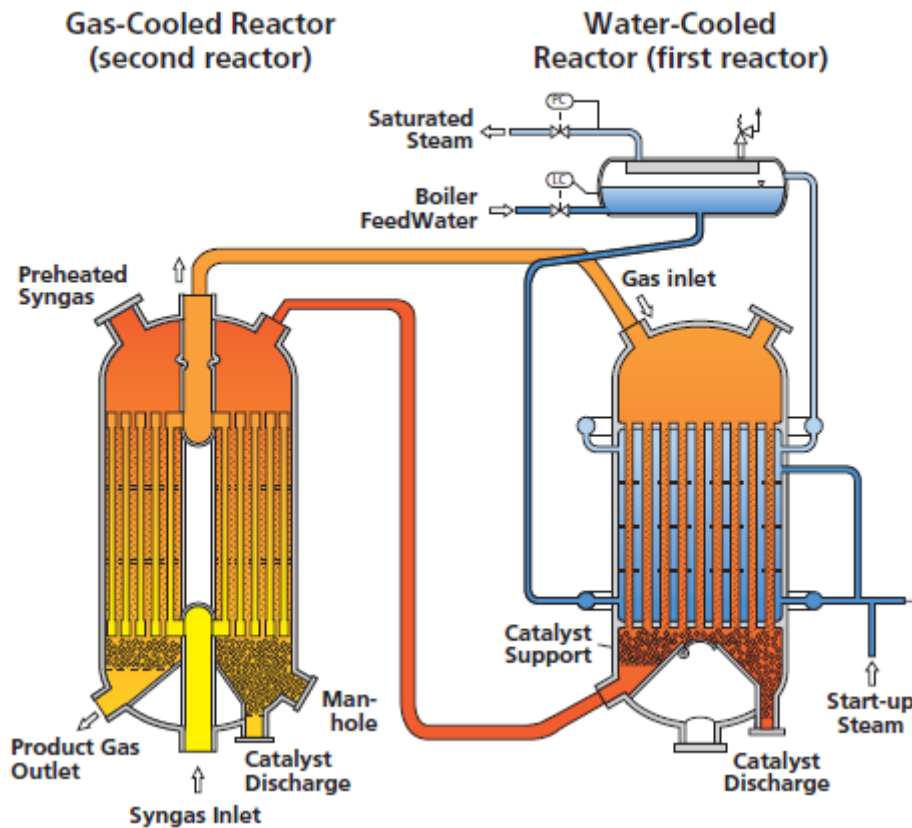


Figure 2.2 Lurgi MegaMethanol Process

Efficient syngas-to-methanol conversion is essential for low cost methanol production. In addition, optimum utilization of reaction heat offers cost advantage and energy savings for the overall plant. From the very beginning of the low-pressure technology era, Lurgi has equipped its methanol plants with a tubular reactor which transfers the heat of reaction to boiling water (Figure 2.2). The Lurgi Methanol Reactor is basically a vertical shell and tube heat exchanger with fixed tube sheets. The catalyst is accommodated in tubes and rests on a bed of inert material. The water/steam mixture generated by the heat of reaction is drawn off below the upper tube sheet. Steam pressure control permits exact control of the reaction temperature. This isothermal reactor achieves very high yields at low recycle ratios and minimizes the production of by-products.

Based on Lurgi Methanol Reactor and the highly active methanol catalyst with its capability to operate at high space velocities, Lurgi has recently developed a dual reactor system (Figure 2.2) featuring higher efficiency. The isothermal reactor is combined in series with a gas-cooled reactor. The first reactor, the isothermal reactor, accomplishes partial conversion of the syngas to methanol at higher space velocities and higher temperatures compared with single stage synthesis reactors. These results in a significant size reduction of the water-cooled reactor compared to conventional processes, while the steam raised is available at a higher pressure.

The methanol-containing gas leaving the first reactor is routed to a second downstream reactor without prior cooling. In this reactor, cold feedgas for the first reactor is routed through tubes in a countercurrent flow with the reacting gas. Thus, the reaction temperature is continuously reduced over the reaction path in the second reactor, and the equilibrium driving force for methanol synthesis maintained over the entire catalyst bed. The large inlet gas preheater normally required for synthesis by a single water-cooled reactor is replaced by a relatively small trim preheater.

As fresh synthesis gas is only fed to the first reactor, no catalyst poisons reach the second reactor. The poison-free operation and the low operating temperature result in a virtually unlimited catalyst service life for the gas-cooled reactor. In addition, reaction control also prolongs the service life of the catalyst in the water-cooled reactor. If the methanol yield in the water-cooled reactor decreases as a result of declining catalyst activity, the temperature in the inlet section of the gas-cooled reactor will rise with a resulting improvement in the reaction kinetics and, hence, an increased yield in the second reactor.

After cooling and separation of the purge gas, the crude methanol is processed in the distillation unit (Figure 2.2). In the hydrogen recovery unit, H_2 is separated from the purge gas and recycled to the syngas loop. The remaining CH_4 -rich gas fraction is used as fuel gas.

The most important advantages of the Combined Synthesis Converters are:

- High syngas conversion efficiency. At the same conversion efficiency, the recycle ratio is about half of the ratio in a single-stage, water-cooled reactor.
- High energy efficiency. About 0.8 ton of 50-60 bar steam per ton of methanol can be generated in the reactor. In addition, a substantial part of the sensible heat can be recovered at the gas-cooled reactor outlet.
- Low investment cost. The reduction in the catalyst volume for the water-cooled reactor, the omission of the large feedgas preheater and savings resulting from other equipment due to the lower recycle ratio translate into specific cost savings of about 40% for the synthesis loop.
- High single-train capacity. Single-train plants with capacities of 5000 mt/day and above can be built [162].

2.6.4 Methanol Distillation

The crude methanol is purified in an energy-saving 3 column distillation unit. With the 3 column arrangement, the low boilers are removed in the pre-run column and the higher boiling components are separated in two pure methanol columns. The first pure methanol column operates at elevated pressure and the second column at atmospheric pressure. The overhead vapors of the pressurized column heat the sump of the atmospheric column. Thus, about 40% of the heating steam and, in turn, about 40% of the cooling capacity is saved. The split of the refining column into two columns allows for very high single-train capacities [26].

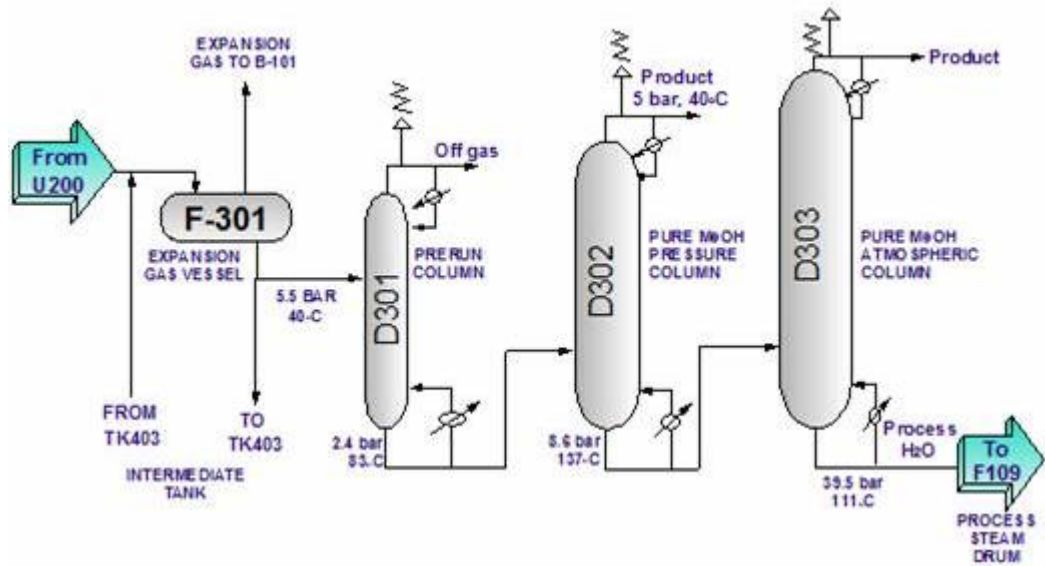


Figure 2.3 Distillation Systems for Methanol

2.7 Carbon Nanotubes

2.7.1 General Information of Carbon Nanotubes

Carbon nanotubes (Figure 2.4a and 2.4b) are allotropes of carbon with a cylindrical nanostructure. Nanotubes have been constructed with length-to-diameter ratio of up to 28,000,000:1[63] which is significantly larger than any other material. These cylindrical carbon molecules have novel properties that make them potentially useful in many applications in nanotechnology, electronics, optics and other fields of materials science, as well as potential uses in architectural fields. They exhibit extraordinary strength and unique electrical properties, and are efficient thermal conductors. Their final usage, however, may be limited by their potential toxicity and controlling their property changes in response to chemical treatment.

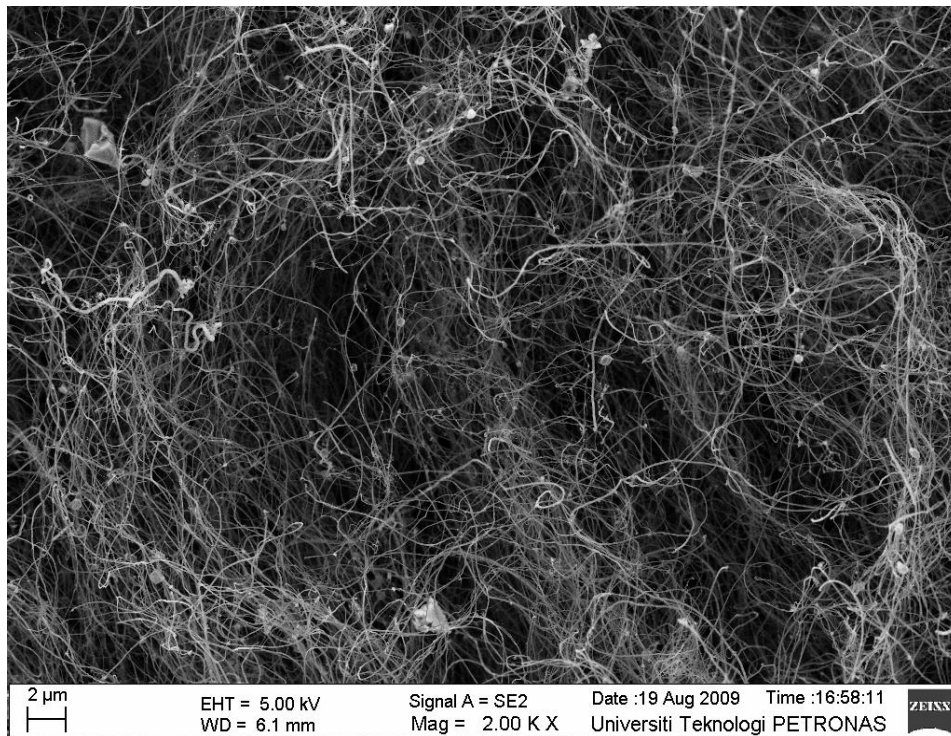


Figure2.4a. Carbon Nanotubes, FESEM Image.

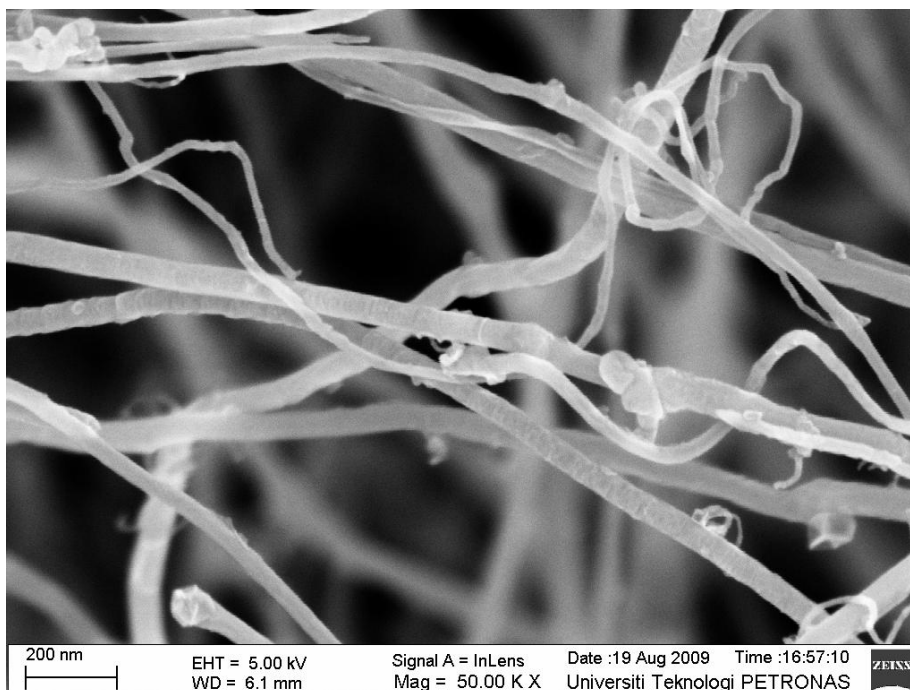


Figure 2.4b. Carbon Nanotubes, FESEM Image.

2.7.2 Properties of Carbon Nanotubes

2.7.2.1 The Strength of CNT

Carbon nanotubes are the strongest and stiffest materials yet discovered in terms of tensile strength and elastic modulus respectively. This strength results from the covalent sp^2 bonds formed between the individual carbon atoms. In 2000, a multi-walled carbon nanotube was tested to have a tensile strength of 63 gigapascals (GPa). This, for illustration, translates into the ability to endure tension of 6300 kg on a cable with cross-section of 1 mm^2 . Since carbon nanotubes have a low density for a solid material of 1.3 to $1.4 \text{ g}\cdot\text{cm}^{-3}$, [64] its specific strength of up to $48,000 \text{ kN}\cdot\text{m}\cdot\text{kg}^{-1}$ is the best of known materials, compared to high-carbon steel's $154 \text{ kN}\cdot\text{m}\cdot\text{kg}^{-1}$.

2.7.2.2 Thermo stability of CNTs

All nanotubes are expected to be very good thermal conductors along the tube, exhibiting a property known as "ballistic conduction," but good insulators laterally to the tube axis. It is predicted that carbon nanotubes will be able to transmit up to $6000 \text{ W}\cdot\text{m}^{-1}\cdot\text{K}^{-1}$ at room temperature; compare this to copper, a metal well-known for its good thermal conductivity, which can only transmits $385 \text{ W}\cdot\text{m}^{-1}\cdot\text{K}^{-1}$. The temperature stability of carbon nanotubes is estimated to be up to $2800 \text{ }^\circ\text{C}$ in vacuum and about $750 \text{ }^\circ\text{C}$ in air [65].

2.8 Preparation of the Catalyst for Methanol synthesis

The copper-based catalysts are usually prepared through conventional coprecipitation method; however, recently, some novel preparation techniques have also been reported. Jensen et al [66] developed a flame-combustion technique to prepare the copper-based catalyst by mixing acetylacetonate vapors of Cu, Zn, and Al with fuel and air, which may efficiently control the uniform dispersion of copper, zinc and aluminum components at the molecular level, and a catalyst with large surface area, high activity, and good thermostability is obtained[67], prepared a ceria-supported copper catalyst through coprecipitation; the catalyst is active for methanol synthesis even at a temperature below 200°C .

Although the conventional precipitation is a mature method to prepare the copper-based catalyst, various modifications have been made, which has attracted much attention. These modifications may be summarized as two categories: (1) addition of different metal elements such as Zr, V, Ce, Ga, and Mn [69-73]; (2) improvement of the precipitation process. Besides the typical precipitation modes such as forward, reverse, and parallel-flow and parallel-drip coprecipitations, some novel coprecipitation techniques like high-speed collision [74], gel-network [75], and urea-hydrolysis [76] coprecipitations have been reported recently. Li *et al.* [77] found that the insonation of the suspension during coprecipitation and aging steps could enhance the activity of copper-based catalysts appreciably. Yu *et al.* [78] reported that the copper-based catalyst prepared using dual-frequency ultrasonic method exhibits higher activity than that obtained by single-frequency ultrasonic method. It should be pointed out that the particles of Al-component precipitate formed in the coprecipitation processes are so fine that an effective washing of the precipitate is rather difficult. Moreover, many researchers on the copper-based catalyst concerned only the effects of Cu and Zn components on its structure and property [75-85], whereas the investigation on the effects of Al component was rarely reported. The study about the effect of Al₂O₃ on catalyst structure and property may offer some useful information to improve the activity and thermostability of copper based catalyst. It has been reported that optimum Cu/Zn ratio is largely dependent on the method of preparation [86], but is not clear whether the optimum Al content is also related to the method of preparation.

CHAPTER III

METHODOLOGY

3.1 Introduction

The catalyst from Cu/ZnO/Al₂O₃ series without CNT includes the catalyst obtained from industry, which is spent catalyst labeled SICat (Spent Industrial Catalyst) and fresh catalyst labeled as CPCat (Commercial pre-catalyst). The in-house made catalyst from Cu/ZnO/Al₂O₃ labeled as In-house Cu/ZnO/Al₂O₃ catalyst. Finally, which were supported with CNT was labeled as 1, 2 or 3% CNT supported catalyst. The catalyst classification and composition is outlined in Table 3.1.

Table 3.1 Catalysts nomenclature

No	Catalyst type	Catalyst's name abbreviation
1	Spent industrial catalyst	(SICat)
2	Commercial pre-catalyst	(CPCat)
3	In-house made Cu/ZnO/Al ₂ O ₃ catalyst (H ₂ reduced)	In-house Cu/ZnO/Al ₂ O ₃ catalyst
4	3% CNT supported Cu/ZnO/Al ₂ O ₃ catalyst	3% CNT supported catalyst
5	2% CNT supported Cu/ZnO/Al ₂ O ₃ catalyst	2% CNT supported catalyst
6	1% CNT supported Cu/ZnO/Al ₂ O ₃ catalyst	1% CNT supported catalyst

The following notes summarize the procedures involved in the methodology of the current study in their respective chronological order.

1. The Commercial catalyst which is currently being used in industry for methanol synthesis as well as the SICat discharged from the plant reactor after 3 years of operation were obtained.
2. The In-house Cu/ZnO/Al₂O₃ catalyst was prepared for the laboratory study of methanol synthesis reaction.
3. The Cu/ZnO/Al₂O₃ type Carbon Nanotubes reinforced catalysts were prepared in the laboratory for research on methanol synthesis.
4. Both commercial and in-house made catalysts were tested in laboratory fixed bed tubular reactor under the same reaction conditions for methanol synthesis.
5. Methanol conversion, yield and selectivity were compared for all the catalysts.
6. The surface morphology, of the commercial as well as in-house made catalysts before and after methanol synthesis in the laboratory reactor, was investigated using FESEM-EDX. TPDRO, XRD, XPS, TEM and only industrial spent catalyst was investigated using LEIS.
7. The surface characteristics obtained on the samples of SICat taken from different part of the PMLSB's reactor were compared with those of fresh catalyst. The aim was to reveal the irregularities in reaction conditions throughout the reactor interior.

3.2 Chemicals and Gases Employed

3.2.1 Catalyst preparation

Table 3.2 is a list of the chemicals which has been used for catalyst preparation. Chemicals were provided by *System* chemicals. Table 3.3 is a list of the gases which has been used for the syngas to methanol conversion process. Gas supplier is MOX Sdn. Bhd. (Malaysia) Company.

Table 3.2 Table of chemicals applied in catalyst preparation

Chemicals	Chemical Formula	Purpose
Copper nitrate trihydrate	$Cu(NO_3)_2 \cdot 3H_2O$	Catalyst reagent – Acid solution
Zinc nitrate hexahydrate	$Zn(NO_3)_2 \cdot 6H_2O$	Catalyst reagent – Acid solution
Aluminum nitrate nonahydrate	$Al(NO_3)_3 \cdot 9H_2O$	Catalyst reagent – Acid solution
Carbon Nanotubess	C	Catalyst reagent
Sodium carbonate	Na_2CO_3	Base solution for Acid titration

Table 3.3 Table of gases used in characterization and methanol synthesis reaction

Gases	Composition	Purpose
Hydrogen	5% in excess N ₂	Reduction / Characterization
Nitrous oxide	2.13% in excess He	Characterization
Nitrogen	pure	Characterization/ Purging
Helium	pure	Characterization
Syngas	30% CO, 70% H ₂	Chemical Reaction

1. The CPCat and SICat were obtained from a methanol synthesis plant. The pre-catalyst was grinded to the crumb state and sifted to mesh 60 to 80 typical for in-house made catalyst.
2. A copper/zinc based catalyst Cu/ZnO/Al₂O₃ was prepared in calculated ratio of metals (Table 3.4). The reactants used are Cu(NO₃)₂.3H₂O, Zn(NO₃)₂.6H₂O, Al₂(NO₃)₃.9H₂O, CNTs and Na₂CO₃.(Manufacturer-***System***) which is shown at Table 3.2. The method of preparation is a novel Acid Alkali Alternating pH developed recently [87]. Acid site solution consisting of copper nitrate, Zinc acetate and Aluminum Nitrate were mixed accordingly to a desired ratio. The base solutions were mixed into the mother solution alternatively to reach a desired low and high pH. The acid site pH was 4.88 and base site pH was 8.8. The mother solution was continuously stirred and temperature was maintained at 70°C. The process was repeated until all acid solution was used and the final pH of mother solution was maintained at 7.1. The base solution contains the highly electropositive Na⁺ ions, which would displace Cu²⁺, Zn²⁺, Zr⁴⁺ and Al³⁺ ions from their respective nitrate anions. The purpose of this displacement is to allow the Cu²⁺, Zn²⁺, Zr⁴⁺ and Al³⁺ cations to disperse and mingle as much as possible to obtain a high metal dispersion in the final precipitate. The solution was aged at 80°C for 2 h under continuous stirring and then filtered. The filtrate was washed with distilled water several times to

remove residual sodium ions from its surface. The filtrate was dried at 110°C for 12 h. consequently, it was pressed and grounded to mesh size 60-80 and then calcined at 300°C for 8 h. After calcining process pre-catalyst was ready for test [87].

3. CuO/ZnO/Al₂O₃ supported by Carbon Nanotubes.

A series of CNTs supported Cu/ZnO catalysts were prepared in different mass% of CNTs. Carbon Nanotubes were purified with treatment of boiling nitric acid (8 mol/L, at 90°C) for 8 hours, followed by rinsing with de-ionized water twice, and then dried at 383° K [87]. Cu/ZnO catalysts supported on the CNTs at different mass percentage as shown in Table 3.2. denoted as CNTs mass%, was prepared by a stepwise incipient wetness method. An aqueous solution containing desired amount of Copper nitrate, Zinc acetate and Aluminum nitrate, have to prepare by dissolving the Copper nitrate, Zinc acetate and Aluminum nitrate into a 300ml of de-ionized water. The aqueous solutions were then impregnated onto the HNO₃-treated CNT-support. The solution was aged at 80°C for 2 h under continuous stirring and then filtered. The filtrate was washed with distilled water several times to remove residual sodium ions from its surface. The filtrate was dried at 110°C for 12 h. consequently, it was pressed and grounded to mesh size 60-80 and then calcined at 370°C for 8 h (Figure 3.1). All samples of catalyst-precursors would be pressed, crushed, and sieved to a size of 60-80 mesh for the activity evaluation [87].

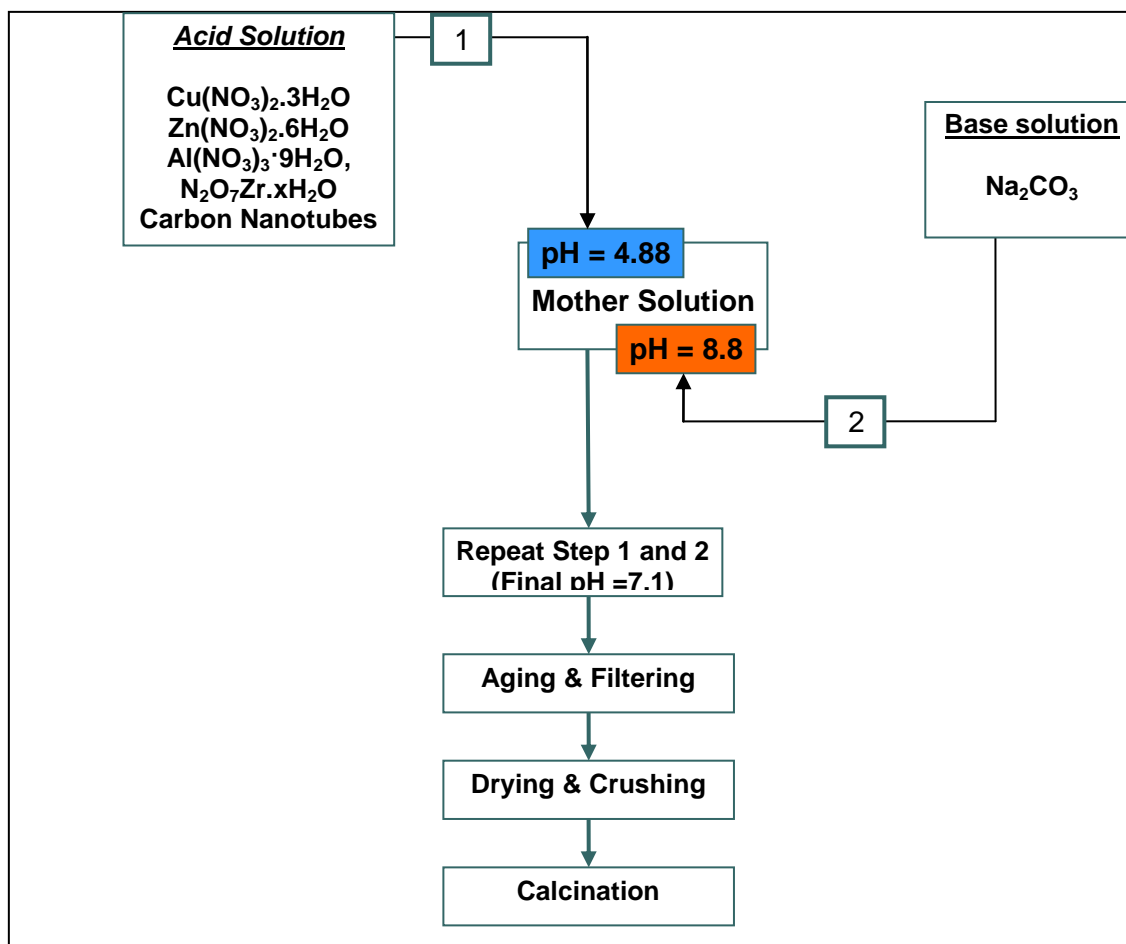


Figure 3.1 Catalyst preparation procedure

Table 3.4: The Ratio of the metals

CNT mass %	mass, g			
	Copper nitrate.3H ₂ O	Zinc acetate	Aluminum nitrate.9H ₂ O	CNT
33.33	0.1369	0.1249	0.0000	0.04
3.00	2.1183	1.7577	0.7309	0.04
2.00	3.1937	2.6501	1.1019	0.04
1.00	6.4525	5.3543	2.2264	0.04

3.3. Methods used for Physico-Chemical Characterization

3.3.1 Catalyst Density Determination

Catalyst density was determined by the Quantachrome Ultrapycnometer 1000 instrument (Figure 3.5). The Ultra pycnometer 1000 is an instrument for measuring the true density and volume of powders, catalysts, pharmaceuticals, ceramics, carbons, building materials, rock cores, etc. Ultra pycnometer 1000 provides high performance and high density accuracy measurement. The relatively simple procedure of density measurement is done:

- The catalyst density, ρ would be calculated using the 3.1 formula:

$$\rho = \frac{\text{mass}}{\text{volume}} \quad (3.1)$$

- Three measurements of density were taken for each sample for greater accuracy.

3.3.2 XRD (X-Ray Diffraction)

X- Ray diffraction is often cited as the fundamental tool in the study of solid states. The XRD analysis was conducted through the Bruker D8 Advanced Diffractometer instrument.

The scattered radiation can be well observed only in directions in which the beams reflected from the crystal plane under each other are amplified by interference.

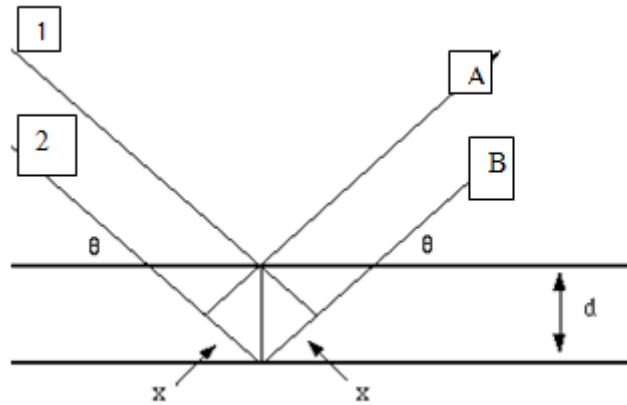


Figure 3.2: X-ray reflection on two atomic planes of a crystalline solid.

The two parallel incident rays 1 and 2 make an angle Θ with these planes. A reflected beam of maximum intensity will result if the waves represented by the x-ray termed 1 and 2 are in phase. The difference in path length between 1 to A and 2 to B or simply labeled as d must then be an integral number of wavelengths, λ (equation 3.2) [92]. This relationship is described mathematically by Bragg's law as:

$$n\lambda = 2d_{hkl} \sin \theta \quad (3.2)$$

Where n is an integer, hkl is the Miller indices of the plane. This equation is a general simplification of a now more elaborate field of x-ray crystallography.

3.3.3 X-ray Photoelectron Spectroscopy

JEOL JPS-9200 High Resolution X-ray Photoelectron Spectrometer for microarea analysis and macroarea chemical state imaging on surface. TRXPS (Total Reflection X-ray Photoelectron Spectroscopy mode) of measurement is a standard feature of this instrument that allows top surface layer (analysis at detection limit: 1×10^{11} atoms/cm² or less).

The quantification procedure used by the JEOL SpecSurf software involves modifying the Scofield cross-sections to account for both an energy dependency and also angular distribution corrections. However, to reproduce the quantification tables in CasaXPS produced by the JEOL SpecSurf software, it is sufficient to use an energy exponent and the unaltered Scofield cross-sections for the RSF (Relative Sensitivity Factor) values.

Given that m elements are so defined and therefore m regions defined on the spectrum, the calculation for the relative proportions of the sample surface or percentage atomic concentration is given by the 3.3 formula:

$$X_i = 100 \frac{A_i}{\sum_{j=1}^m A_j} \quad (3.3)$$

The percentage atomic concentration for the i^{th} element X_i is defined by the adjusted intensity A_i as follows (3.4):

$$A_i = \frac{I_i}{T(E_i)R_iE_i^n} \quad (3.4)$$

The terms contributing to the adjusted intensity are: the measured intensity for a peak I_i (either integrated peak area or peak height), the transmission function evaluated at the peak position $T(E_i)$, the relative sensitivity factor R_i , kinetic energy E_i and escape-depth exponent n .

3.3.4 Low Energy Ion Scattering Spectroscopy (LEIS)

In LEIS analysis the sample surface is bombarded with noble gas ions at energy of a few keV. Ions are scattered by the atoms of the surface following the laws of the conservation of energy and momentum. By measuring the energy of the backscattered ions the masses of the scattering surface atoms are determined.

LEIS Features are below as below shown:

- Reliable and straight-forward quantification
- Ultra-high surface sensitivity – top atomic layer analysis
- Detection of all elements > He
- Non-destructive in-depth analysis
- Sensitive to isotopes
- Detection limits: Li - O \geq 1 %; F - Cl 1 % - 0.05 %; K - U 500 ppm- 10 ppm

1) Modes of Operation

- i) Surface Spectroscopy and Imaging
- ii) Surface Spectroscopy and Surface Imaging provide quantitative elemental information of the top atomic layer for elements above He.

2) Static Depth Profiling

- i) By measuring the energy loss of ions scattered at sub-surface layers the elemental in-depth information can be obtained non-destructively.

3) Sputter Depth Profiling

- i) By using a low-energy sputter ion source in a dual beam mode with LEIS analysis, high-resolution chemical depth profiles are obtained [91].

3.3.5 Field Emission Scanning Electron Microscopy (FESEM)

Field Emission Scanning Electron Microscopy (FESEM) is a technology used to capture the image of the surface of a solid sample, determine its elemental composition as well determine the distribution of the elements on its surface. The model of the FESEM used for analysis was the SUPRA 55VP by Carl Zeiss.

Two groups of microscopy instruments are available i.e. the scanning (SEM) and transmission electron microscope (TEM). The transmission electron microscope provides surface resolution as small as 0.2 nm while a conventional scanning electron microscope provides only up to 10 nm [89]. This would also effectively explain the low cost of a scanning electron microscope.

The backscattered and/or secondary electrons from the surface at particular energies could determine the composite material that makes the surface. Backscattered or reflected source electrons are detected by the BSE detector while the secondary electrons ejected from the sample are detected by the SE detector. The SE detector is placed at an angle above horizontal so as to enable topographical information to be analyzed [90].

Another detector, the In lens detector is placed vertically and inside the electron acceleration column to detect high energy secondary electrons which provides extremely high resolution of the sample surface.

Quantitative compositional analysis of materials that make up the catalyst on the surface assuming homogeneity can be determined by the Energy Dispersive Spectrometer (EDS) which detects X-rays released by the surface after electron bombardment and the X-rays are characteristic of an element. Also, Wavelength Dispersive Analysis (WDS) allow elemental mapping on the sample surface by introducing false colors for each element.

3.3.6 Energy Filter Transmission Electron Microscope

The new generation field emission analytical TEM provides atomic scale resolution combined with nano-scale crystal structure _CBED, chemical _EDS, and electronic structure _EELS. Libra 200 FE is an analytical transmission electron microscope compatible for biology and material science. Equipped with high efficient Field Emission cathode and energy Omega-filter it is suitable for high-accuracy measurements of structure and atomic composition of nano-sized objects at ultimate resolution. This new imaging filter provides full 2nd order aberration correction and is minimized for 3rd order aberrations. In the LIBRA 200 FE it is firmly integrated in the column and fully embedded in the digitally controlled electron optical system. This in-column Omega energy filter fulfils the highest requirements for EFTEM applications in imaging and analysis. Its high acceptance results in the respectable transmissivity of 190nm². The energy resolution of less than 0.7 eV at 200 eV enables the transfer of large and highly resolved energy filtered images with excellent isochromaticity.

Cross-section TEM is an extremely useful technique, which has been applied to study film thickness, step coverage, implant damage, etch profile, via or contact filing, interface contamination, particle identification and failure analysis. As the scale of semiconductor devices shrink to sub-half micron regime, it becomes more and more difficult to make the interconnection. Typically, multiple-layer metallization is required to improve contact resistance, adhesion and wetting property and the performance of the devices is extremely sensitive to the quality of those layers. However, to characterize those materials at the bottom of a 0.25 mm contact or via structure to a few nanometers thick is beyond the ability of any other instrument.

3.3.7 Temperature Programmed Reduction (TPR)

Temperature Programmed Reduction or TPR is a crucial method to analyze the surface reducibility and optimum reduction Temperature of a catalyst species. It involves the adsorption of H₂ on the active metal surface and allows for qualitative analysis of reduction conditions on catalyst surfaces.

The TPR analysis was conducted on the catalyst by means of the Thermo Finnigan TPDRO 1100 equipment. The procedure requires the pretreatment of catalyst sample before the TPR study could be conducted on its surface

TPR analysis is conducted in a 5% H₂ in N₂, which is a reducing hydrogen gas in inert nitrogen. The catalyst sample was heated from room Temperature to 600°C at a ramp rate of 10°C with the gas flowing at 20cm³/min and was held at final temperature for 10 minutes. The analysis gas consisting Hydrogen and nitrogen have a thermal conductivity of 39.6x10⁻⁵ and 5.68 x10⁻⁵ each at 0°C temperature. The difference between the thermal conductivities of the two gases is detected by the Thermal Conductivity Detector (TCD) as a voltage signal in mV. The concentration of hydrogen in the gas mixture decreases as it adsorbs on catalyst surface. This change in gas concentration is detected by the TCD as a positive change in signal (mV) as the Thermal conductivity difference in the gas mixture is reduced [88]. The highest peak in the spectrum is identified as the optimum reduction Temperature where highest amount of hydrogen gas is adsorbed. The area under the spectrum curve is defined as the total amount of gas adsorbed in mV and the signal is converted to mmol of gas adsorbed by a pre-calibrated factor of 1.067x10⁻⁷ mmol/mV.

3.4 Micro Tubular Reactor (MTR) / GC System

3.4.1 System Description

The High Pressure Reactor Analysis system involves a micro tubular reactor (MTR) with an on-line gas chromatograph used to analyze the gaseous products from the reactor. Figure 3.3 shows the ensemble of the system placed in a room specially designed for high pressure systems.



Figure 3.3: Micro Tubular Reactor

3.4.2. Micro Tubular Reactor

The micro tubular reactor is supported on the top by a support flab with a cylindrical opening. This cylindrical opening is connected to the reactor tube via a lock-system with Allen type bolts, which keeps the reactor tube suspended in mid-air. The micro tubular body of the reactor consists of an outer shell and inner shell. There are four inlet openings at the top of the reactor which are connected to all the inlet gases. The inner and outer shells were fabricated from stainless steel SS 316. At the bottom of the reactor, there is another lock system, which connects the bottom of the shells to the Reactor outlet. The top and bottom of each lock system are secured tightly by a gasket in between each lock system and six Allen bolts that together ensure that the reactor is air tight. The dimensions of the outer reactor shell are 2.55cm I.D., 4.90cm O.D and Height of 45.5 cm. The dimensions of the inner shell are 1.3cm I.D., 2.5cm O.D., and a Height of 47.4. The volume of the inner shell is 62.92 cm³. Catalyst sample is place in the centre of the inner tube. At the bottom of the inner tube, a filter (Figure 3.4) of the mesh size 90µm is placed to avoid catalyst powder from escaping the reactor into the product line.



Figure 3.4: Standard Cleaning Filter of the Reactor (316 stainless steel)

The dual sensor thermocouple is placed in between the outer and inner shell of the reactor bottom as to maintain the accuracy of the reading and avoid damage to its body. One sensor of the thermocouple is placed at the centre of the reactor as to allow control of the catalyst bed temperature. This reactor system is equipped with a split-type electric tubular heating element with controllable temperature from ambient to 600°C and accuracy of $\pm 0.5^\circ\text{C}$. The reactor has a design Temperature of 50 bars.

The inner shell that holds the catalyst is a hollow cylinder as described earlier (Figure 3.4). The catalyst is placed in the middle of the reactor in between two layer of quartz wool to avoid catalyst diffusion. The top and bottom of the tube are filled with inert alumina balls as support to the catalyst in the middle.

3.4.3. Reactor Inlet System

The reactor inlets used 3 types of gas to flow into the systems listed in Table 3.3. Which module reduction gas, purge gas and reactant gas. The reduction gas (5% H_2 in excess N_2) used to activate the catalyst, while the purge gas is pure N_2 gas. The reactant gas is a mixture with the composition 30% CO and 70% H_2 for methanol synthesis reaction. All these gases were supplied by MOX Malaysia Sdn Bhd. The gas cylinders were connected to the reactor inlets via $\frac{1}{4}$ inch high-pressure stainless steel tubing. High-pressure gas regulators were used to control the outlet pressure of gas cylinder at 30 bars. The design pressure of the MTR is 50 bar and its equipped with a pressure relief valve with the same pressure

The reactor flow was controlled using the Swagelok type $\frac{1}{4}$ -inch needle valve and gas flow is measured by the Brooks 5860i series mass flow meter that has a flow rate ranging between 1-200 sccm. The pressure in the reactor was indicated by a Pressure gauge located at the top of the reactor cabinet as well as the pressure transducer that displays the Pressure digitally on the control panel. A schematic diagram of the reactor assemble is represented in Figure 3.5 and process flow is Figure 3.6

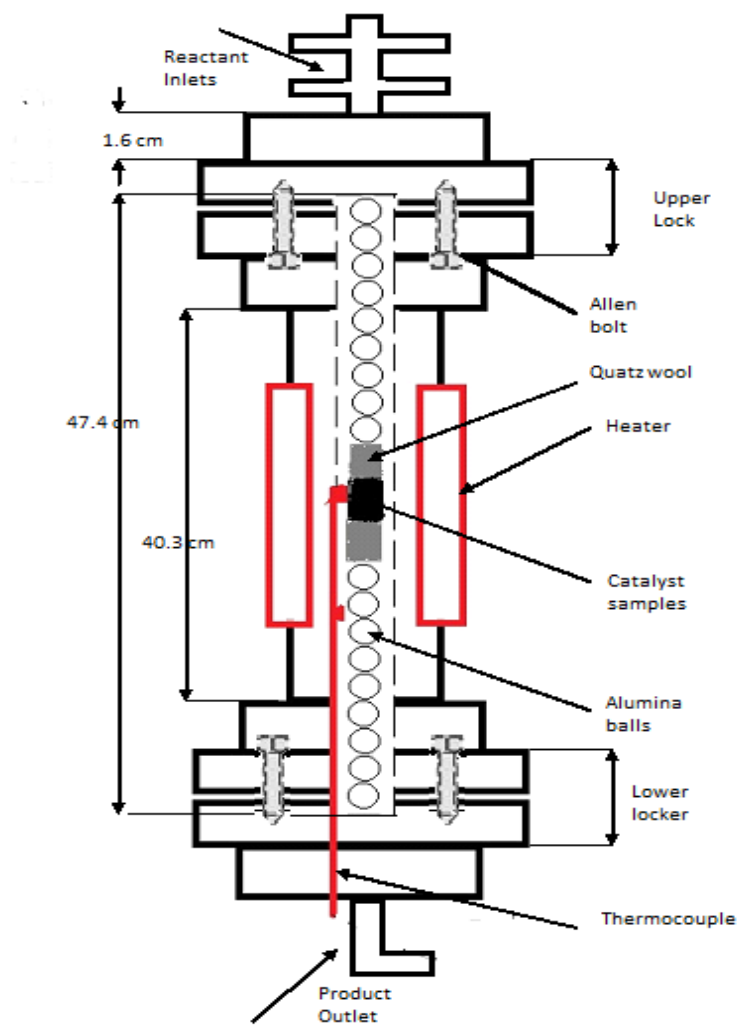


Figure 3.5: High-pressure micro tubular reactor schematic diagram - Side view

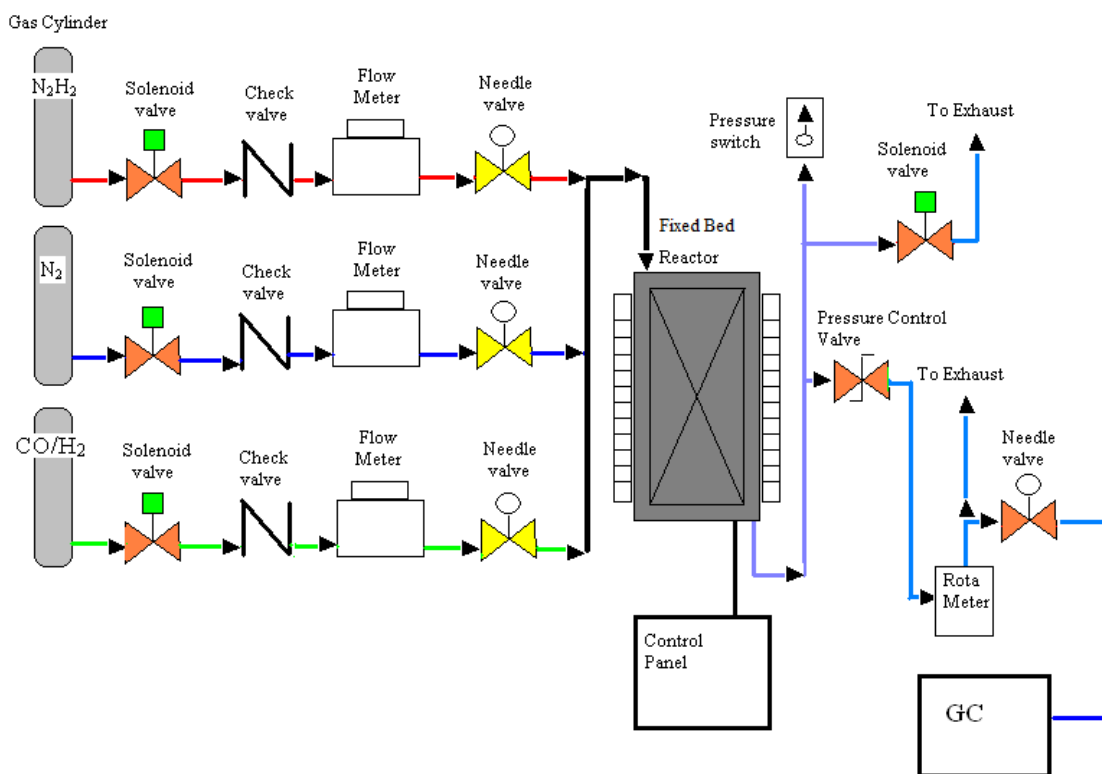


Figure 3.6: Process Flow diagram of the Micro Tubular Reactor

3.4.4 Reaction preparation and procedure

1g of catalyst was inserted into the center of the inner tube of the reactor and sandwiched immediately between cotton wool and then alumina balls.

Catalyst activation which was conducted to reduce the catalyst surface area carried out using a 5% H₂ in N₂ gas stream at a flow rate of 76.5 ml/min from room temperature to the sample reduction temperature at a ramp rate of 10°C/min. H₂ reduces the copper oxide in the catalyst to copper giving off heat and water by the following reactions as shown by equation 3.5:



Above reaction is exothermic and subject to pyramiding action. The concentration of the reducing agent in an inert carrier gas and the temperatures of reduction are used as a means of controlling the reaction. There is a linear relationship

between the amount of H₂ in the carrier gas and the temperature rise observed in the reactor. The temperature rise per percent H₂ is 10 to 12°C with natural gas or steam carrier [1]. The bed temperature was maintained for the next 1 hour. This is followed by reactor line purging and sample cooling with pure nitrogen gas at 110ml/min and 10 bars for 1 hr .

3.5 Activity Study

A gas mixture of 30% CO/ 70% H₂ was then flowed in to the system at a flow rate of 210ml/min and Temperature was maintained at 250°C and 30 bars. The product line was heated to 150°C to maintain product gaseous phase. An on-line GC analyzed effluent gases from the reactor at every ½-hour interval to obtain the gas concentration in mol%.

The products determined by on-line GC analysis on time intervals of 30min and the process is continued until methanol conversion from syngas has reached its maximum peak.

CO conversion X_{CO} is calculated using equation 3.6.

$$X_{CO} = \frac{(n_{CO})_1 - (n_{CO})_{i+1}}{(n_{CO})_1} \times 100 \quad (3.6)$$

Where $(n_{CO})_1$ - Inlet Flow of CO (mol %).

$(n_{CO})_{i+1}$ - Outlet Flow of CO (mol %).

The methanol selectivity S_{meth} was calculated by using formula 3.7

$$S_{Meth} = \frac{n_{Meth}}{X_{CO}} \quad (3.7)$$

n_{Meth} - mol % of produced methanol

Methanol conversion and selectivity are calculated for each run of experiments. The same reaction procedure applies for all the catalysts which had been prepared.

3.6 Gas Chromatography

Gas chromatography (GC) is a useful mechanism to analyse qualitatively and quantitatively gaseous product by means of retention in multi-coiled columns. It is a separation method in which components of a sample partition between two phases. One of these phases is a stationary bed with a large surface area and the other is a gas that filters through the stationary bed. The sample is vaporized and carried by the carrier gas through the column. Sample partition into the stationary liquid phase based on their solubilities at any given Temperature. The components of the sample separate from one another based on their relative vapor pressures and their affinities for the stationary bed. This chromatographic process is called elution [111].

The gas chromatograph (GC) employed for the identification and quantification of the reaction effluents was the GC 6890 series by Hewlett Packard as shown in Figure 3.7. A 3-way valve connected the reactor outputs with the GC gas-sampling valve creating an online gas sampling system. The reactor was connected to the GC by a ¼ inch stainless steel tub which was heated by a heating element and Temperature controlled by a Watlow Controller. The temperature of the line was maintained at 150°C to maintain the gaseous phase of the reactor outputs.



Figure 3.7: The GC 6890 series by Hewlett Packard

The 890 GC was equipped with 3 columns for gas retention. They were the DB-1, HP-Plot U and HP-Molesieve columns. In addition, 2 detectors to determine gas types are included, the thermal conductivity detector (TCD) and a flame ionization detector (FID). The details of the GC columns are shown in Table 3.5.

Table 3.5 Details of the 6890 GC column

Type	Column Details			Max Temp. (°C)	Gas Flow (ml/min)
	Length (m)	Film (µm)	I.D. (µm)		
HP-Plot U	30	20	530	190	3
HP-Molesieve	15	50	530	300	3
DB-1	30	3	530	280	5

HP-PLOT U consists of bonded, divinylbenzene/ethylene glycol dimethacrylate coated onto a fused silica capillary, and is suitable for analyzing hydrocarbons such as natural gas, refinery gas, C1-C7, all C1-C3 isomers except propylene and propane as well as CO₂, methane, air, CO, water and polar compounds.

HP Molesieve is a PLOT column for the analysis of permanent gases such as O₂, N₂, CO and CH₄ that are resolved in less than 5 minutes. This column has a durable molecular sieve 5A coating that minimizes baseline spiking and damage to multiport valves.

DB-1 column is made of 100% Dimethylpolysiloxane. It is suitable for analyses of non-polar molecules such as methanol and dimethyl ether. It has a High temperature limit and is bonded and cross-linked. It is also rinsable with solvent for cleaning [112]. Figure 3.8 shows an image of a column with its coiled capillary tubes.



Figure 3.8: Image of a Gas chromatograph column [112].

CHAPTER IV

RESULTS AND DISCUSSION

4.1 Catalyst Physic-Chemical Properties

4.1.1 Density of Catalysts

Catalyst density was measured for the 3 catalyst series prepared by the Acid Alkali Alternating pH precipitation method [93]. The In-house Cu/ZnO/Al₂O₃, Cu/ZnO/Al₂O₃ supported with Carbon Nanotubes catalyst series were prepared to determine the effect of absence and presence of Cu and/or CNT in the catalyst. Catalysts density was measured by the Quantachrome Ultrapycnometer 1000 instrument. The density for each sample was measured 3 times to account for deviation in densities of different sample group. The average of these 3 readings was taken as the density of the catalyst sample. The average densities are tabulated in Figure 4.1. The bulk density of the catalyst is a very important characteristic in determining the volume of the catalyst inside the reactor.

From the figure 4.1, it can be seen that Sample 1% CNT supported catalyst has the highest density of 9.16 g/cm³ while CPCat sample has the lowest density of 4.73g/cm³. For, CPCat, it has been found through FESEM EDX study, that it contains 4.21 wt% graphitic carbon possibly inserted into the catalyst as a binding agent during pelletization process. As it can be noticed from the results, catalysts which contain higher amount of carbon nanotubes show lower density when compared with that of lower carbon nanotubes content as well as the alumina based catalysts. This is related to the lower apparent density of carbon nanotubes itself. Since carbon nanotubes have a low density for a solid of 1.3 to 1.4 g·cm³ it would significantly reduce the catalyst weight and hence lower its density [94].

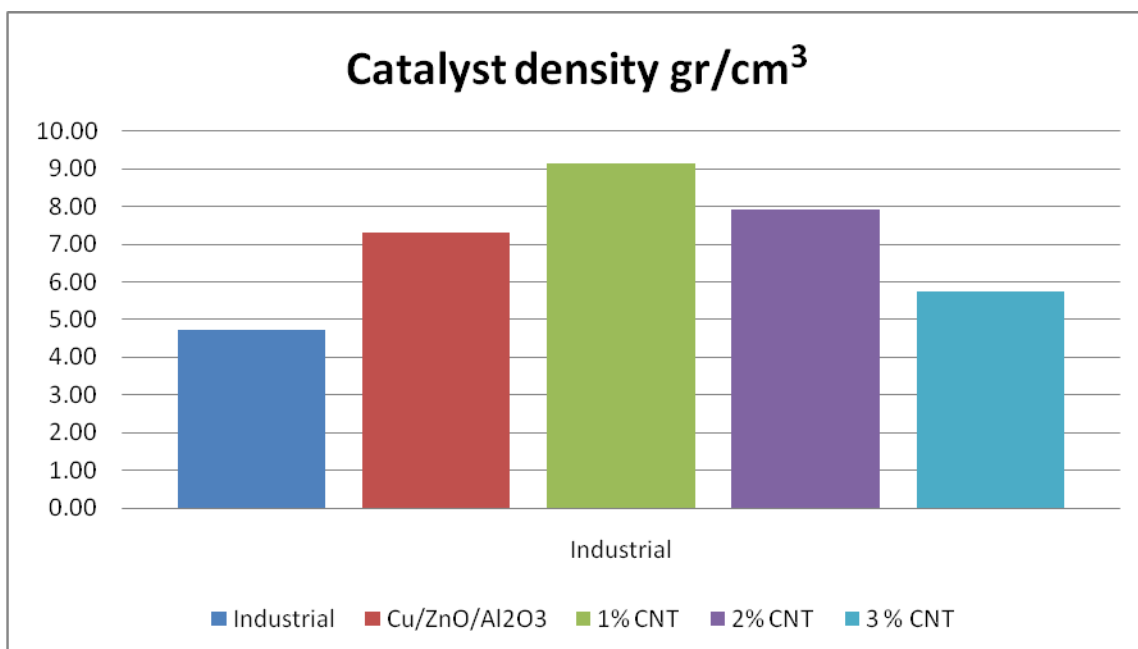


Figure 4.1: Density of all catalyst samples

4.1.2 Phase Analysis by XRD

X-Ray Diffraction analysis was done at a scanning angle range of 2 - 80° and the scanning speed of 1.2°/min. The crystallite types present in the catalysts were identified by comparing the scanning angles and d-spacings of each peak in the resultant curves with the ones existing in the material library. The XRD analysis was conducted through the Bruker D8 Advanced Diffractometer instrument that uses CuK α radiation as its source.

XRD analysis was done on 3 samples, 1% CNT, 2% CNT and 3% CNT supported catalysts to investigate the metal oxide phases and their intensity as corresponding to their compositions. Figure 4.2 shows the spectrum of metal oxides phases formed in each catalyst sample. The actual phase of metal oxide formed is listed in Table 4.1.

The Bragg's angle for copper oxide phase is shown in Figure 4.2 at 35.44 and 38.66°, for zinc oxide at 30.05°, for alumina at 37.8°. Peaks for all other metal oxides are almost the same.

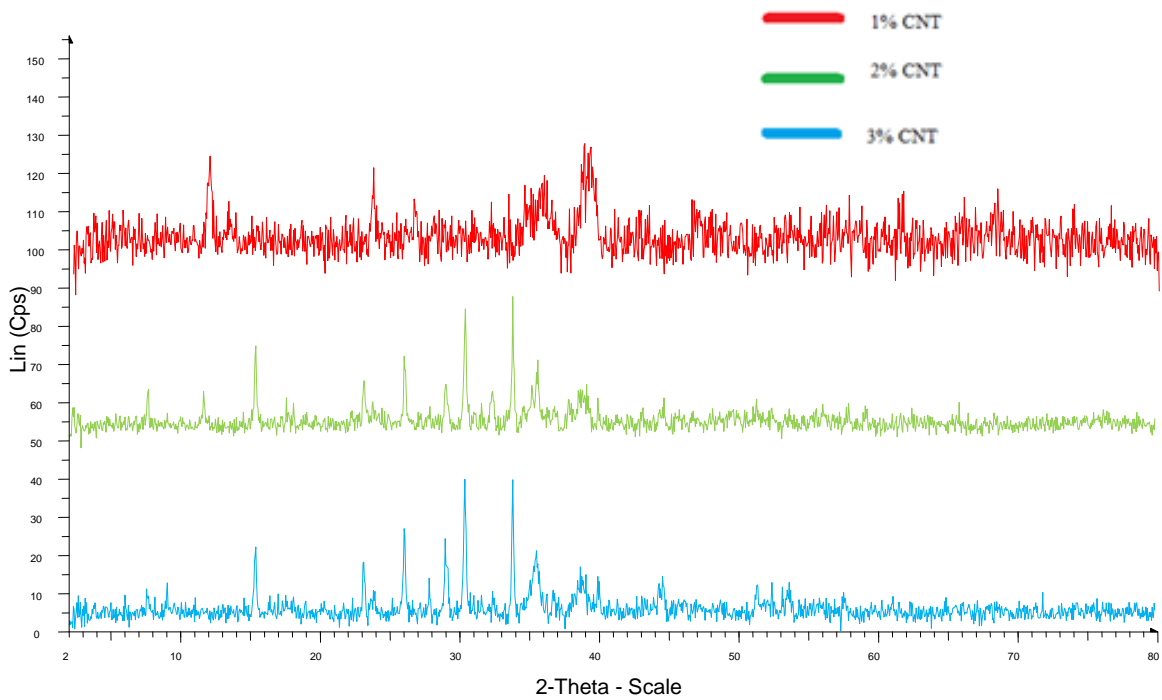


Figure 4.2: Spectrum of metal oxides phases formed in each catalyst sample

Table 4.1: Phases of metal oxides formed for each catalyst sample.

Catalyst Series	Sample	Copper Oxide	Zinc Oxide	Alumina
Cu/ZnO/Al ₂ O ₃ supported with CNT	1% CNT	Tenorite- Monoclinic	Zincite - Hexagonal	Tetragonal
	2% CNT	Tenorite- Monoclinic	Zincite - Hexagonal	Tetragonal
	3% CNT	Tenorite- Monoclinic	Zincite - Hexagonal	Tetragonal

As it can be seen in Table 4.1, the phase of oxide formed for copper oxide is monoclinic Tenorite and for zinc oxide is hexagonal Zincite. This is true for all catalyst samples containing Cu and Zn. [79]. Rhodes et al reports that formation of monoclinic zirconia is 5 times more active than other forms of zirconia due to increase in CO and CO₂ adsorption capacity [114]. The increase in CO adsorption capacity could mean higher activity influenced by the Zr phase alone. The Zinc phase

also has the ability of CO adsorption to produce methanol. Zr and Zn are the sites for hydrogen atoms spillover for the formation of methanol [8].

In methanol synthesis process, the high Al_2O_3 acidity causes the formation of dimethyl ether as a byproduct. This is because the large Bronstead Acid sites (Al-OH) where hydroxyl sites are present and the methanol is catalyzed into dimethyl ether [56]. Our need for a support which has low acidity and high inertness is very crucial. γ -alumina has high surface area but medium Bronstead acidity. θ -alumina has low acidity and high inertness despite its lower surface area. α -alumina has the lowest surface area and lowest acidity.

4.2 Catalyst Structure and Morphology

4.2.1 Surface Chemistry by XPS

The special analytical procedure was worked out and debugged in this study and the surface chemical analysis of all Industrial spent catalysts (from 3 parts of PML syngas to methanol conversion reactor, is obtained from top, middle and bottom) (Figure 4.3) and CNT supported catalyst samples (Figure 4.4) were performed with Photoelectron Spectrometer JPS 9200 (courtesy of Dr. Yoshitoki Iijima, JEOL Ltd. Japan). JPS 9200 is equipped with differential pumping ion gun that allows elemental depth-profile analysis in an ultra-high vacuum environment. The analysis chamber is evacuated by an ion pump and this chamber incorporates an internal backing heater. XPS measurements were performed to determine how the surface composition and the valence state of the surface copper vary between the different catalysts.

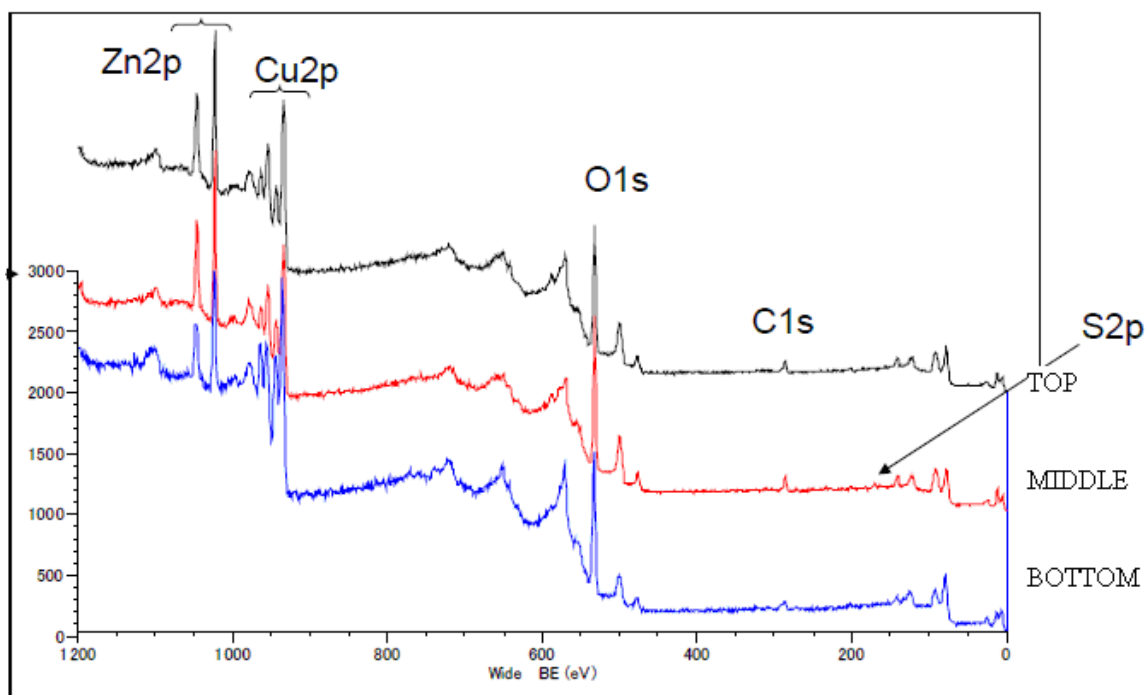


Figure 4.3 Quantitative Elemental phases Spectrum formed in Industrial catalysts.

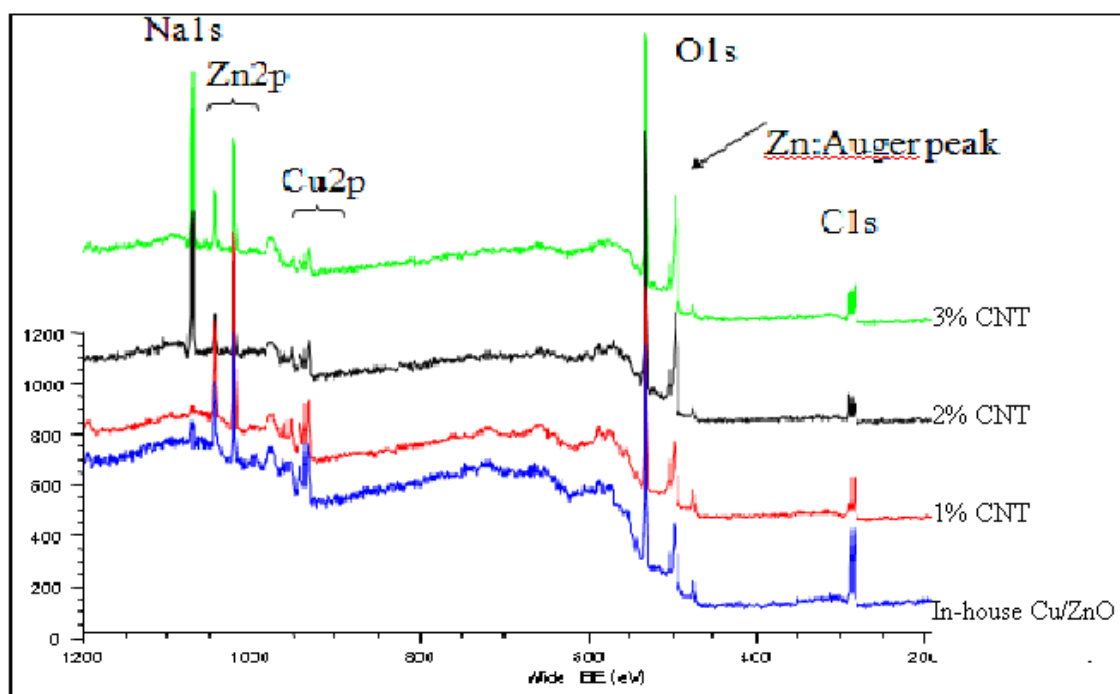


Figure 4.4 Quantitative Elemental phase Spectrum formed in CNT supported and Cu/ZnO catalysts (Blue: In-house Cu/ZnO/Al₂O₃, Red: 1% CNT supported, Black: 2% CNT supported, Green: 3% CNT supported)

In accordance with adopted experimental procedure the samples did not undergo any special pretreatment, before analysis to retain neat composition of the surface of catalyst. The catalysts were just degassed in the preparation chamber at high vacuum ($\sim 10^{-7}$ torr) about 20 minutes before being transferred to the ultrahigh vacuum analytical chamber ($\sim 10^{-9}$ torr). The spectra of the untreated surface were recorded first, then the surface material in analytical microarea was sputtered down till 500 nm and next down till 1000 nm. The spectra at depth 500 nm and 1000 nm were measured. Monochromatic X-rays used in this analysis and spectra were taken in high energy resolution mode, analytical signal of photoelectrons is normally collected from 5-6 nm thick top atomic layer for each specified depth.

XPS analysis was done on all catalysts to investigate the elemental and chemical state phases and their intensity as corresponding to their compositions. Figure 4.3 and 4.4 shows the spectrum of elemental and chemical state phases formed in each catalyst sample. The actual phase of elements formed in catalysts shown in Figure 4.5.

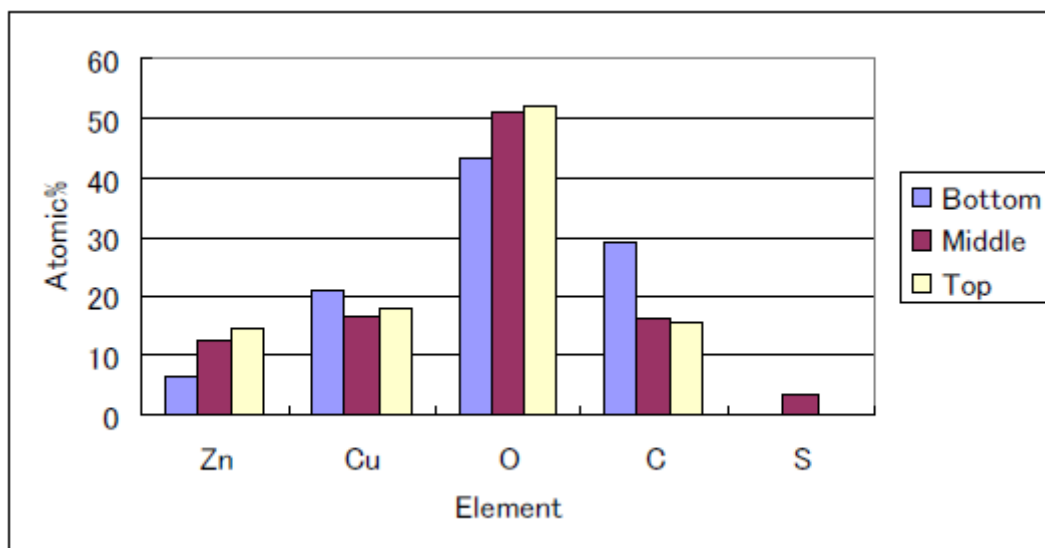


Figure 4.5 Result of Quantification for Industrial spent catalyst (Atomic %)

From XPS analysis (Figure 4.3 and 4.5) it is shown that SICat (from Middle part of Reactor) contains low amount of Sulfur compounds. ZnO have the ability to adsorb poison species that are present in syngas streams. Traditionally, copper catalysts are extremely sensitive to very low levels of sulfur poisoning. Twigg and Spencer50 corroborated that Cu/ZnO/Al₂O₃ catalysts retained a higher activity and even accumulated quite a large amount of sulfur. With an average of 2% sulfur, the methanol synthesis activity of Cu/ZnO/Al₂O₃ catalysts was approximately dropped to 80% of the fresh catalyst. In addition, ZnO can form a special interface or surface defects between Cu and ZnO, which might be an active surface domain [97].

The spectra of Zn 2p is shown in Figure 4.6a and b. The spectra of Zn2p for all catalysts are coincident with each other, whose binding energies for Zn (1021.8) are 1021 and 1022 eV. The spectra of Cu2p for all catalysts were also consistent Figure 4.7a and b, whose binding energies (932.7) are 932.5 and 934 eV. The presence of the satellite peak is attributed to the interaction of the ejected photoelectron with another valence band electron, and/or to the metal-to-ligand charge transfer which has been demonstrated to occur in Cu²⁺ [103,98]. Satellite peaks are not present in Cu⁰ or Cu⁺ spectra due to the full 3d bands [107,98]. The presence of a Cu²⁺ species is in agreement with the XRD data, which indicates that CuO is the main Cu species before reduction and reaction [124].

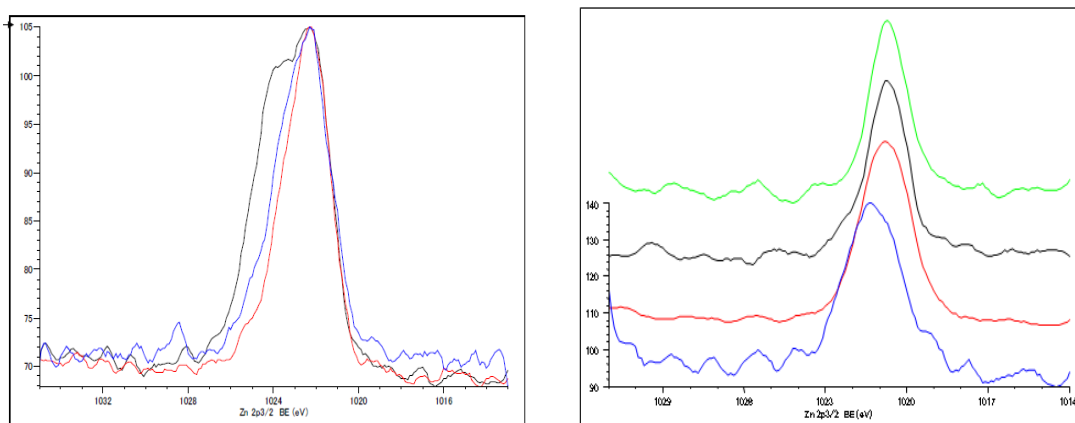


Figure 4.6 A (Left) and B (Right): (A) Binding Energies spectra of Zn on Industrial Spent Catalyst. (B) Binding Energies Spectra of Zn on CNT Supported Catalysts.

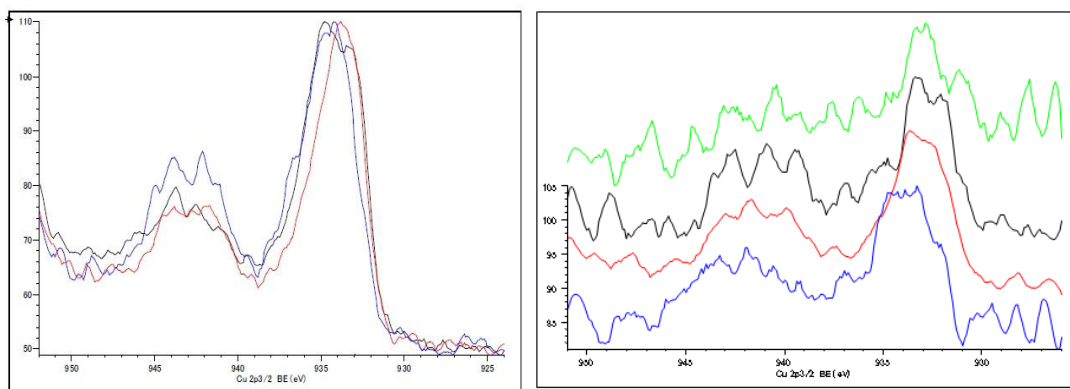


Figure 4.7 A (Left) and B (Right): (A) Binding Energies spectra of Cu on Industrial Spent Catalyst. (B) Binding Energies Spectra of Cu on CNT Supported Catalysts.

After reductive treatment and exposure to the reaction conditions, the Zn/Cu ratio increases on all catalysts. This indicates that after reaction more ZnO covers the active Cu phase compared to before the reaction. This explains at least part of the catalyst deactivation since the active Cu surface area is reduced. In contrast, the C/Al ratio is relatively constant before and after reaction on all catalysts. After exposure to the reaction conditions the binding energy of the Cu $2p_{3/2}$ peak is shifted to a lower value revealing reduction of the CuO (Figure 4.8). The binding energies of the spent catalysts are located at 932.7 eV for Cu₂O, which is in agreement with Cu₂O and Cu metal [109] 935.2 eV for Cu(OH)₂ and 933.9 eV for CuO. However, the peaks are broader than what would be expected for pure Cu₂O or pure Cu metal, which again suggests that more than one Cu species are present on the surface.

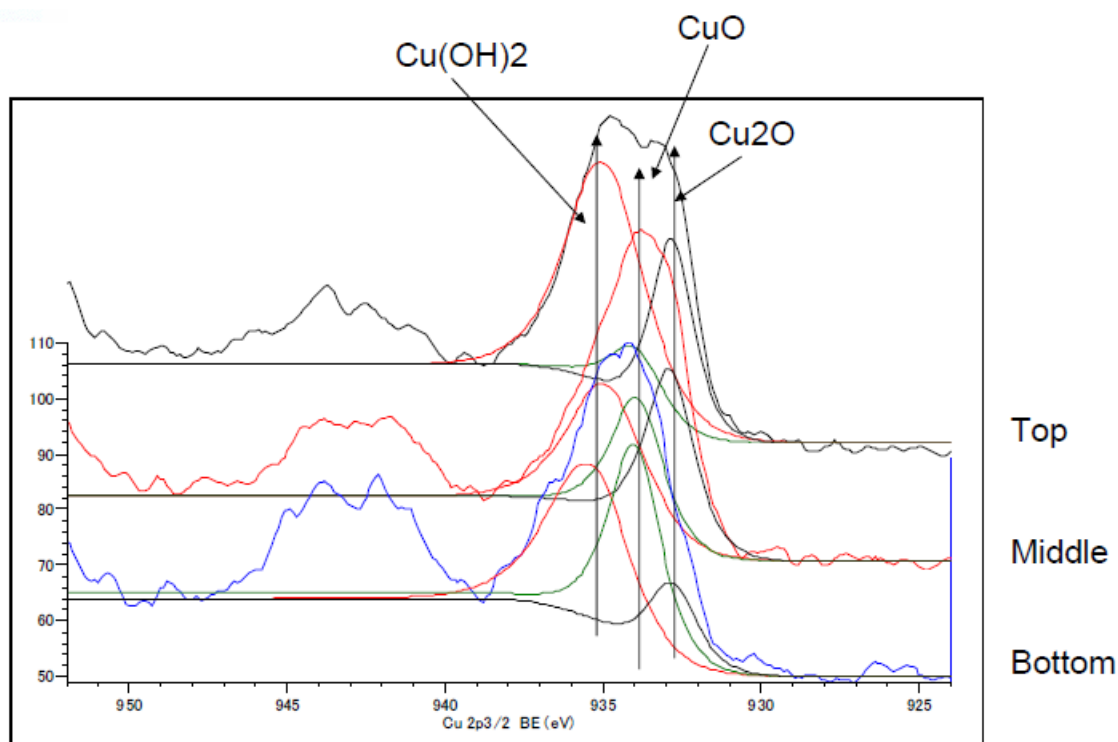


Figure 4.8 Cu chemical state on Industrial catalyst.

The Zn 2p and O 1s binding energy regions were also examined for all catalysts after reaction. However, these regions do not vary significantly between the catalysts and do not provide new information about the catalyst surface. For example, the Zn 2p peaks in ZnO and Zn(OH)₂ are located at 1022.1 and 1023.7 eV (Figure 4.9), respectively and thus the XPS data alone cannot be used to differentiate between the two species [109].

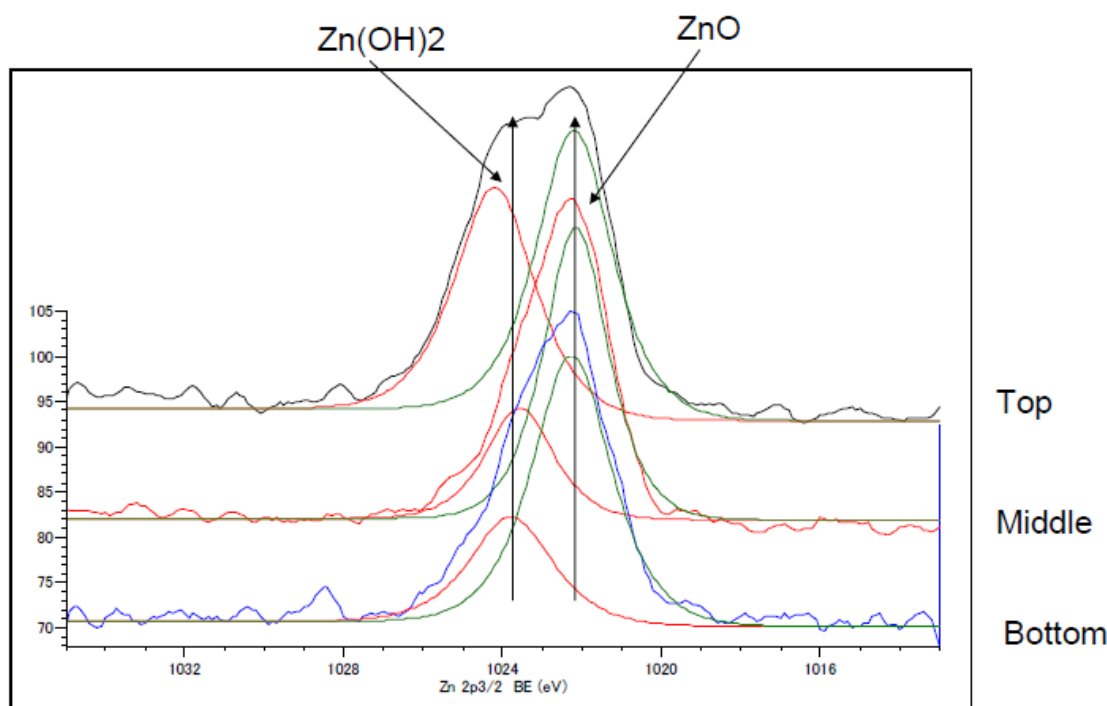


Figure 4.9 Zn chemical state on Industrial catalyst.

In summary, all catalysts contain Cu_2O at the surface after exposure to the reaction conditions. While some Cu^+ likely is required for a high catalytic activity, it is possible that over oxidation. Formation of CuO or bulk Cu_2O , decreases the catalytic activity [110].

4.2.2 LEIS Data

The LEIS experiments were carried out using the Qtac100 (High Sensitivity LEIS Spectrometry) setup. The energy distribution of the scattered ions is analyzed through a fixed angle (142°) with a kind of cylindrical mirror analyzer. During the measurements, the pressure increases to the low 10^{-8} mbar range because of the ion beam. In this study a 5 keV Ne^+ beam was used to measure Cu and Zn. Because it is not possible to detect light elements such as O. Ne^+ beam, a 3 keV $^4\text{He}^+$ beam was used to check the purity of the surface. As a consequence of the ion bombardment, atoms are sputtered from the target surface. This procedure allows determination of the depth distribution of the elements in the sample. The sputter yield - the number of target atoms sputtered from the surface of the catalyst per incident ion - 1.4×10^{13} atoms per cm^2 were sputtered from the sample surface during the analysis.

SICats were analysed. The catalysts were taken from different areas of a reactor. It was expected that the varying conditions in the reactor induce different surface compositions (Figure 4.10).

#	Label on Sample
1	Top Left AT (L) (1)
2	Middle Left AM(L) (2)
3	Bottom Left BB(L) (3)
4	Top Right AT(R) (4)
5	Middle Centre AM(C) (5)
6	Bottom Centre BB(C) (6)
7	Bottom (2) AB (2) (7)
8	Bottom (1st) AB (1st) (8)
9	Bottom Right BB(R) (9)
10	AM Middle (10)
11	CuZnO Reference

Figure 4.10 Nomenclature of catalysts

For preparation sample, first catalyst treated with atomic oxygen at room temperature until complete removal of organic contaminants. After these pretreatments catalysts surface is clean and oxidized. This can be observed by the increase of the interfering Cu/Zn surface peak and the increase of the O surface peak. $^4\text{He}^+$ ions scattering on the cleaned samples allows screening for elemental surface components.

The following measurement and evaluation concept for Ne scattering was performed:

- All atomic oxygen cleaned samples were analyzed. The results are presented assorted by the samples' distribution in the reactor.
- The peak areas of the combined Zn/Cu signals were determined and used for a normalization of the spectra.
- Using normalized spectra the samples were clustered in groups of identical Cu/Zn ratio. The results of this normalization procedure are presented assorted by the three determined groups.

- The Zn and Cu surface coverage area of one representative of each of these groups was quantitatively evaluated by fitting the nonnormalized spectra to those of the Zn and CuO standards.
- The quantitative evaluation of the spectra of the other samples was performed taking the determined Cu/Zn ratio and the determined combined Cu/Zn surface peak area into account.

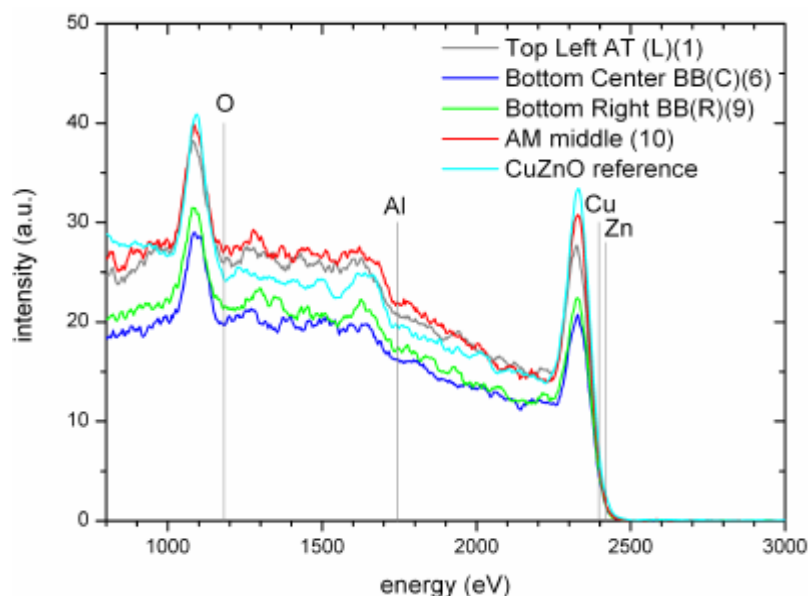


Figure 4.11 The typical spectra of catalysts collected from different part of the reactor.

The vertical lines marked by chemical element correspond to the high energy onset of the expected peak, not the centre of the peak. On all five samples analyzed in this experimental set-up, O is at 1182 and Cu/Zn are detected at 2397/2421 eV (Figure 4.11). In addition, an increase of the signal at a scattering energy of -1700 eV is indicative for the existence of Al at and below the outermost atomic layer of the samples.

In order to determine the Al surface content further studies would be necessary. As the key interest in this study was the Cu and Zn surface content this was not further pursued. Neon scattering provides a higher mass resolution in the high mass range. Accordingly, neon scattering was performed to study the Zn and Cu content of the samples' surfaces (Figure 4.12).

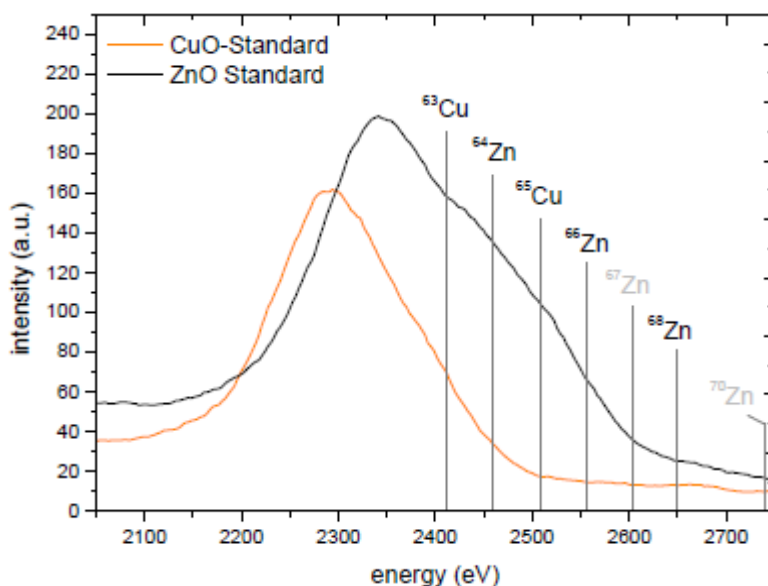


Figure 4.12. The typical spectra of ZnO and CuO References catalysts.

Isotopes of low abundance are marked in grey in table and figure.

Scatter Ion: 20Ne @ 8keV			
Element	Isotope (Atomic No)	Abundance	High Energy Onset / eV
Cu	63	69,2	2411
Zn	64	48,6	2460
Cu	65	30,8	2508
Zn	66	27,9	2556
Zn	67	4,1	2603
Zn	68	18,8	2649
Zn	70	0,6	2740

Figure 4.13 High energy Onset/eV for Cu, Zn and isotopes

Analyzing pure CuO and ZnO samples, two main differences in these two LEIS spectra are observed:

- Due to heavier isotopes the high energy onset of the ZnO surface peak is located at higher scatter energies than the one of the CuO surface peak.
- Due to a greater number of isotopes, the ZnO surface peak is broader than the Cu surface peak.

Whereas using ${}^4\text{He}^+$ scattering a separation of the elements Cu and Zn was not possible, such a separation is possible using ${}^{20}\text{Ne}^+$ scattering (Figure 4.14). This approach is used to qualitatively and quantitatively study the Cu and Zn content of the catalysts' surfaces.

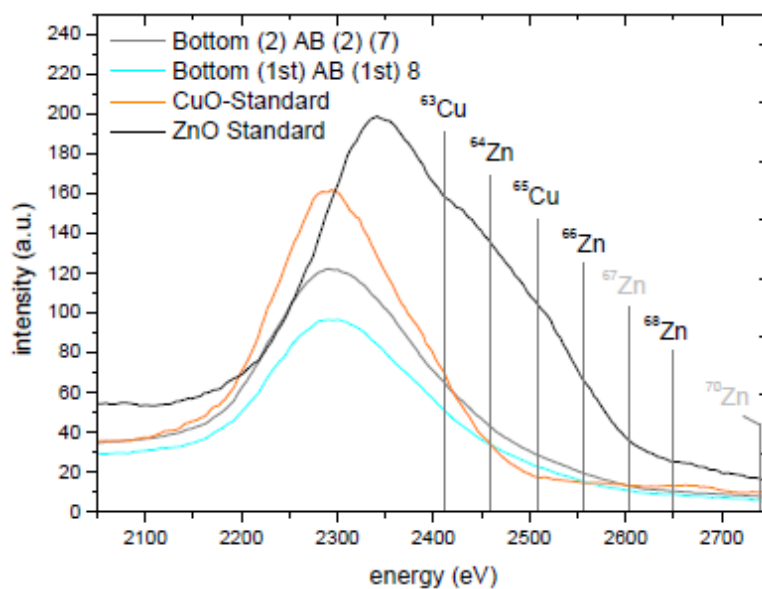


Figure 4.14. The typical spectra of catalysts from the bottom of the reactor.

Figure 4.16 the Ne scattering spectra of the samples “Bottom (2) AB (2) (7)” and “Bottom (1st) AB (1st) (8)” are shown. The combined Zn/Cu surface peak detected on sample “Bottom (1st) AB (1st) (8)” shows a lower intensity than the one of sample “Bottom (2) AB (2) (7) “. Thus a lower surface coverage by these two elements is revealed.

Comparing the combined Cu/Zn surface peaks of the sample with those of the pure standards qualitatively, it can be stated that they are located at relatively low energies, indicating a high Cu content.

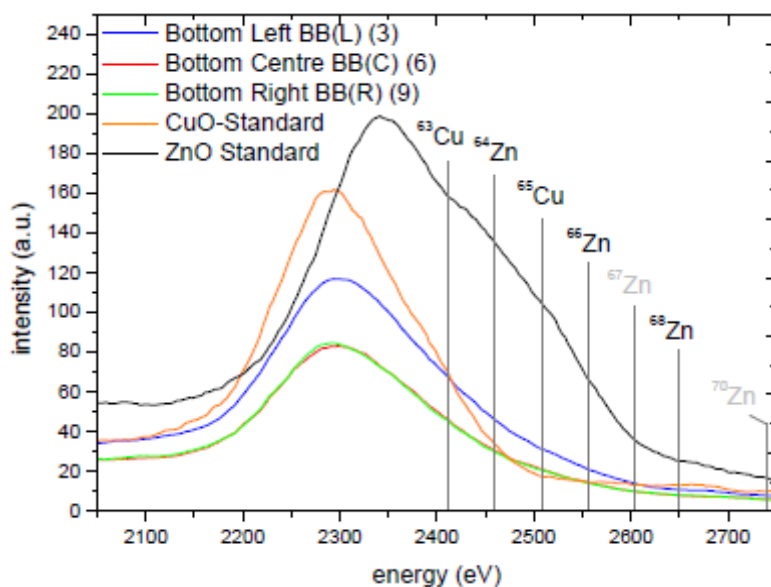


Figure 4.15 The typical spectra of catalysts from the bottom of the reactor (2).

Sample “Bottom Centre BB(C) (6)” and “Bottom Right BB(R) (9)” show almost identical spectra. Thus, the Cu/Zn surface content is very similar (see previous page).

Compared to these samples sample “Bottom Left BB(L) (3)” has a higher Cu/Zn content. All three samples show a relatively high Cu/Zn ratio.

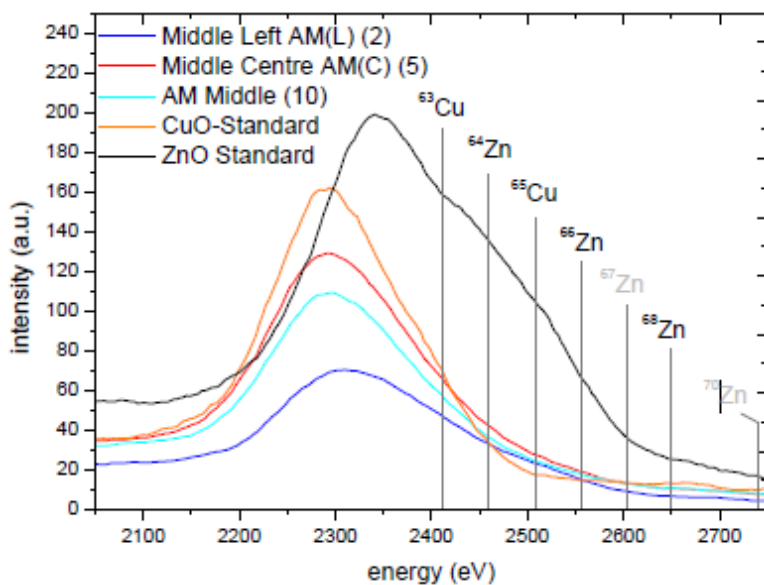


Figure 4.16 The typical spectra of catalysts from middle part of the reactor.

The sample “AM Middle (10)” and “Middle Centre AM(C) (5)” show relatively high surface contents of Cu and Zn (Figure 4.16).

In contrast sample “Middle Left AM(L) (2)” shows a low surface content of Cu and Zn. The combined Cu/Zn surface peak of sample “Middle Left AM(L) (2)” is shifted towards higher scatter energies. This is indicative for a lower Cu/Zn ratio. A similar shift like the one observed for sample “Middle Left AM(L) (2)” is found for sample “CuZnO Reference“. This shift is not observed for samples ”Top Left AT (L) (1)” and “Top Right AT(R) (4)”. These two samples show the Cu/Zn surface peak in relatively high intensities (Figure 4.17).

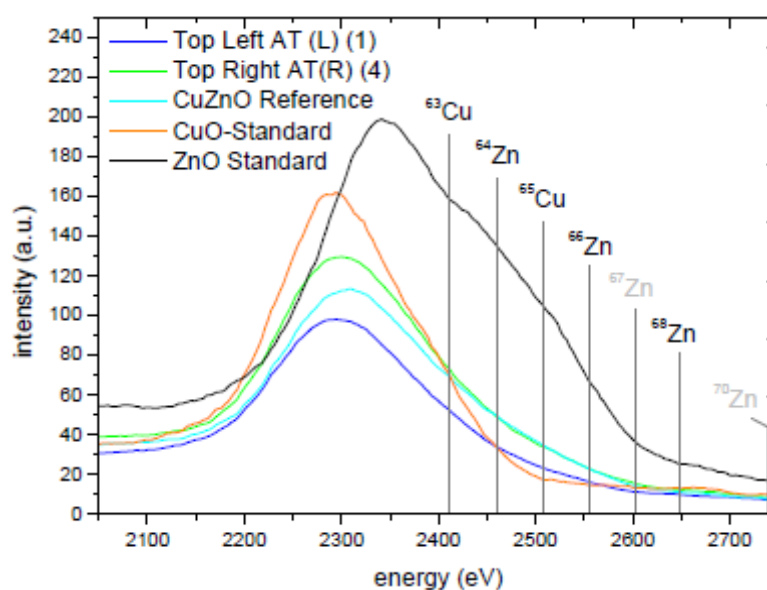


Figure 4.17 The typical spectra of catalysts from the top part of the reactor.

4.2.3 Surface Imaging

Field Emission Scanning Electron Microscopy (FESEM) is a technology used to capture the image of the surface of a solid sample, determine its elemental composition as well determine the distribution of the elements on its surface. The model of the FESEM used for analysis was the SUPRA 55VP by Carl Zeiss. Two sets of images, fresh and spent images were obtained for each catalyst, from the FESEM. The images are captured in a high resolution at 10000X magnification.

Figures 4.18a and 4.18b are pre-catalysts, before reduction process. Catalyst activation which was conducted to reduce the catalyst surface was done with a 5% H₂ in N₂ gas stream at a flow rate of 76.5 ml/min from room temperature to the sample reduction temperature at a ramp rate of 10°C/min. Hydrogen reduces copper oxide in the catalyst to copper giving off heat and water. Figures 4.19a and 4.19b are industrial spent catalyst and 2% CNT supported catalyst tested in a laboratory scale [95].

Figures 4.18a and 4.18b shows FESEM data of a fresh, untreated commercial pre-catalyst and CuO/ZnO/Al₂O₃ catalyst supported with 2% CNT. They showed that the majority of the CuO and ZnO appear in large agglomerates in the order of 5-15 nm in size. Additional structures existed consisting of Al₂O₃ and carbon added as supports. It appeared that the bulk CuO/ZnO amalgamations are relatively separated from the Al₂O₃ and the carbon filler. It is well known that Al₂O₃ and carbon have little activity for methanol oxidation at the lower temperatures representative of this study. It is likely then, that either CuO or ZnO or both are the active phases with the other components being inert [115].

Figures 4.19a and 4.19b are industrial spent catalyst and 2% CNT supported catalyst. SEM observation of the precursors of the Cu/ZnO catalyst clearly showed the formation of spherical fine particles in the magnifications of 10KX. Spherical fine particle seems to be assembly of thin plate-like structures and the surface is not smooth. Spherical fine particles were evidently observed for the samples showing the strong reflection of aurichalcite in the XRD. Such spherical fine particle structure with high surface area was maintained even after the calcination at 300 °C for 3 h in air, and is supposed to possess an important role in the catalytic activity.

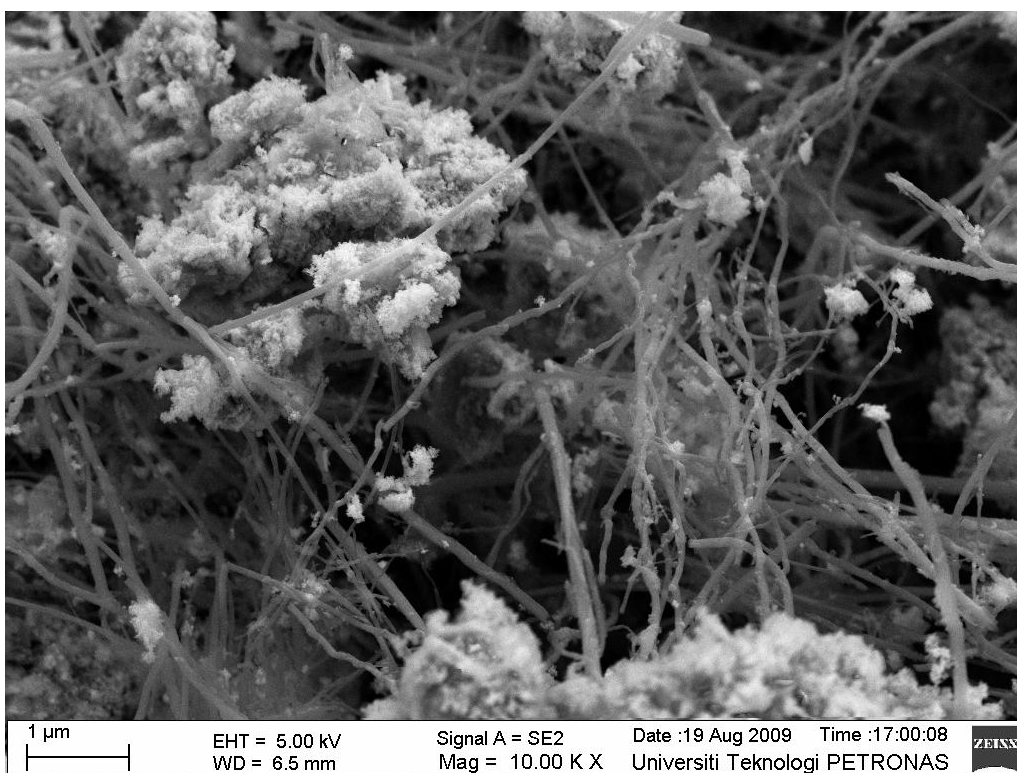
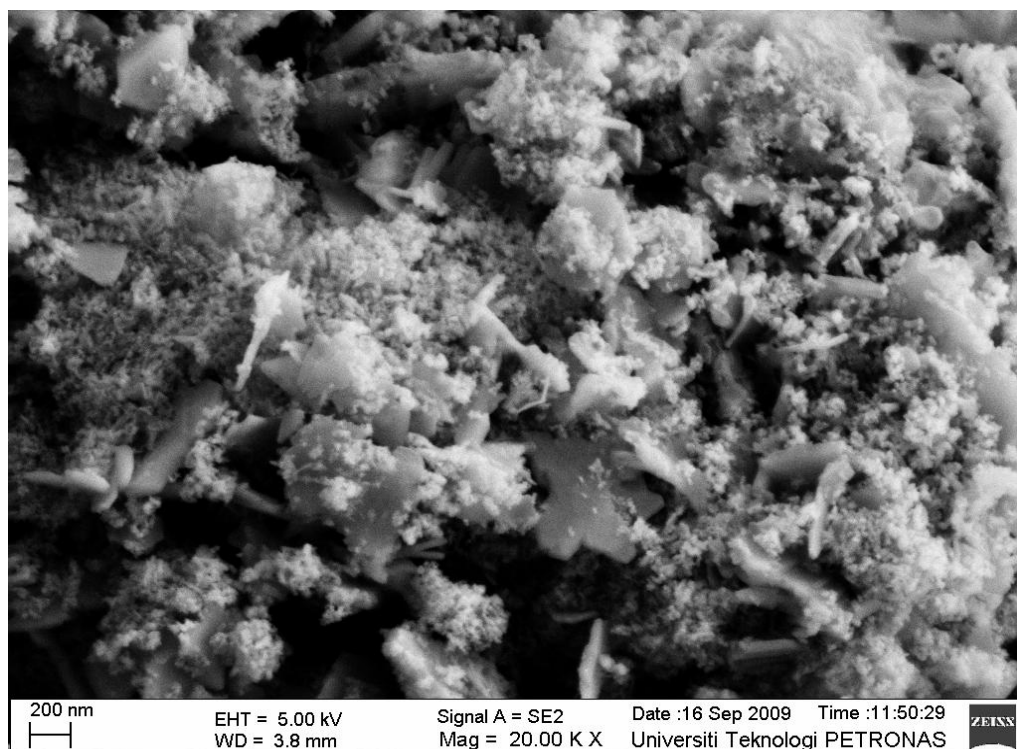


Figure 4.18a and b: (a) (TOP) Commercial pre-catalyst.
(b) (BOTTOM) 2% CNT supported pre-catalyst

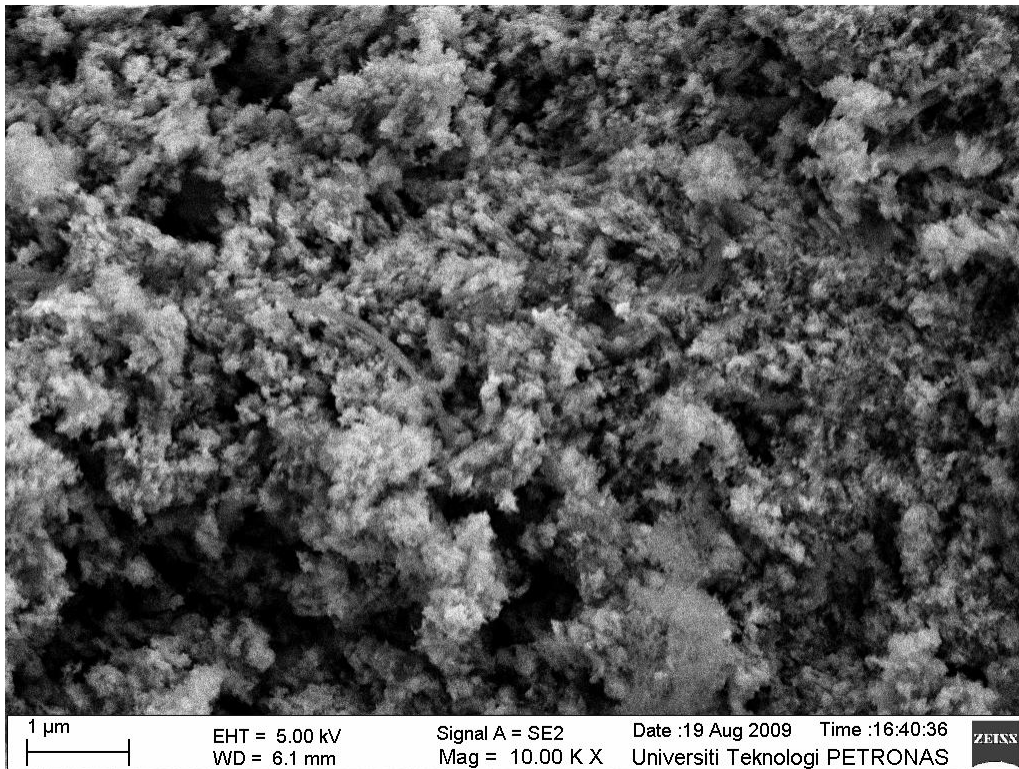
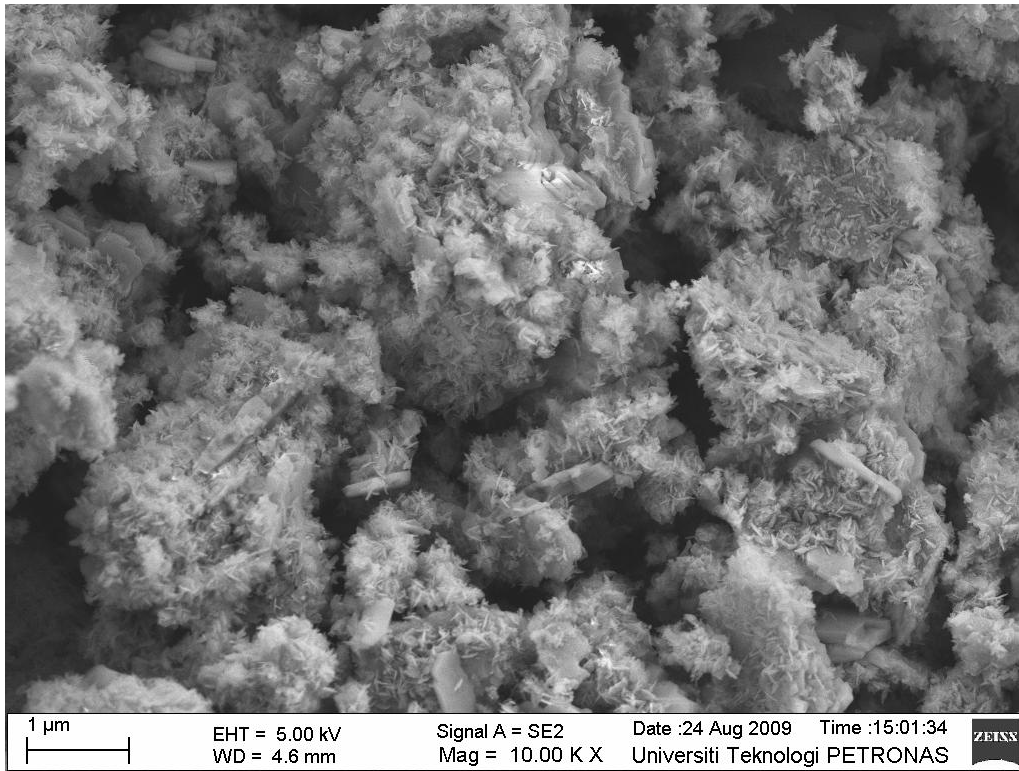


Figure 4.19a and b: (a) (TOP). Commercial spent catalyst
(b) (BOTTOM) 2% CNT supported catalyst.

4.2.4 Elemental Composition Analysis by EDX

Elemental composition of the sample at its surface is obtained by X-Ray Energy Dispersive Analysis (EDX) analysis (Table 4.2). X-rays are released by the sample surface after electron bombardment and each element releases x-rays of a particular energy (keV). EDX was conducted on an image of width 6 μ m.

Table 4.2: SEM-EDX metal ratios of SICat and in-house made catalyst samples

Catalyst	SICat	In-house Cu/ZnO/ Al ₂ O ₃	1%CNT supported catalyst	2%CNT supported catalyst	3%CNT supported catalyst
Element					
C	10.56	3.31	3.96	2.48	24.57
O	26.74	28.65	22.93	24.45	34.82
Al	4.12	2.50	3.11	2.88	2.11
S	1.30	0	0	0	0
Cu	38.08	26.49	29.01	31.19	5.29
Zn	20.05	39.10	40.99	38.99	8.27
Na	0	0	0	0	24.62

Only metal compositions are taken into account during theoretical calculations while oxygen, carbon and nitrogen are considered together with metals in an EDX detected composition. From the table 4.2 it's obvious shown that SICat contains itself low amount of sulfur, which is known as a poison for catalysts [108]. It can be seen SICat contains some amount of carbon. Carbon is very strong material, and it can block, deactivate some spots on the surface. In 3% CNT supported catalyst Sodium appears in high amount. This can be explained that Na₂CO₃ was base solution, while catalysts preparation process. Sodium decreases amount of Cu and Zn. But the catalyst is still keeps its high conversion property.

4.2.5 EFTEM study of CNT promoted catalysts

The structural features of Cu/ZnO/Al₂O₃ supported with CNTs were analyzed by TEM to observe the dispersion and size of catalyst particles. The Cu particles had a larger size of about 250 nm with a higher aggregation, and were not absorbed on the surface of CNT. The results by TEM analysis are illustrating that a better dispersion and effective adsorption of catalyst particles on the CNT surface can be achieved. These data suggested that Cu/ZnO catalyst existed in fine particles, which showed distinctive surface physical properties from Cu/ZnO/Al₂O₃ supported with CNTs.

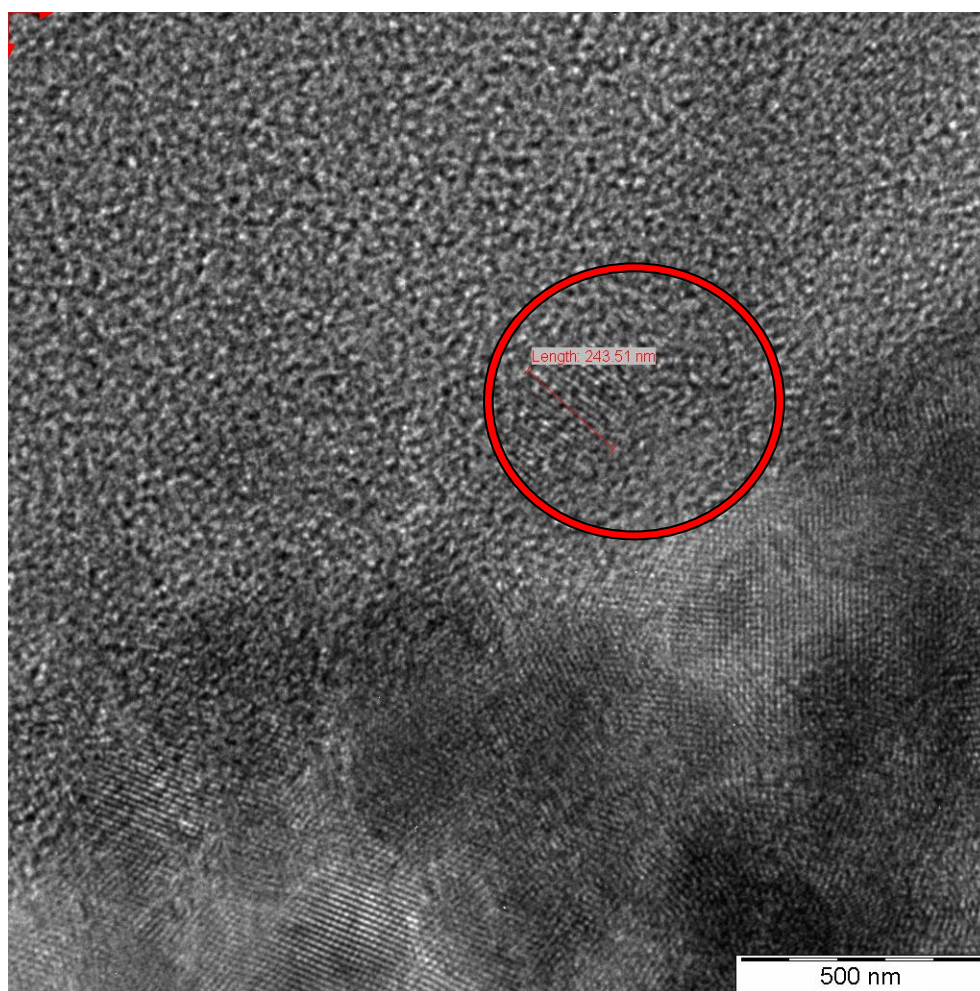


Figure 4.20 TEM surface imaging of 2% CNT supported Catalyst

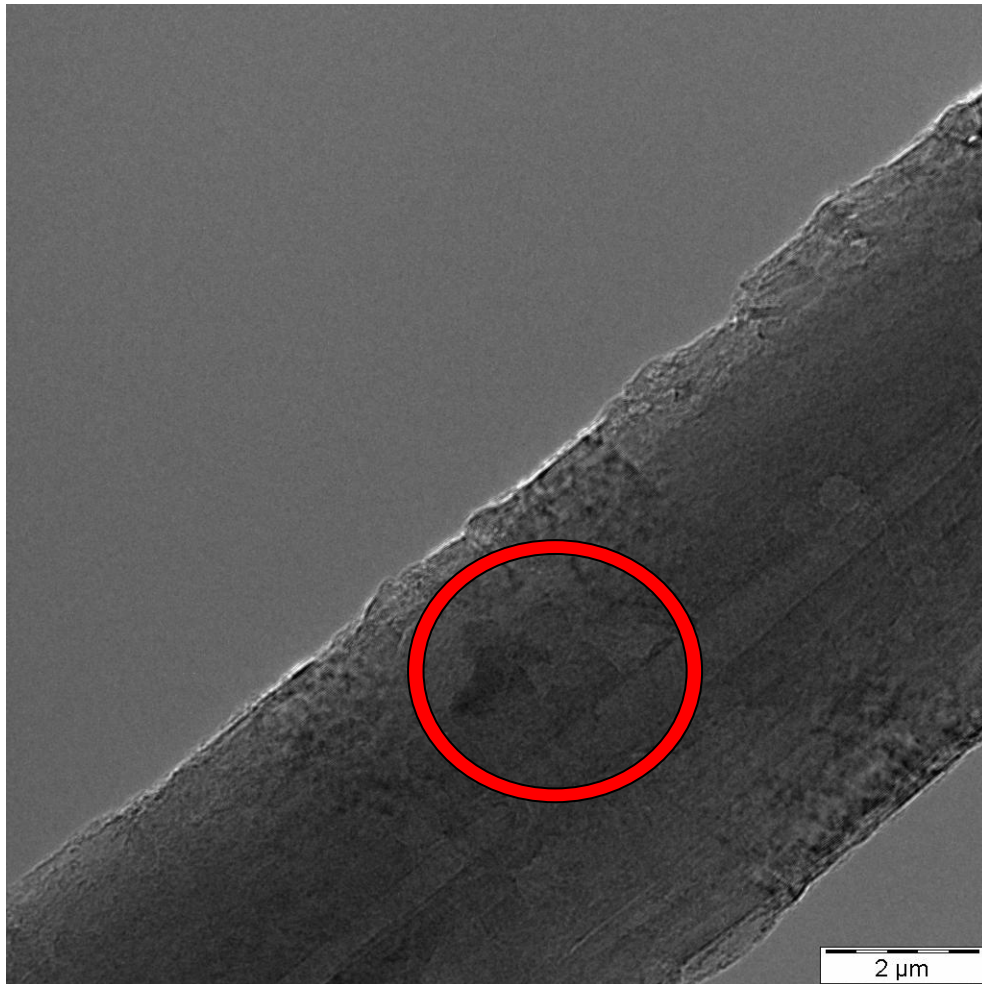


Figure 4.21 TEM surface imaging of 2% CNT supported Catalyst

Electron energy loss spectroscopy (EELS) identified only metallic Cu as copper phase in all samples studied. However, EFTEM analysis of selected areas evidences the presence of amorphous materials Cu and ZnO in addition to the main phases. Aluminum was hardly detected and mainly found as amorphous phase. In rare cases Al has been identified as crystalline α -Al₂O₃ by EFTEM. Various morphologies of Cu and ZnO particles were detected for the Cu/ZnO/Al₂O₃ supported with CNTs catalyst, such as round and irregular shaped Cu particles as well as plate and needle like ZnO particles (Figure 4.21)

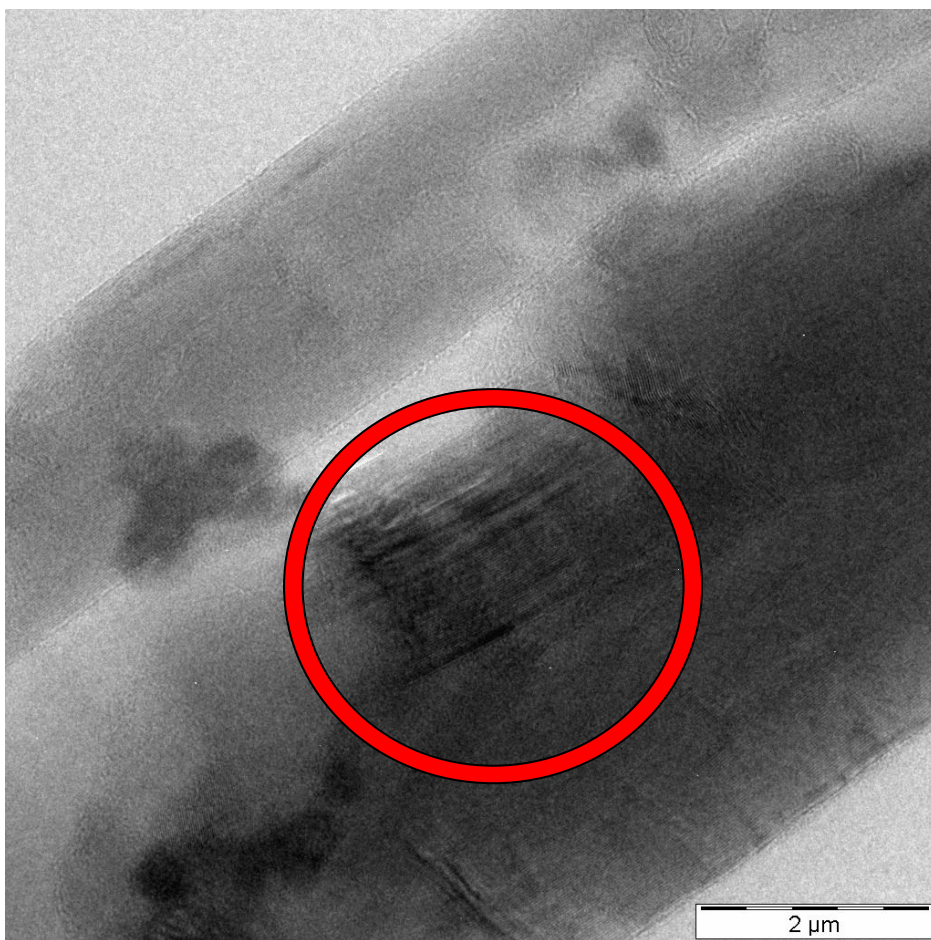


Figure 4.22 TEM surface imaging of 2% CNT supported Catalyst

4.2.6 Reducibility and Temperature Optimization

Temperature Programmed Reduction (TPR) of all catalyst samples were conducted by means of the Thermo Finnigan TPDRO 1100 equipment. All samples were pretreated with nitrogen to remove impurities and then the reduction process was commenced from room temperature to 600°C. The resulting Signal peaks (mV) vs. reduction temperature are plotted for all catalyst samples and for comparison are grouped together in Figure 4.23. The Signal (mV) here represents the amount of H₂ adsorbed at each Temperature. The area under the curves of each sample is defined as the total amount of H₂ gas adsorbed in mV and the signal is converted to mmol of gas adsorbed by a pre-calibrated factor of 1.067×10^{-7} mmol/mV. This adsorption value would be further corrected by taking into account the gas adsorbed by Cu metal alone through inclusion of metal Cu wt% area. The graph of total H₂ adsorbed for each sample is plotted and shown in Figure 4.34.

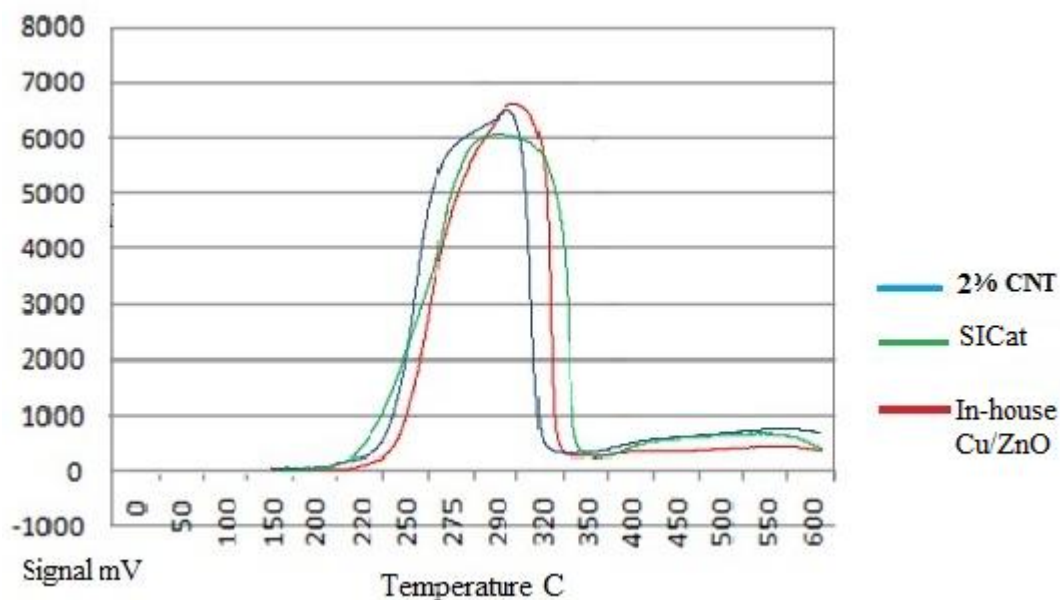


Figure 4.23: Graph of reduction Temperature and their corresponding H₂ gas adsorbed as Signal (mV).

From Figure 4.23, it can be seen that for catalyst samples, the H₂ adsorption or the reduction was zero until 200°C when H₂ adsorption commenced. At about 200 to 275°C H₂ adsorption steadily increased for all catalyst samples. H₂ adsorption peaked around 280°C and remained constant until 320°C for all catalyst samples. The latter samples remained at highest reduction peak until 295°C. After this peak reduction period, H₂ adsorption dwindled and thus and zeroed at 350°C.

The data for most optimum temperature for reduction is crucial for catalyst activation before activity is studied in the methanol synthesis process. For each sample it was determined as follows: SiCat is 295°C, 2% CNT is 295°C and sample In-house Cu/ZnO/Al₂O₃ is 285°C. This temperature is in effect the highest peak obtained for each sample graphs in Figure 4.23 i.e. Temperature at highest signal is the temperature at which highest amount of H₂ adsorption took place.

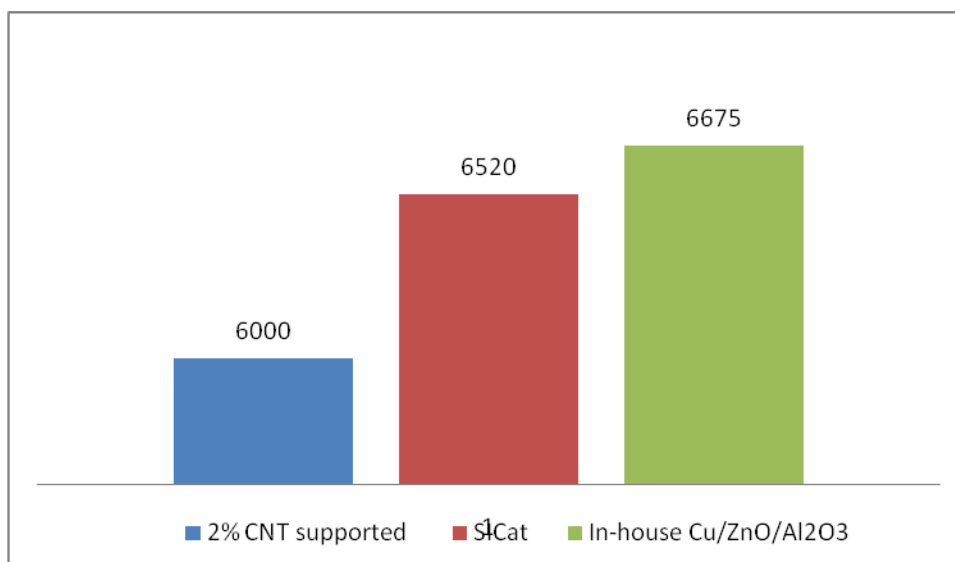


Figure 4.24: Total Hydrogen gas adsorbed by each catalyst sample in TPR analysis

In Figure 4.24, it is shown that the amount of H₂ adsorbed by Cu metal crystals alone in 2% CNT supported catalyst, SiCat and In-house Cu/ZnO/Al₂O₃ catalyst samples. This graph somewhat qualitatively suggests the potential catalyst activity as far as Cu active sites is concerned. It has been established that greater number of available Cu active sites is an indicator of greater activity. The hydrogenation of CO on Zn sites still depends heavily on Zn amount in catalyst samples [95].

4.3 Catalyst Activity Study

Catalyst activity was studied in a catalytic micro tubular reactor as described in Section 3.5. The 30% CO/70% H₂ mix gas was flowed from the top of the reactor through the catalyst bed and the effluent gas was directed onto on-line Gas Chromatograph (GC) to analyze the composition of the reaction products. Two key properties are used as gauges for comparison of catalyst activity for all catalyst samples with variant metal compositions as displayed in Table 4.2. They are CO Conversion (Equation 4.1) and Methanol Selectivity (Equation 4.2) [96].

$$X_{CO} = \frac{(n_{CO})^i - (n_{CO})^f}{(n_{CO})^i \times g_{cat}} \times 100\% \quad 4.1$$

$$S_{MeOH} = \frac{(n_{MeOH})^f}{\sum (n_x)^f} \times 100\% \quad 4.2$$

$$S_x = \frac{(n_x)^f}{\sum (n_x)^f} \times 100\% \quad 4.3$$

CO conversion X_{CO} , on the other hand was defined as change in CO concentration over initial CO concentration and catalyst mass at any given time during the reaction. Methanol selectivity S_{MeOH} was defined as concentration in mol% of methanol in the product gas over total concentration of all other products $\sum (n_x)^f$ in the product gas. The Selectivity, S_x of all other products was defined as mol% of product, n_x in the product gas over total concentration of all other products. Effluent gas concentrations were measured by on-line GC at every 15 minutes interval although Methanol Selectivity and CO conversion for each catalyst sample was calculated for every 30 minutes for a period of 3.5 hours.

The concentration of reactant gas was evaluated in the GC prior to the reaction for a number of times and the average concentration of the mixture gas was 30.98mol% CO and 70.1 mol% H₂. The gas mixture was flowed in to the reactor system at a flow rate of 210ml/min and catalyst bed Temperature was maintained at 250°C and Pressure at 30 bars. In the reactor, catalysts mass for all samples loaded was 1g.

4.3.1 CO conversion

In the methanol synthesis reaction, CO conversion is a primary indicator of catalyst activity as CO is the limiting reactant. The amount of H₂ in syngas mixture is excess in industrial settings. This is because the conventional prior reaction that produces syngas from natural gas and H₂O is the steam reforming and the stoichiometric ratio of H₂ produced to CO produced in this reaction is 3:1 as shown in equation 4.4. This syngas mixture is then directly injected into the methanol synthesis reactor for catalytic conversion to methanol.



CO conversion into methanol is defined by Equation 4.1. The results of comparison between all catalyst samples are shown in Figure 4.25 and Figure 4.26. Table 4.4 lists the composition of all elements in each catalyst samples. Figure 4.25 shows the CO conversion comparison between catalyst samples of type In-house Cu/ZnO/Al₂O₃, CPCat and 2% CNT supported catalyst at time interval of 30 minute for 3.5 hours.

It can be clearly seen from Figure 4.25 that the highest CO conversion among 2% CNT, CPCat and In-house Cu/ZnO/Al₂O₃ catalyst samples is obtained for Sample In-house Cu/ZnO/Al₂O₃. Although the conversion rate changes throughout the period of study, it is still within the range of 3% to 8%. 2% CNT supported catalyst has low CO conversion rates of 1.5 to 4.5 %. The conversion rate of Industrial CPCat is higher than 2% CNT supported catalyst but lower than In-house Cu/ZnO/Al₂O₃ at around 2 to 6.0%. CO hydrogenation to methanol over the Cu/ZnO/Al₂O₃ catalysts supported on CNT showed that the supporter could significantly affect the activity of CO hydrogenation.

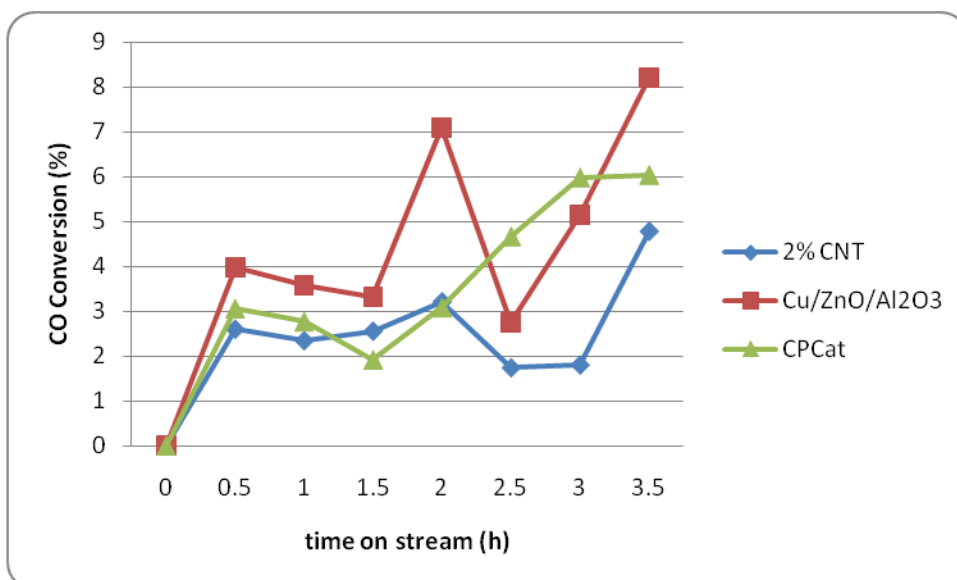


Figure 4.25: CO conversions in % for 2% CNT supported catalyst, CPCat and In-house Cu/ZnO/Al₂O₃ type catalysts.

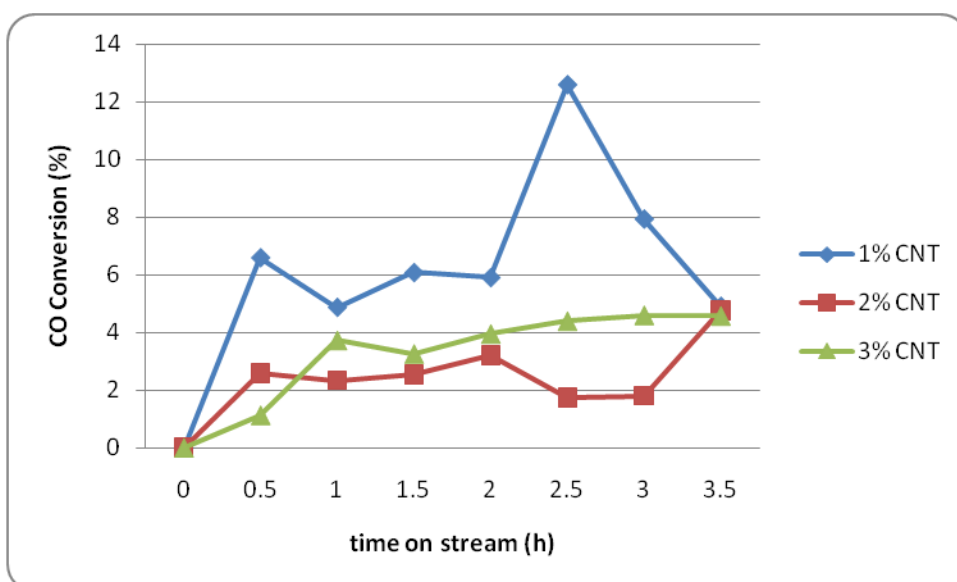


Figure 4.26: CO conversions in % for 1, 2 and 3% CNT supported catalysts.

From Figure 4.26 it can be seen that 1% CNT supported catalyst has the highest CO conversion up to 12% and this followed by 3% CNT supported catalyst up to 4.5%. 2% CNT supported catalyst has low activity as well in the range of 1.8 to 4.5%. 1% CNT supported catalyst and 2% CNT supported catalyst shows a unique set of CO conversion rates over a period of 3.5 hours study. For the first 2.5 hours the CO conversion of 1% CNT supported catalyst is much higher than 2% CNT supported,

but after 2.5 hours conversion rate is decreases to the same rate as 2% CNT supported catalyst, the CO conversion of 2% CNT supported catalyst increased especially towards the last ½ hour of the study. This could be due to the effect of hysteresis in 1% CNT supported catalyst which is not so obvious in 2% CNT supported catalyst. Hysteresis happens when after a period of adsorptions of gas on catalyst surface and the formation of multilayer of adsorbed molecules on the catalyst surface occurs. This hinders the motion of the desorbed product gas away from the surface of the catalyst and thus impedes the reaction rate.

4.3.2 MeOH Yield

The Methanol synthesis process through syngas route is outlined in Equation 4.5 – 4.8. The reactant gas which contains only H₂/CO mixture hypothetically produces Methanol with the stoichiometric MeOH/CO ratio of 1:1 as shown in Equation 4.7. However, this is not the case generally observed. Klier *et al* proposed that the water gas shift (Equation 4.5) will occur in the forward direction for low CO₂ feed concentration to convert CO to CO₂ and thus encourage the hydrogenation of methanol as outlined in Equation 4.6 [96]. This reaction would also give a stoichiometric MeOH/CO ratio of 1:1. The stoichiometric ratio of CO /H₂ of 1:2. In our reaction, the molar ratio of CO/H₂ was set to 3:7. This was done so as to provide excess H₂ in the reaction. This precaution is crucial in order to discourage the Boudouard reaction (Equation 4.8) from occurring. This reaction involves the direct conversion of CO to CO₂ and C and is a major source of catalyst deactivation as carbon clogs the catalyst pore and reduces excess to active metal surface area. The presence of excess H₂ would discourage the formation of Carbon and encourage the route in Equation 4.5 for CO instead of equation 4.7.



As the stoichiometric ratio for CO/MeOH conversion is 1:1, MeOH yield is thus defined as mol MeOH produced in effluent gas over mol CO in reactant gas as shown in Equation 4.9.

$$Y_{CH_3OH} = \frac{(n_{CH_3OH})^f}{(n_{CO})^i} \times 100\% \quad 4.9$$

Figure 4.27 is a plot of calculated (Appendix 1) MeOH yield (%) for commercial catalyst samples, CPCat and CNT mixed catalysts at time interval of 30 minutes over a period of 3.5 hours. From Figure 4.38, it can be clearly seen that from the beginning of the reaction until 2.5 hours of study, MeOH yield by all catalyst samples increases quickly.

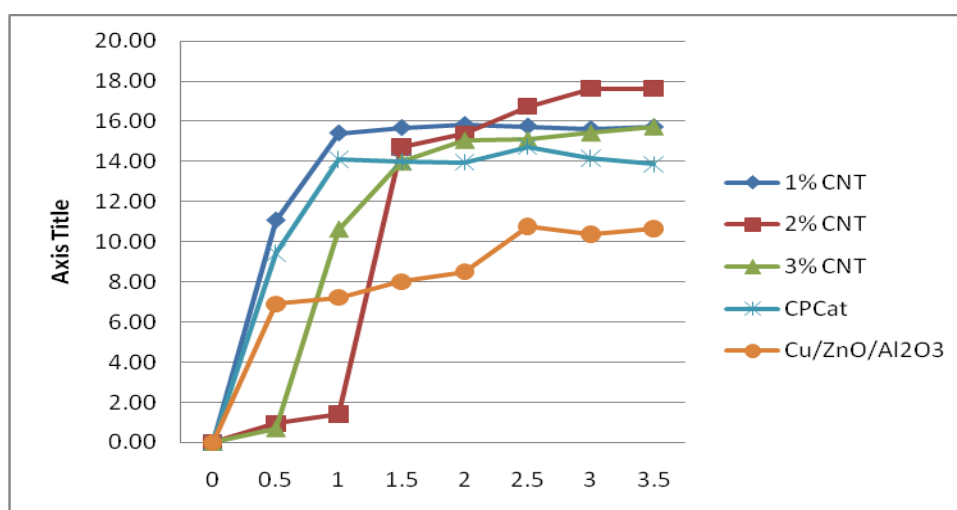


Figure 4.27: MeOH Yield in % for CPCat samples, In-house Cu/ZnO/Al₂O₃ and CNT supported Catalysts

This phenomenon is explained as modification of metal oxide surfaces into a form of Cu-Zn metal alloy which work in tandem with each other to break the H₂ bond into H atoms and simultaneously hydrogenate hydrated CO into subsequent species before methanol is formed [80]. This surface modification usually requires time before an optimum metal-chemical structure is obtained and an equilibrium steady state MeOH yield is achieved.

1% CNT supported catalyst and 2% CNT supported catalysts reached optimum MeOH yield quickly at around 1.5 hr, but 3% CNT supported catalyst reached slower than 1% CNT supported catalyst and 2% CNT supported catalyst at around 2hr of reaction time, suggesting that the combination of Cu/Zn and CNT alloys evolve faster to reach equilibrium chemical state as compared to CPCat and In-house Cu/ZnO/Al₂O₃ which reach steady state MeOH yield at around 2.5 hours of reaction time.

Figure 4.28 shows the MeOH yield comparison between 3 catalyst samples Cu/ZnO/Al₂O₃, CPCat and 2% CNT supported catalyst at hour 3.5 of reaction study. At this point, methanol yields by all catalyst samples have somewhat stabilized. It can be seen clearly that the highest MeOH yield among this catalyst type is given by 2% CNT supported catalyst closely by CPCat and finally by In-house Cu/ZnO/Al₂O₃. This trend of MeOH yield is exactly the same as CO conversion given in Figure 4.26. This enforces that the catalyst activity is strongly dependent on both Zn and CNT composition but that Zn composition has precedence over CNT in order of importance of metals that increase catalyst activity, facilitate the CO hydrogenation process on its surface.

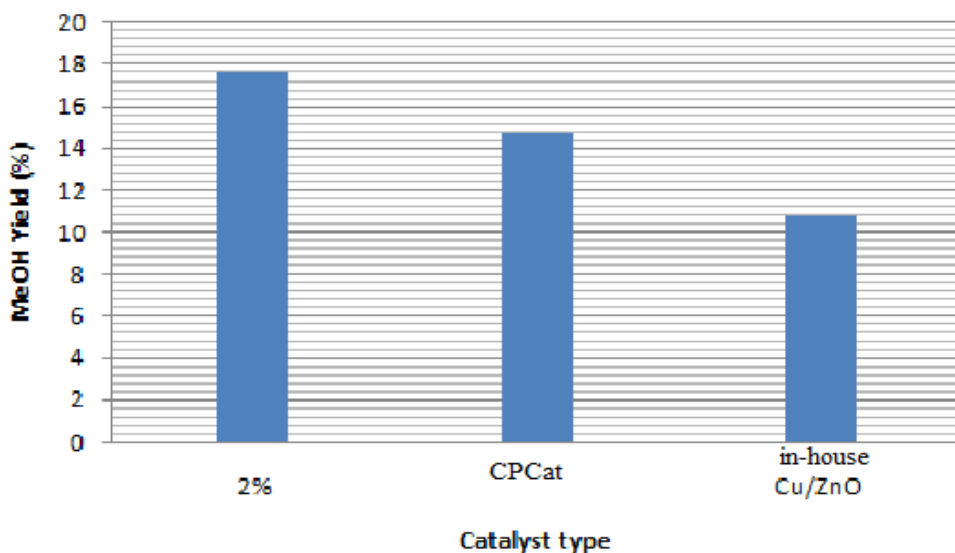


Figure 4.28: MeOH Yield in % for In-house Cu/ZnO/Al₂O₃, CPCat and 2% CNT supported catalysts.

Figure 4.29 however, shows the MeOH Yield at hour 3.5 for catalysts supported with different % of CNT. 1%, 2% and 3% CNT supported catalysts. MeOH yield given by catalyst 2% CNT is much higher up to 17.5% , the similar yield given by the 1% CNT and 3% CNT catalysts from 15.8 to 15.9. The optimum amount for MeOH synthesis has between 1 to 3% CNT supported catalyst, 2% gave the best conversion. Therefore, it appears that the high activity of the CNT supported catalyst for CO hydrogenation to methanol is also closely associated with the peculiar structure and properties of the CNTs as supporter. In view of chemical catalysis, in addition to its high mechanical strength, nanosize channel, sp^2 -C constructed surface and graphite-like tube-wall, the excellent performance of the CNTs in hydrogen-adsorption and electron transport is also very attractive [77].

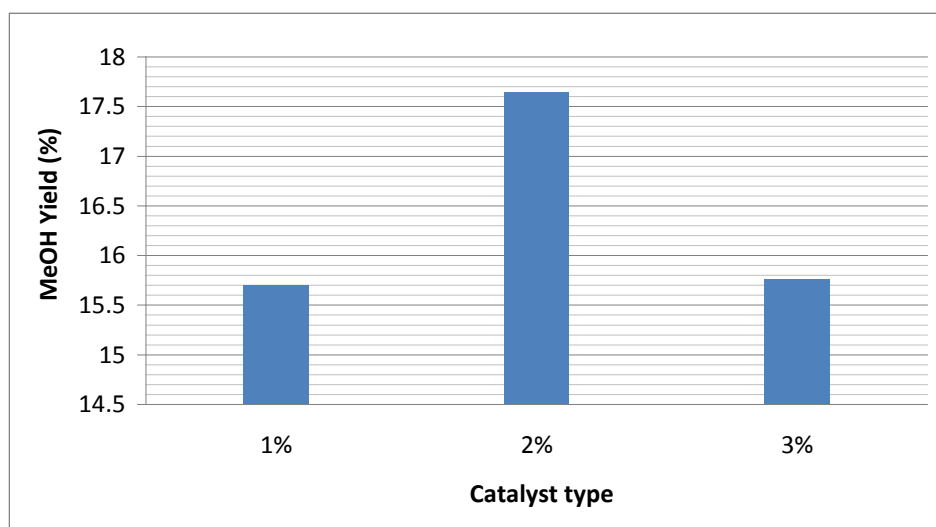


Figure 4.29: MeOH Yield in % for CNT supported catalysts.

4.3.3 MeOH Selectivity

MeOH selectivity is a measure of the composition of Methanol (in mol %) present in the product gas over the amount all considered compounds (in mol %) detected in the product gas as outlined by Equation 4.2. Conventional products of the methanol synthesis reaction by Cu/Zn and Cu/Zr based catalysts can also produce others such as higher alcohols, dimethyl ether, methyl formate, ketones, and aldehydes as well as

various paraffinic hydrocarbons. However all these products are often present in small amounts especially hydrocarbons which are present in amounts of less than 5000 ppmwt. Even water is produced in a CO₂ free syngas feed but usually below detection limits of the Thermal Conductivity Detector (TCD) [96].

In the wake of limitations, the compounds in the product gas that were calibrated in the Gas Chromatograph (GC) compounds analyzed in this MeOH synthesis in this study were Methanol (CH₃OH), Ethanol (C₂H₅OH), Dimethyl Ether (CH₃OCH₃), Methyl Formate (HCOOCH₃), Methane (CH₄), Carbon Dioxide (CO₂), Water (H₂O) as well the unreacted Carbon Monoxide (CO) and Hydrogen (H₂). $\sum (n_x)^f$ in Equation 4.2 refers to the sum of all these compounds.

Figure 4.30 shows the MeOH Selectivity comparison between all CNT supported and CPCat, over a time on stream of 3.5 hours and 30 minutes reaction interval. It can be seen that selectivity of MeOH in these samples is well above all other byproducts throughout the study period. It can also be seen that MeOH selectivity increases over time until reaching a staggering value above 95% after 3.5 for all CNT supported catalyst, CPCat and In-house Cu/ZnO/Al₂O₃. All prepared catalyst samples reach optimum selectivity of MeOH above 95% at hour 3.5. This is consistent with the MeOH Yield progress as shown in Figure 4.27 and most likely due to the surface modifications and synergy between the Cu-Zn alloys over time which produces the optimum amount of MeOH.

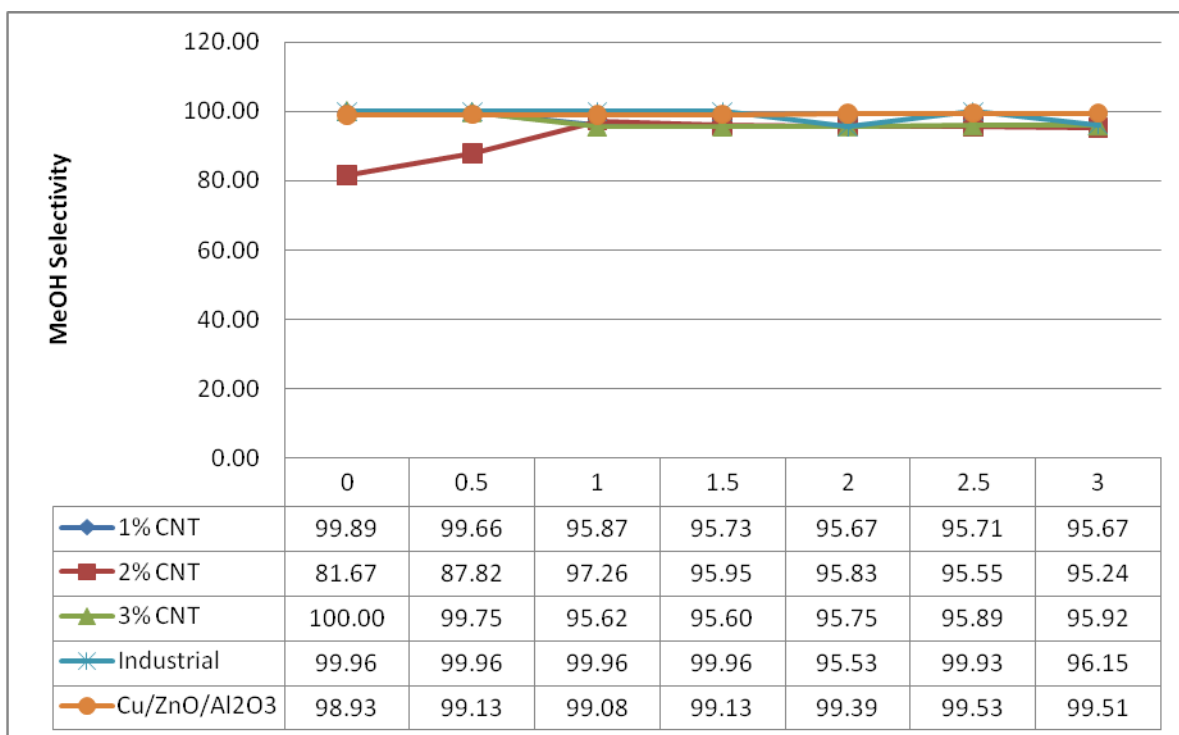


Figure 4.30: MeOH Selectivity in % for all CNT supported catalysts, In-house Cu/ZnO/Al₂O₃ and commercial pre-catalyst.

Figure 4.31 shows the steady state MeOH selectivity of all catalyst samples at the end of 3.5 hours time on stream. This is termed the optimum amount of selectivity of MeOH given by that particular catalyst sample and thus used to gauge its performance. The types of products given by a catalyst sample are largely dependence on the composition of active metals as well as the morphology of the catalyst species. The Cu metal surface area and consequently the size of Cu aggregates have been stated as a primary factor in dictating the activity and selectivity of the catalyst species [97-98].

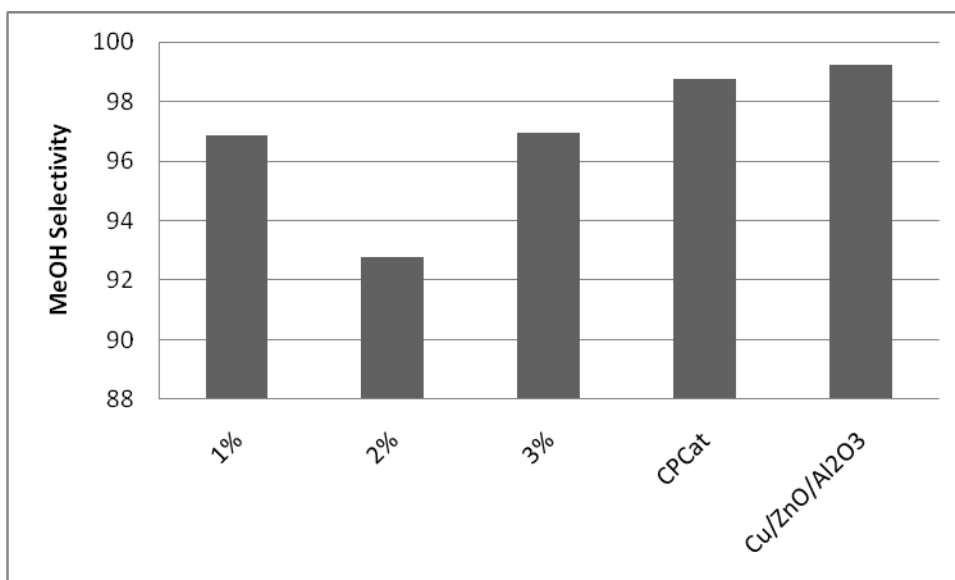


Figure 4.31: MeOH Selectivity at hour 3.5 in % for all catalyst samples.

An activity up to 99.9% has been reported achieved from the Cu/ZnO/Al₂O₃ catalyst at pressure 50 bars and temperature 225°C [99]. In the prior study, most of the samples have achieved MeOH selectivity well above 98% at a pressure of 30 bars and temperature 250°C. Of all catalyst analyzed In-house Cu/ZnO/Al₂O₃ has achieved the highest MeOH selectivity of 99.94%.

4.3.4 Ethanol Yield and Selectivity

Higher alcohols (other than MeOH) are typical byproducts in the methanol synthesis process catalyzed by the Cu-ZnO catalysts type [1]. Although present in very low amount in conventional MeOH product (typically 60ppm in Grade AA [101]), it still has been considered for analysis in the product gas. Equation 4.10 outlines a general stoichiometric equation for the equilibrium production of higher alcohols from syngas of CO and H₂ feed. Equation 4.11 on the other hand, outlines a more specific stoichiometric equation for the reaction of syngas to produce Ethanol and water.

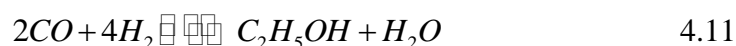
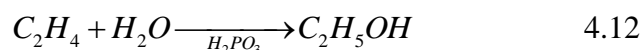


Figure 4.32 shows the ethanol yield for all catalysts samples in a 3.5 hour time on stream at a 30 minute interval of analysis. It can be seen clearly that ethanol is only present as a product in 1% CNT, 2% CNT, 3% CNT supported catalysts and in a CPCat sample, and very low amount appears in In-house Cu/ZnO/Al₂O₃ sample.



Industrially, Ethanol is usually produced by hydration of ethylene in phosphoric acid acting as the catalyst (Equation 4.12) at 250°C and 60-70 bar [102]. This however is an easy procedure as the carbon-carbon bond is already established in the ethylene (C₂H₄) compound and the process only requires the reduction in activation energy of the water molecule(i.e. O-H bond breaking) by forming an intermediate species of ethylene and phosphoric acid compounds.

However, the process of ethanol synthesis directly from CO and H₂ requires the formation of carbon-carbon bond. This requires a reagent having nucleophilic carbon atom (C^{δ-}) and a reagent with an electrophilic carbon atom (C^{δ+}). These opposite polarities in carbon reacting species leads to the formation of a carbon-carbon bond [103]. The species of C-O has an electrophilic C site while a C-H species has a nucleophilic C site. These two sites could be instrumental in the formation of ethanol precursors and eventually ethanol as a byproduct in the catalysts.

An instance of an Ethanol production process is the MeOH homologation with H₂ and CO as shown in Equation 4.13. Such reaction is reported to occur on Cobalt carbonyl (Co-CO) complex surfaces at temperature 290°C and pressure 18.4 MPa as well as H₂/CO ratio of 1.05 [104]. The high pressures in these reactions are necessary as the reaction involves a C-C bond formation as described earlier. This process could explain the formation of ethanol as a byproduct albeit in small amount on the surface of Cu-Zn catalysts systems.



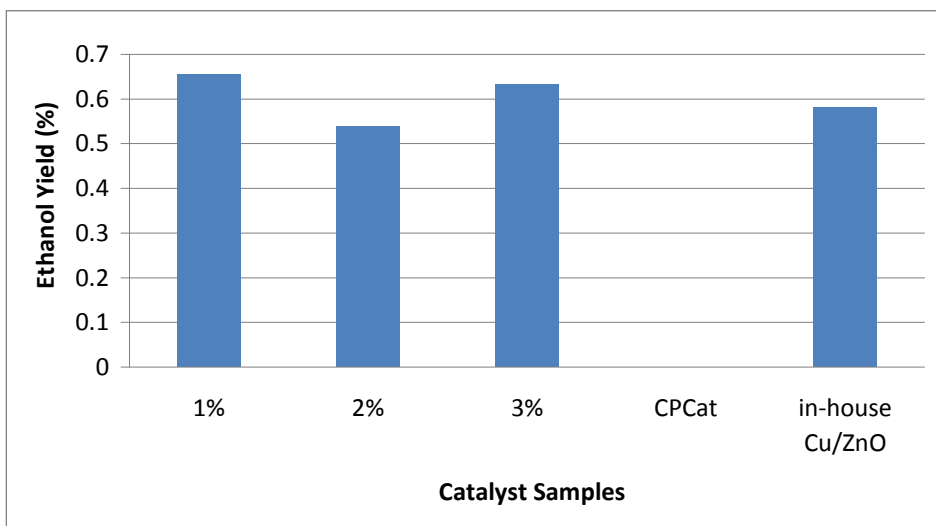


Figure 4.32: Ethanol yield in % for all catalyst samples in a 3.5 hour study

The Ethanol selectivity trend from Figure 4.33 for 1% CNT, 2% CNT, 3% CNT supported catalysts consistent with the Ethanol yield trends. It is clear that ethanol selectivity does increase over time but reaches optimum at below 4% for all catalysts sample studied.

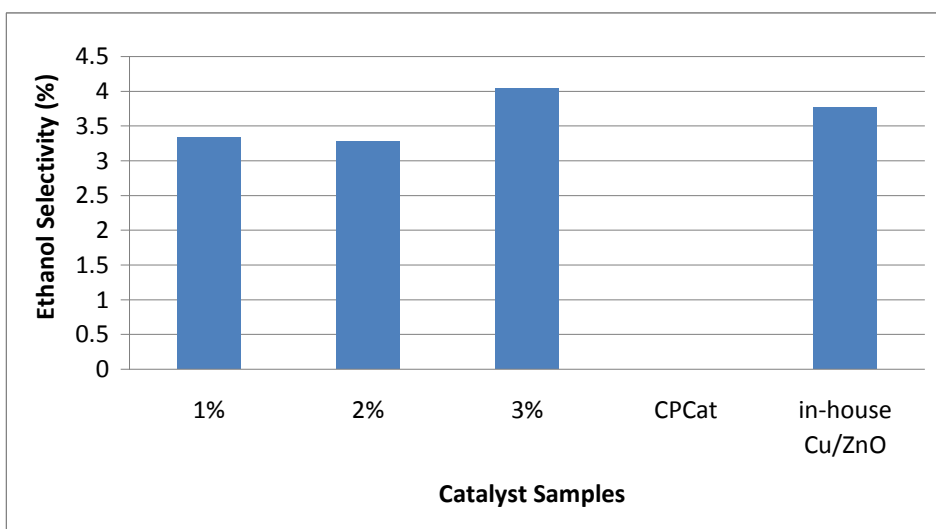


Figure 4.33: Ethanol Selectivity in % for all CNT supported catalysts, CPCat and In-house Cu/ZnO/Al₂O₃ type catalyst samples in a 3.5 hours study.

4.3.5 DME and Methyl Formate

Dimethyl Ether (DME) is an ether compound which is conventionally a byproduct in MeOH synthesis reactions. It is usually present in trace amounts when the Methanol synthesis process is catalyzed by the conventional Cu-ZnO based catalysts. The process which involves the formation of dimethyl ether is the dehydration of MeOH as shown in Equation 4.6. Methanol dehydration to DME is reported to occur on the surface of γ -Al₂O₃ and γ -Al₂O₃ modified with Phosphates or titanates [3].

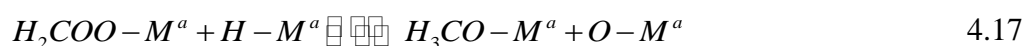


DME Yield is measure of amount of DME produced in the MeOH synthesis reaction. DME Yield (%) is defined as 2 times the unit mols of DME detected in the product gas after the reaction over the amount of CO in the reactant gas. The 2 unit mol of DME used is the result of the equilibrium stoichiometry of CO to DME which is 2:1 as shown in Equation 4.8. Thus the mol of CO has to be divided by 2 to gain normalized Yield. Equation 4.8 is the net equation derived from the MeOH synthesis process (Equation 4.7) and MeOH dehydration to form DME (Equation 4.16).

$$Y_{DME} = \frac{2 \times (n_{DME})^f}{(n_{CO})^i} \times 100\% \quad 4.16$$

Figure 4.43 shows the DME Yield in % for all catalyst samples at a 30 minutes interval in a 3.5 hour study. It can be seen that DME Yield is extremely low in all catalyst samples, i.e. well below 0.017%. This suggests that DME production is a trivial process among the catalysts samples studied. However for some catalyst samples, the DME Yield is more significant than others. For instance, it can be seen Figure 4.43 that the DME Yield for In-house Cu/ZnO/Al₂O₃, 2, 3% CNT supported catalyst types are well below 0.01%. For CPCat and 1% CNT supported catalyst type however, the amount of DME produced is greater and hence investigatiable.

It was outlined in previous sections that the MeOH synthesis process is a process that occurs on two regimes. Cu is the region where H₂ bond breaking occurs, while Zn is the region where CO and CO₂ hydrogenation to MeOH precursors and eventually MeOH occurs. It has been established by Askgaard et al [84] that the rate limiting step in the MeOH synthesis process is the formation of the methoxy species on the catalyst surface(H_3CO-M^a) as shown by equation 4.9 where M^a is the surface where hydrogenation of the H_2COO-^* species occurs. M^a could be Zn.



For sample Industrial this Ma species is Zn. This Zn site is extremely crucial as the rate limiting step (Equation 4.9) could be impeded if this site was deactivated. For sample Industrial, the low Zn/Cu ratio than other samples meant that the Zn sites are insufficient and there would be an excess of H atoms on the Cu surface from the H₂ bond breaking step. This would encourage the H atom spillover onto the Al₂O₃ support which would form highly acidic Al-OH Bronstead acid sites. These sites have been reported to be the prime location for DME formation. This would explain greatly the larger amount of DME Yield in sample Industrial as compared to all other Zn containing samples.

Methyl formate ($HCOOCH_3$) has been a crucial chemical in industries predominantly in the production of formamide and dimethylformamide and latex coagulant. It is also a common byproduct in Cu-based MeOH synthesis reactions. It has been discovered that Methyl Formate has been predominantly produced from further reactions of MeOH and not directly from CO and H₂ in the Methanol synthesis reactions.

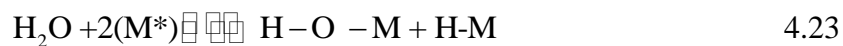
There are two main possible routes for production of Methyl formate from MeOH. They are the dehydrogenation of MeOH (Equation 4.19) and carbonylation of MeOH (Equation 4.20). MeOH dehydrogenation reaction usually occurs on transition metals such as Cu and Pd based catalysts. It has been reported that a conversion of 18% and selectivity to Methyl formate of 94% from MeOH in a reaction conditions of 270°C and 10bar. These conditions are comparable to the ones studied in our reaction [105].

MeOH carbonylation however occurs conventionally on alkali metal catalysts such as sodium methoxide at pressure of 810MPa and Temperature 80°C [106]. This reaction Therefore is unlikely to be occurring in our study due to the high Pressure requirement as well as the need for Na based catalyst which is not present in our catalysts systems.



4.3.6 CO₂ formation Study as an Intermediate species type

Carbon dioxide is a crucial intermediate in the MeOH synthesis process from a CO/H₂ feed system. It has been a favorable hypothesis that MeOH is produced mainly from the route of CO₂ hydrogenation on the surface of Zn (Zn site is represented as M*). A generic 4 step procedure for the production of MeOH in a gas feed system where no H₂O and CO₂ is present is outlined in Equation 4.20 to 4.23.



The first step (Equation 4.20) is the formation of CO₂ from CO in a H₂O-free feed mixture. It involves the adsorption of CO on the hydrogenation site M-O (Zn-O) and the consequent bonding of with the O on the M-O lattice to form an intermediate site of O-C-O -M. These intermediary sites are of significant consequence in the next step (Equation 4.21) where the spillover H atoms (Cu sites breaks the bond in H₂ molecule and H atoms are transferred unto the M sites) react with this intermediary O-C-O -M site to produce desorbed MeOH and H₂O as well 2 sites of M* (Zn²⁺).

These positively charged sites M* are crucial in the readsorption of H₂O molecule and the formation of the H-O-M sites. These H-O-M sites are crucial for they have available excess O atoms which are necessary to continue the formation of the intermediary O-C-O-M sites (Equation 4.22). The formation of water as an intermediate O source (Equation 4.23) is thus the reason why it was not detected in the TCD signal as it was fully reutilized in the reaction process.

Figure 4.33 shows the formation of CO₂ yield for all catalyst samples throughout a 3.5 hour study at an interval of 30 minutes. It can be seen that a clear trend of CO₂ production which increases in the beginning of the reaction and reduces towards the end of the study period.

As was outlined, the rate limiting step as proposed by Askgaard *et. al* is the methoxy species production methoxy species on the catalyst surface (H_3CO-M) as shown by equation 4.24 where M is the surface where hydrogenation of the H_2COO- species occurs.



However, since the Methoxy production step is rate limiting it is conceivable that the effect would be rippled off all the way back (Equation 4.20) of CO oxidation to CO₂ would be as well affected. The bond of Metal-Oxygen in H₂COO-M is stronger than the bond of Metal -Oxygen in O-C-O-M. The Zn-O bond of H₂COO-Zn has a bond disassociation energy of 133.9kJ/mol while the Zn-O bond in O-C-O-Zn has a bond disassociation energy of 43.6 kJ/mol [150]. Bond disassociation energy (BDE) is the amount of energy required to break a particular bond.

It is evident that the weaker bond (O-C-O-M) would be broken prematurely by the excess of formation of the stronger bonds (H₂COO-M) and lead to the formation of free CO₂ gas in all catalyst samples which would be detectable in all samples as evident from the data in Figure 4.54.

This scenario however does not continue throughout the process as it can be seen in Figure 4.33 that the amount of CO₂ drops to zeros after a period of 2-3 hours of reaction. This would suggest a change in CO adsorption capacity on the surface to account limited surface sites as a lot of M* sites are still engaged in the methoxy formation process. The amount of CO adsorbed would naturally decrease due to the limited sites available at every moment in time and thus the amount of prematurely desorbing CO₂ too will decrease until none is seen.

Another factor to be considered would be the period before stability of Yield and zero CO₂ byproduct is reached. As a rule of thumb, lower Zn sites would lead to quicker halt of CO₂ formation as less time would be required for the ripple effect of CO₂ desorption and hysteresis on Zn surface to cease. Less total sites would mean less initial amount of CO adsorbed (and oxidized to CO₂) and therefore less forced desorption of CO₂. That would explain why CPCat reaches zero-CO₂ state quicker as shown in Figure 4.33. This is because it has less Zn sites in comparison to other Zn containing catalyst samples.

All catalyst samples reaches zero-CO₂ state at around 3- 3.5 hours suggesting optimum catalyst activity after that period of study. Another evidence of this theory that number of Zn sites available dictates the speed at which a zero-CO₂ free state is reached is the initial conversion of CO for all catalysts samples. The higher conversion of CO simply means that less CO is detected by TCD in the product gas. Therefore, if less CO is detected in product gas more is adsorbed on the catalyst surface. This contention is consistent with the evolution of CO conversion for commercial catalyst sample, CPCat in Figure 4.33. It is evident that the amount of CO adsorbed increases in the beginning of the reaction before reducing at 2 hour of study.

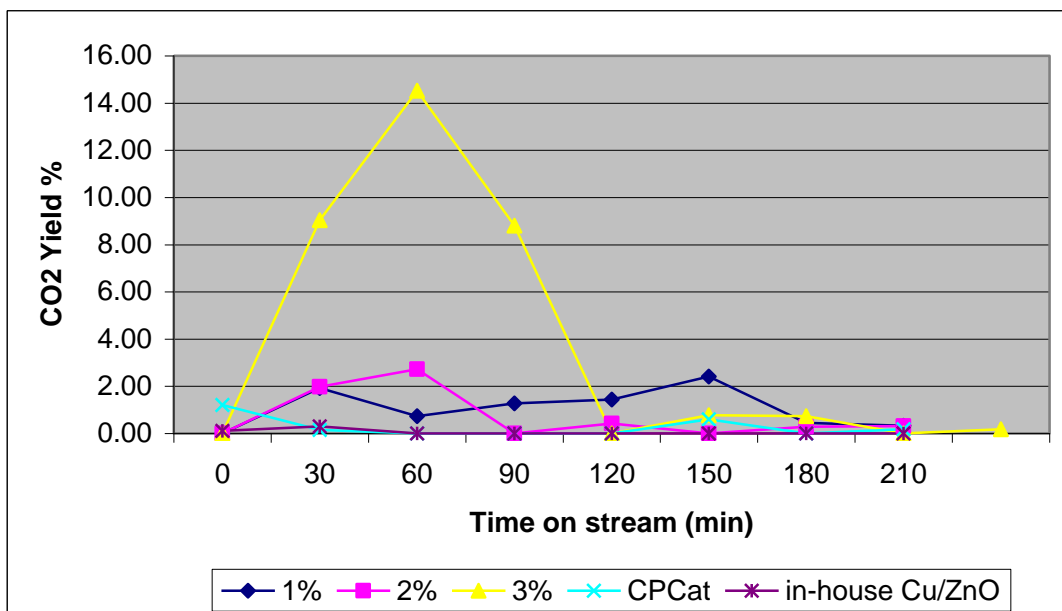


Figure 4.34: Formation of CO₂ yield for all catalysts

5 CONCLUSIONS AND RECOMMENDATIONS

5.1 Conclusions

The study addresses the bottle-necks related to industrial methanol production. The origins of catalyst-specific problems were revealed and prospective solutions explored by utilizing advanced methods of modern physical chemistry, such as scanning and transmission electron microscopy, photoelectron spectroscopy, low energy ion scattering spectroscopy, x-ray diffraction, temperature programmed reduction, kinetic study of catalytic activity by flow microreactor hyphenated with gas chromatograph and original in-house synthesis of the catalysts promoted with carbon nanotubes. The study data and their analysis can be summarised as follows

- The deficiencies of industrial technology which affect a performance and handling of commercial Cu/ZnO/Al₂O₃ catalyst in industrial settings are likely associated with nonuniformity of reaction conditions throughout the industrial tube type fixed bed reactor;
- It was experimentally proven that the heterogeneity of the reactor conditions results in substantial modification of initially homogeneous chemical surface composition of the catalyst in the course of its 3 year operation;
- Local overheating in the industrial methanol production reactor leads to deterioration of mechanical strength of the catalyst that results in massive pellets disintegration (crumbling) and blocking gas pathways while concomitant sintering causes seizure during catalyst replacement;
- This study makes clear that promoting the Cu/ZnO/Al₂O₃ catalyst with Carbon Nanotubes is a straight track towards development novel thermoresistent and mechanically robust catalyst;

- The in-house developed novel Cu/ZnO/Al₂O₃ prototype-catalyst supported with about 2% Carbon Nanotubes was proven to have doubled turnover frequency of that of conventional commercial catalyst;

5.2 Recommendations

1. As long as TEM & XPS are now available in UTP it is much desirable to upgrade them in such a way to enable the experiments under elevated pressure over catalyst surface to study the catalysis at more realistic conditions.
2. This study has a promise of development of highly active and long lasting Cu/ZnO/Al₂O₃-CNT industrial catalyst.

References:

- [1] G.A. Olah, A. Goepfert, G.K. Surya Prakash, *Beyond Oil and Gas: The Methanol Economy*, Wiley-VCH, Weinheim (2006).
- [2] Lee S. *Methanol Synthesis Technology*, CRC Press: Boca Raton, Florida, 1990.
- [3] Henrici-Olive, G.; Olive, S. *Catalyzed Hydrogenation of Carbon Monoxide*; Springer-Verlag: Berlin, 1984.
- [4] Chang, C. *Methanol Production And Use*; Marcel Dekker: New-York, 1994.
- [5] Kung, H. H.; Smith, K. *Methanol Production and Use*; Marcel Dekker: New-York, 1994.
- [6] Natta, G. *Catalysis* 1954.
- [7] P. Davies, F.F. Snowden, G.W. Bridger, D.O. Hughes, P.W. Young, *UK 1,010,817* ICI.
- [8] H. Sakurai, M. Haruta, *Appl. Catal. A* 127 (1995) 93.
- [9] H. Sakurai, M. Haruta, *Catal. Today* 29 (1996) 361.
- [10] Davies, P.; Snowden, F. F. *Production of Oxygenated Hydrocarbons*: U.S., 1967
- [11] Supp, E. *Hydrocarbon Processing*. 1981, 60, 71.
- [12] A. E. Hokanson and R. M. Rowell; *Methanol from wood waste: a technical and economic study*.
- [13] S.A. French, A.A. Sokol, S.T. Bromley, C.R.A. Catlow, S.C. Rogers, F. King, P.Sherwood, *Angew. Chem. Int. Ed.* 40 (2001) 4437.
- [14] S.A. French, A.A. Sokol, S.T. Bromley, C.R.A. Catlow, P. Sherwood, *Top. Catal.* 24(2003) 161.
- [15] G.C. Chinchin, P.J Denny, J.R. Jennings, M.S. Spencer, K.C. Waugh, *Appl. Catal.*36 (1988) 1.
- [15] A. Y. Khodakov, A.Griboval-Constant, R. Bechara, V.L. Zholobenko, *J. of Catal.* 206 (2002) 230–241.
- [17] W. Chen, X. Pan, X. Bao, *J. Am. Chem. Soc.* 129 (2007) 7421-7426.
- [18] W. Chen, Z. Fan, X. Pan, X. Bao, *J. Am. Chem. Soc.*130 (2008) 9414-9419.

- [19] M. C. Bahome, L. L. Jewell, K. Padayachy, D. Hildebrandt, D. Glasser, A. K. Datye, N. J. Coville, , *Appl. Catal. A: Gen.* 328 (2007) 243–251.
- [20] P. Serp, M. Corrias, P. Kalck, *Appl. Catal. A: Gen.* 253 (2003) 337–358.
- [21] I. Eswaramoorthi, V. Sundaramurthy, A.K.Dalai, *Appl. Catal. A: Gen.* 313 (2006) 22-28.
- [23] C.H.Bartholomeow, R.J Farrauto, Chapter 5 & 6: Fundamentals of Industrial Catalytic, Wiley-Interscience, 2007.
- [26] PETRONAS Methanol Labuan (PMLSB) Presentation, *New Method: Unloading Catalyst under Inert Condition*.
- [27] R. D. Srivastaya, L. M. Campbell, and B. D. Blaustein, *Chem. Eng. Prog.*, 86(12):45 (1989).
- [28] I. Dybkyjaer and J. B. Hansen, *Chem. Economy Eng. Rev.*, 17(5):13 (1985).
- [29] G. C. Chinchin, *Appl. Catal.*, 36:1 (1988).
- [30] K. Kiler, *Adv. Catal.*, 31:243 (1982).
- [31] H. H. Kung, *Catal. Rev.*, 22:235 (1980).
- [32] G. D. Short and J. R. Jennings, European Patent 117944, ICI.
- [33] T. E. O’Hare, R. S. Sapienza, D. Mahajan, and G. Skaperdas, paper presented at the 21st State-of-the-Art Symposium, *Ind & Eng. Chem. Div.*, ACS Florida, June 1986.
- [34] Breakthrough claimed in gas-to-methanol catalyst, *Eur. Chem. News.*, May 27:32 (1991).
- [35] New ICI gas to methanol process, *Chem. Week*, April14:28 (1993).
- [36] K. Westerterp, *Ind. Eng. Chem. Res.*, 28(6):763 (1989).
- [37] A. K. Rhodes, *Oil and Gas J.*, November30:48-50 (1992).
- [38] J. Shearman, *Chem. Eng.*, October: 57-59 (1991).
- [39] C. A. Macfoy and E. I. Cline, *J. Ethnopharmacol.*, 28:323 (1990).
- [40] M. M. Iwu, D.J. Klayman, *J. Ethnopharmacol.*, 36:133 (1992).
- [41] M. M. Iwu, J. E. Jackson, T. D. Tally, and D. L. Klayman, *Planta Med.*, 58:436 (1992).
- [42] Y. Y. Cui, S. Y. Feng, G. Zhao, and M. Z. Wang, *Acta Pharm. Sin.*, 27(8):603 (1992).
- [43] P. Swart, K. J. Van der Merwe, A. C. Swart, P. C. Todres, and J. H. Hofmyer, *Planta Med.*, 59(2):139 (1993).

- [44] J. R. Pellon and A. J. Sinskey, Genetic engineering for food and additives (T. A. Roberts and F. A. Skinner, eds.), Academic Press, London, 1983, pp. 287-292.
- [45] P. Rotheim, Business Communication Co., Stamford, Connecticut, July 1985, pp. 119-120.
- [46] P. Ruffio and A. Crull, *Business Opportunity Report C-018N: Modern Fermentation Processes and Products*, Business Communication Co., Stamford, Connecticut, October 1987, pp. 10-11.
- [47] Metcalf and Eddy, Inc., *Wastewater Engineering: Treatment, Disposal and Reuse*, 3rd ed., McGraw-Hill, New York, 1991, Chap. 11.
- [48] M. A. Winkler, *Biological Treatment of Waste-Water*, Ellis Howard, Ltd., New York, 1981, Chap. 7.
- [49] R. L. Culp, G. M. Wesner, and G. L. Culp, *Handbook of Advanced Wastewater Treatment*, 2nd ed., Van Nostrand-Reinhold, New York, 1978, Chap. 7.
- [50] Methanol business in looking up in '92, *Chem. Marketing Reporter*, January 6:3 (1992).
- [51] T. Wett, *Chem. Business*, july/August: 23-24 (1991).
- [52] G. L. Farina and E. Supp, *Hydrocarbons Proc.*, March: 77-79 (1992).
- [53] D. M. Monti, M. A. Kohler, M. S. Wainwright, D. L. Trimm, and N. W. Cant, *Appl. Catal.*, 22:123 (1986).
- [54] J. W. Evans, M. S. Wainwright, N. W. Cant, and D. L. Trimm, *J. Catal.*, 88:203 (1984).
- [55] S. C. Chen, C. C. Chu, F. S. Lin, and F. J. Huang, U.S. Patent 5,189,214, Dairen Chemical Corp. (1993).
- [56] C. R. Marston, European Patent 177,824, Reilly Tar & Chemical (August 10, 1988).
- [57] W. S. Fong, Acetic acid by low pressure carbonylation of methanol with a supported rhodium catalyst, *PEP Review No. 88-3-4*, SRI International, Menlo Park, California, 1990.
- [58] J. F. Gaillard, B. Juguin, and D. Duee, DE3813721, Institute Francais du Petrole (1988).
- [59] M. Soudek and J. J. Lacatena, *Hydrocarbon Proc.*, 69(5):73 (1990).
- [60] P. R. Pujado and B. V. Vora, *Hydrocarbon Proc.*, 69(3):65 (1990).
- [61] J. F. Knifton, EP333078, Texaco (1993).

- [62] J. F. Knifton, U. S. Patent 5,214,218, Texaco (1993).
- [63] Wang, X.; Li, Q.; Xie, J.; Jin, Z.; Wang, J.; Li, Y.; Jiang, K.; Fan, S. (2009). "Fabrication of Ultralong and Electrically Uniform Single-Walled Carbon Nanotubes on Clean Substrates".
- [65] Demczyk, B.G.; Wang, Y.M.; Cumings, J.; Hetman, M.; Han, W.; Zettl, A.; Ritchie, R.O. (13 June 2002). "Direct mechanical measurement of the tensile strength and elastic modulus of multiwalled carbon nanotubes". *Materials Science and Engineering A* 334.
- [66] Wang G L, Li C Y. Catalysts for methanol synthesis. *Chemical Industry and Engineering Progress*, 2001, 20(3): 42–46.
- [67] Jensen J R, Johannessen T, Wedel S, Livbjerg H. A study of Cu/ZnO/Al₂O₃ methanol catalysts prepared by flame combustion synthesis. *J Catal*, 2003, 218(1): 67–77.
- [68] Shen W J, Ichihashi Y, Matsumura Y. Low temperature methanol synthesis from carbon monoxide and hydrogen over ceria supported on copper catalyst. *Appl Catal A*, 2005, 282(1–2): 221–226.
- [69] Shen B S, Wu X M, Zhang H B, Lin G D, Dong X. Study of highly active Cu-based catalyst promoted by nickel-modified multi-walled carbon nanotubes for methanol synthesis. *Acta Chimica Sinica*, 2004, 62(18): 1721–1728.
- [70] Kanoun N, Astier M P, Pajonk G M. Catalytic properties of new copper-based catalysts containing zirconium and/or vanadium for methanol synthesis from a carbon dioxide and hydrogen mixture. *Catal Lett*, 1992, 15(3): 231–235.
- [71] Walker, A P, Lambert R M, Nix R M, Jennings J R. Methanol synthesis over catalysts derived from CeCu₂: Transient studies with isotopically labeled reactants. *J Catal*, 1992, 138(2): 694–713.
- [72] Toyir T, de la Piscina P R, Fierro J L G, Homs N. Highly effective conversion of CO₂ to methanol over supported and promoted copper-based catalysts: Influence of support and promoter. *Appl Catal B*, 2001, 29(2): 207–215.
- [73] Li J T, Zhang W, Gao L, Gu P, Sha K, Wan H. Methanol synthesis on Cu-Zn-Al and Cu-Zn-Al-Mn catalysts. *Appl Catal A*, 1997, 165(1–2): 411–417.
- [74] Zhang X T, Chang J, Wang T J, Fu Y, Tan T W. Methanol synthesis catalyst prepared by two-step precipitation combined with addition of surfactant. *Journal of Fuel Chemistry and Technology*, 2005, 33(4): 479–482.

- [75] Li J T, Zhang W D, Zhou Y X. Study on high dispersion catalysts for methanol synthesis. *Petrochemical technology*, 1998, 27(1): 1–4.
- [76] Hong Z S, Deng J F, Fan K N, Cao Y. Preparation of methanol synthesis catalyst Cu/ZnO/Al₂O₃ by gel-network coprecipitation method. *Chemical Journal of Chinese Universities*, 2002, 23(4): 706–708.
- [77] Li J F, Chang J, Yin X L, Lu P M. Preparation of Cu/ZnO/Al₂O₃ catalysts for methanol synthesis by urea-hydrolyzed precipitation method. *Journal of Fuel Chemistry and Technology*, 2004, 32(3): 378–380.
- [78] Yu F W, Ji J B, Zhang Y F, Liu H Z. Copper-based catalyst for methanol synthesis prepared with dual-frequency ultrasonic technology. *Petrochemical technology*, 2004, 33(9): 824–827.
- [79] Choi Y, Futagami K, Fujitani T, Nakamura J. The role of ZnO in Cu/ZnO methanol synthesis catalysts-morphology effect or active site model. *Appl Catal A*, 2001, 208(1–2): 163–167.
- [80] Yurieva T M. Mechanisms for activation of hydrogen and hydrogenation of acetone to isopropanol and of carbon oxides to methanol over copper-containing oxide catalysts. *Catal Today*, 1999, 51(3–4): 457–456.
- [81] Fujitani T, Nakamura J. The effect of ZnO in methanol synthesis catalysts on Cu dispersion and the specific activity. *Catal Lett*, 1998, 56(2–3): 119–125.
- [82] Klier K. Methanol synthesis. In: Eley D D, Pines H, Weisz P B. Eds. *Advances in Catalysis*. New York: Academic, 1982, 243–313.
- [83] Zhao Y Q, Chen J X, Zhang J X, Zhang J Y. *Study on direct synthesis of dimethyl ether by hydrogenation of carbon dioxide: II Effects of Cu/Zn ratio on structure and properties of catalysts*. *Journal of Fuel Chemistry and Technology*, 2005, 33(3): 334–338.
- [84] Jansen W P A, Beckers J, Heuvel J C, Gon A W D, Bliiek A, Brongersma H H. Dynamic behavior of the surface structure of Cu/ZnO/SiO₂ catalysts. *J Catal*, 2002, 210(1): 229–236.
- [85] Zhao J S, Chen B S, Ma F S, Zhu L C, Kang H M. *The effect of the composition of a Cu-based catalyst for methanol synthesis on its structure and property*. *Journal of Chemistry Industry and Engineering (China)*, 1988, 39(5): 562–569.
- [86] Grunwaldt J-D, Molenbroek A M, Topsøe N-Y, Topsøe H, Clausen B S. In situ investigations structural changes in Cu/ZnO catalysts. *J Catal*, 2000, 194(2): 452–460.

- [87] P. Chen, H.B. Zhang, G.D. Lin, Q. Hong and K.R. Tsai, *Carbon* 35 (1997), p. 1495.
- [88] Instruction Manual, TPD/R/O 1100 Catalyst Surface Analyzer, Thermo Finnigan Italia S.P.A, 2002.
- [89] M.Dunlap, J. E. Adaskaveg, Introduction to the Scanning Electron Microscope Theory, Practice, & Procedures, Facility for Advanced Instrumentation, U. C. Davis, 1997.
- [90] Presentation, 'Introduction to FESEM Technology', Hi- Tech Instruments, UTP, 2009.
- [92] W. R. M. Robinson, J. C. Mol, Characterization and catalytic activity of copper/alumina methanol synthesis catalysts, *Appl. Catal.*, Vol. 44, pp. 165-176. 1988
- [93] *Chin J Catal*, 2006, 27(3): 210–216.
- [94] Collins, Philip G.; Phaeton Avouris (2000). "[Nanotubes for Electronics](#)" (PDF). *Scientific American*: 67-69.
- [95] F.Arena, G. Italiano , K. Barbera, S. Bordiga, G. Bonura ,L. Spadaro , F.Frusteri , Solid-state interactions, adsorption sites and functionality of Cu-ZnO/ZrO₂ catalysts in the CO₂ hydrogenation to CH₃OH, *Applied Catalysis A: General* 350 (2008) 16–23
- [96] Klier K., 1982, *Adv. Catal.*, 31:243.
- [97] Recent Advances in Catalysts for Methanol Synthesis via Hydrogenation of CO and CO₂. Xin-Mei Liu, G. Q. Lu, Zi-Feng Yan, and Jorge Beltramini.
- [98] M. Kalliomaki, V. Meisalo, A. Laisaar, *Phys. Status Solidi* 56 (1979) K127–K131.
- [99] J.B. Hansen, *Handbook of Heterogeneous Catalysis*, Weinham Germany, 1997.
- [100] Dimethyl Ether Technology and Markets 07/08-S3 Report, ChemSystems, December 2008.
- [101] *Federal Specification O-M 232 F*, U.S. Government Printing Office, Washington, D.C., June 5, 1975.
- [102] H.F. Rase, *Handbook of commercial catalysts: heterogeneous catalysts*, pg 93, CRC Press LLC, 2000.
- [103] M.N. Barroso, M.F. Gomez, J.A. Gambo, L.A. Arru´ a, M.C. Abello, *J. Phys. Chem. Solids* 67 (2006) 1583–1589.

- [104] Wender, in *Catalysis and Surface Science* (H. Heinemann and G. A. Somorjai, eds.), p. 321, Marcel Dekker, New York, 1984.
- [105] N. Iwasa, O. Yamamoto, T. Akazawa, S. Ohyama, and N. Takezawa, *J. Chem. Soc., Chem. Commun.*(18):13221323 (1991).
- [106] A. Aguilo and T. Horlenko, *Hydrocarbon Proc., November*:120130 (1980).
- [107] B. Strohmeier, D. Leyden, R. Field, D. Hercules, *J. Catal.* 94 (1985) 514–530.
- [108] D. E. Grove, *Platinum Metals Rev.*, 2003, **47**, (1), 44.
- [109] C.D. Wagner, A.V. Naumkin, A. Kraut-Vass, J.W. Allison, C.J. Powell, J.R. Rumble Jr., NIST Standard Reference Database 20, Version 3.4 (Web Version),
- [110] Wei-Lin Dai, Qi Sun. *XPS studies of Cu/ZnO ultra fine catalysts derived by a novel gel oxalate co-precipitation for methanol synthesis by Co₂+h₂.*
- [111] H. Wilmer, M. Kurtz, K.V. Klementiev, O.P. Tkachenko, W. GrÄunert, O. Hinrichsen, A. Birkner, S. Rabe, K. Merz, M. Driess, C. WÄoll, M. Muhler, *Phys. Chem. Chem. Phys.* 5 (2003) 4736.
- [112] Y.B. Kagan, A.Ya. Rozovskii, L.G. Liberov, E.V. Slivinskii, G.I. Lin, S.M. Loktev, A.N. Bashkirov, *Dokl. Akad. Nauk SSSR* 224 (1975) 1081.
- [113] Steam reforming of methanol using Cu-ZnO catalysts supported on nanoparticle alumina Samuel D. Jones, Luke M. Neal, Helena E. Hagelin-Weaver.
- [114] M. Bowker, H. Houghton, K.C. Waugh, *J. Chem. Soc. Faraday Trans. I* 77 (1981) 3023.
- [115] Characterization of CuOrZnO under oxidizing conditions for the oxidative methanol reforming reaction. T.L. Reitz, S. Ahmed, M. Krumpelt, R. Kumar, H.H. Kung.
- [116] H.H. Kung, *Catal. Rev.-Sci. Eng.* 22(2) (1980) 235.
- [117] V.E. Heinrich, P.A. Cox, *The Surface Science of Metal Oxides* Cambridge University Press, 1996.
- [118] H. KnÄozinger, *Science* 287 (2000) 1407.
- [119] A.F. Holleman, N. Wiberg, *Lehrbuch der Anorganischen Chemie*, 101. Au°,., Verlag Walter deGruyter, Berlin (1995).
- [120] V. Ischenko, S. Polarz, D. Grote, V. Stavarache, K. Fink, M. Driess, *Adv. Funct.Mater.* 15 (2005) 1945.
- [121] R. Kov¶a·cik, B. Meyer, D. Marx, *Angew. Chem. Int. Ed.* 46 (2007) 4894.

- [122] O. Dulub, U. Diebold, G. Kresse, *Phys. Rev. Lett.* 90(1) (2003) 016102-1.
- [123] B. Meyer *Phys. Rev. B* 69 (2004) 045416.
- [124] R.G. Herman, K. Klier, G.W. Simmons, B.P. Finn, J.B. Bulko, T.P. Kobylinski, *Prepr. Am. Chem. Soc. - Div. Petr. Chem.* 23 (1978) 595.
- [125] R.G. Herman, K. Klier, G.W. Simmons, B.P. Finn, J.B. Bulko, T.P. Kobylinski, *J. Catal.* 56 (1979) 407.
- [126] S. Metha, G.W. Simmons, K. Klier, R.G. Herman, *J. Catal.* 57 (1979) 339.
- [127] J.B. Bulko, R.G. Herman, K. Klier, G.W. Simmons, *J. Phys. Chem.* 83 (1979) 3118.
- [128] K.C. Waugh *Catal. Today* 15 (1992) 51.
- [129] W.X. Pan, R. Cao, D.L. Roberts, G.L. Griñn, *J. Catal.* 114 (1988) 440.
- [130] G.C. Chinchén, K.C. Waugh, D.A. Whan, *Appl. Catal.* 25 (1986) 101.
- [131] G.C. Chinchén, M.S. Spencer, K.C. Waugh, D.A. Whan, *J. Chem. Soc. Faraday Trans. I* 83 (1987) 2193.
- [132] M. Muhler, E. Törnqvist, L.P. Nielsen, B.S. Clausen, H. Topsøe, *Catal. Lett.* 25(1992) 1.
- [133] M. Kurtz, N. Bauer, C. Bäuscher, H. Wilmer, O. Hinrichsen, R. Becker, S. Rabe, K. Merz, M. Driess, R.A. Fischer, M. Muhler, *Catal. Lett.* 92 (2004) 49.
- [134] R. Burch, R.J. Chappell, *Appl. Catal.* 45 (1988) 131.
- [135] H. Wilmer, O. Hinrichsen, *Catal. Lett.* 82 (2002) 117.
- [136] J. Greeley, A.A. Gokhale, J. Kreuser, J.A. Dumesic, H. Topsøe, N.-Y. Topsøe, M. Mavrikakis, *J. Catal.* 213 (2003) 63.
- [137] J.B. Wagner, P.L. Hansen, A.M. Molenbroek, H. Topsøe, B.S. Clausen, S. Helveg, *J. Phys. Chem. B* 107 (2003) 7753.
- [138] J. Nakamura, Y. Choi, T. Fujitani, *Top. Catal.* 22(3-4) (2003) 277.
- [139] B.S. Clausen, J. Schiøtz, L. Grabaek, C.V. Ovesen, K.W. Jacobson, J.K. Nørskov, H. Topsøe, *Top. Catal.* 1 (1994) 367.
- [140] J.-D. Grunwaldt, A.M. Molenbroek, N.-Y. Topsøe, H. Topsøe, B.S. Clausen, *J. Catal.* 194 (2000) 452.
- [141] H. Wilmer, T. Genger, O. Hinrichsen, *J. Catal.* 215 (2003) 188.
- [142] B.H. Sakakini, J. Tabatabaei, M.J. Watson, K.C. Waugh, *J. Mol. Catal. A* 162(2000) 297.

- [143] Y. Kanai, T. Watanabe, T. Fujitani, M. Saito, J. Nakamura, T. Uchijima, *Catal.Lett.* 27 (1994) 67.
- [144] K.-D. Jung, O.-S. Joo, S.-H. Han, *Catal. Lett.* 68 (2000) 49.
- [145] J.C. Frost, *Nature* 334 (1988) 577.
- [146] I. Nakamura, H. Nakano, T. Fujitani, T. Uchijima, J. Nakamura, *Surf. Sci.* 402-404 (1998) 92.
- [147] J. Nakamura, I. Nakamura, T. Uchijima, Y. Kanai, T. Watanabe, M. Saito, T. Fujitani, *Catal. Lett.* 31 (1995) 313.
- [148] J. Nakamura, I. Nakamura, T. Uchijima, Y. Kanai, T. Watanabe, T. Fujitani, *J.Catal.* 160 (1996) 65.
- [149] T. Fujitani, I. Nakamura, T. Watanabe, T. Uchijima, J. Nakamura, *Catal. Lett.* 35(1995) 297.
- [150] J. Nakamura, I. Nakamura, T. Uchijima, T. Watanabe, T. Fujitani, *Stud. Surf. Sci.Catal.* 101 (1996) 1389.
- [151] T. Fujitani, I. Nakamura, S. Ueno, T. Uchijima, J. Nakamura, *Appl. Surf. Sci.* 121/122 (1997) 583.
- [152] T.S. Askgaard, J.K. Nørskov, C.V. Ovesen, P. Stoltze, *J. Catal* 156 (1995) 229.
- [153] R. Kieffer, E. Ramaroson, A. Deluzarche, Y. Trambouze, *React. Kinet. Catal. Lett.* 16 (1981) 207.
- [154] Y. Amenomiya, T. Tagawa, *8th International Congress on Catalysis (Berlin), Vol II*, Verlag Chemie, Weinheim (1984) 557.
- [155] E. Shustorovich, A.T. Bell, *Surf. Sci.* 253 (1991) 386.
- [156] K.M. VandenBussche, G.F. Froment, *J. Catal.* 161 (1996) 1.
- [157] K. Klier, *Adv. Catal.* 31 (1982) 243.
- [158] Y. Choi, K. Futagami, T. Fujitani, J. Nakamura, *Appl. Catal. A: General* 208(2001) 163.
- [159] Jennifer Strunk *On the Role of the Various Active Sites on ZnO-based Catalysts for the Heterogeneously Catalyzed Methanol Synthesis.*
- [160] By J.J. Spivey, Chemical Society (Great Britain), Royal Society of Chemistry (Great Britain) 170.
- [161] D.S. King, R.M. Nix, *J. Catal.* 160 (1996) 76.

APPENDIX A

XRD SPECTRUMS

1%

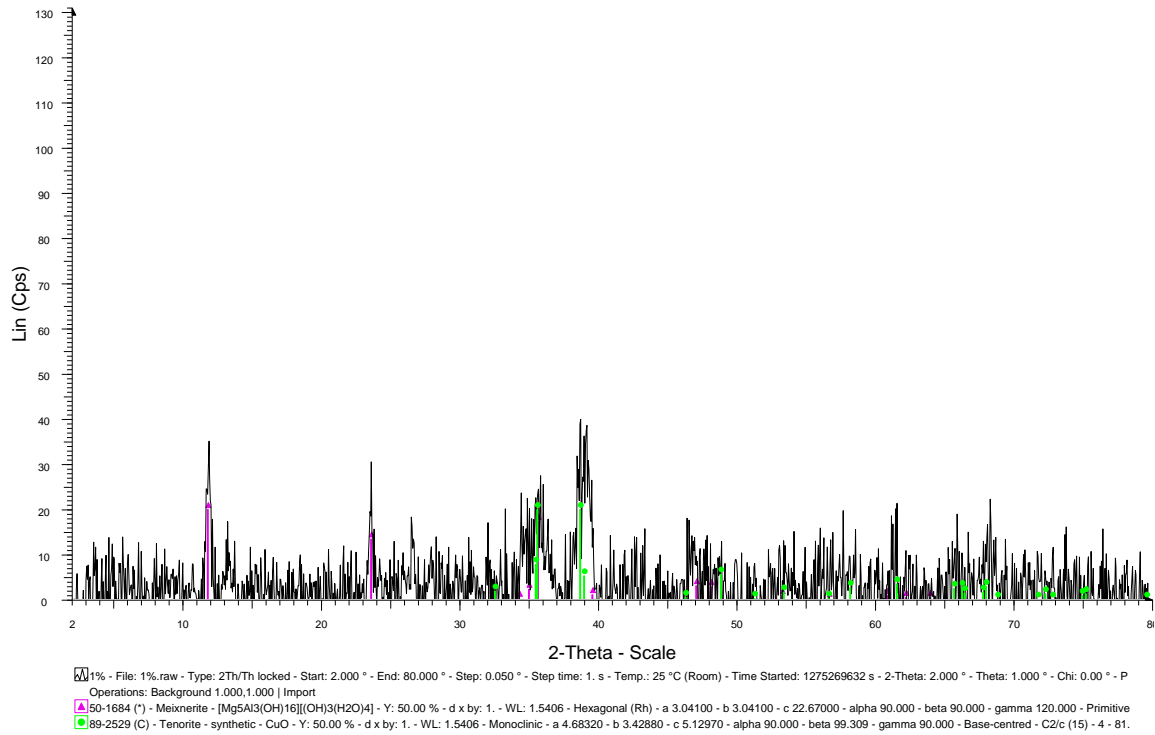


Figure B-1: XRD Spectrum of 1% CNT supported Catalyst

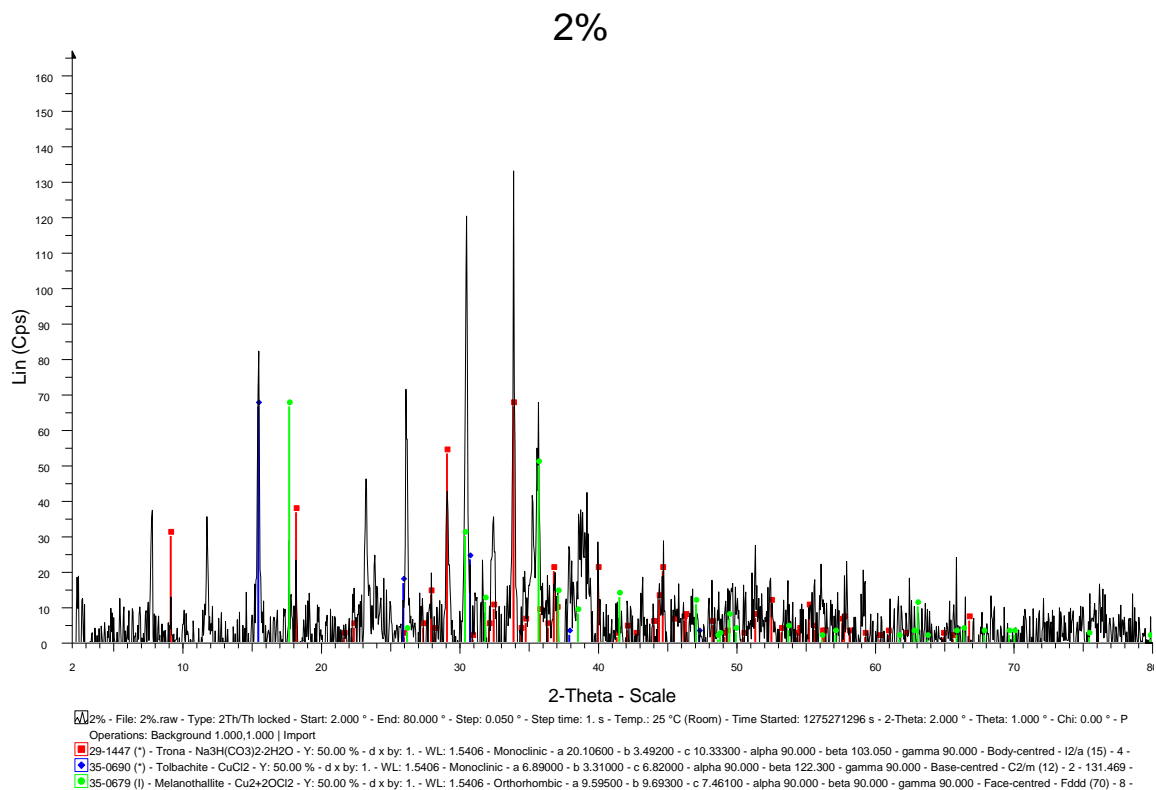


Figure B-2: XRD Spectrum of 2% CNT supported Catalyst

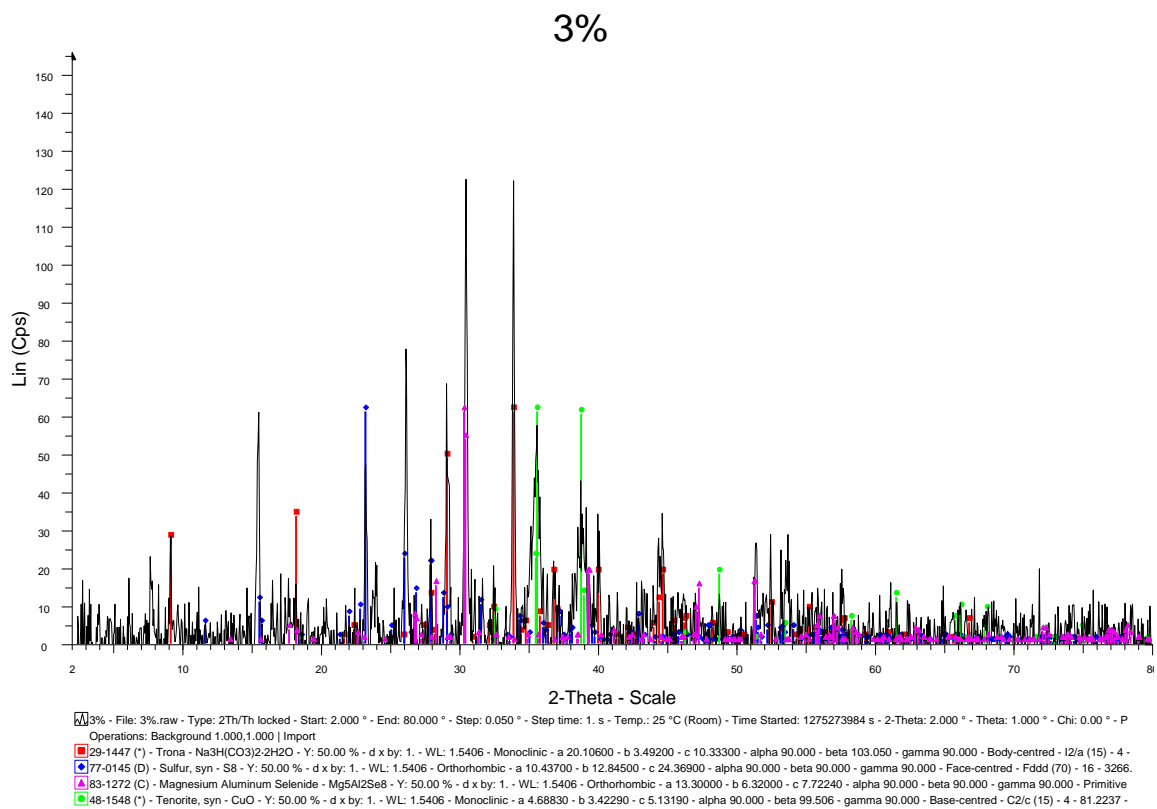


Figure B-3: XRD Spectrum of 3% CNT supported Catalyst

APPENDIX B

Fesem Images for all catalyst samples

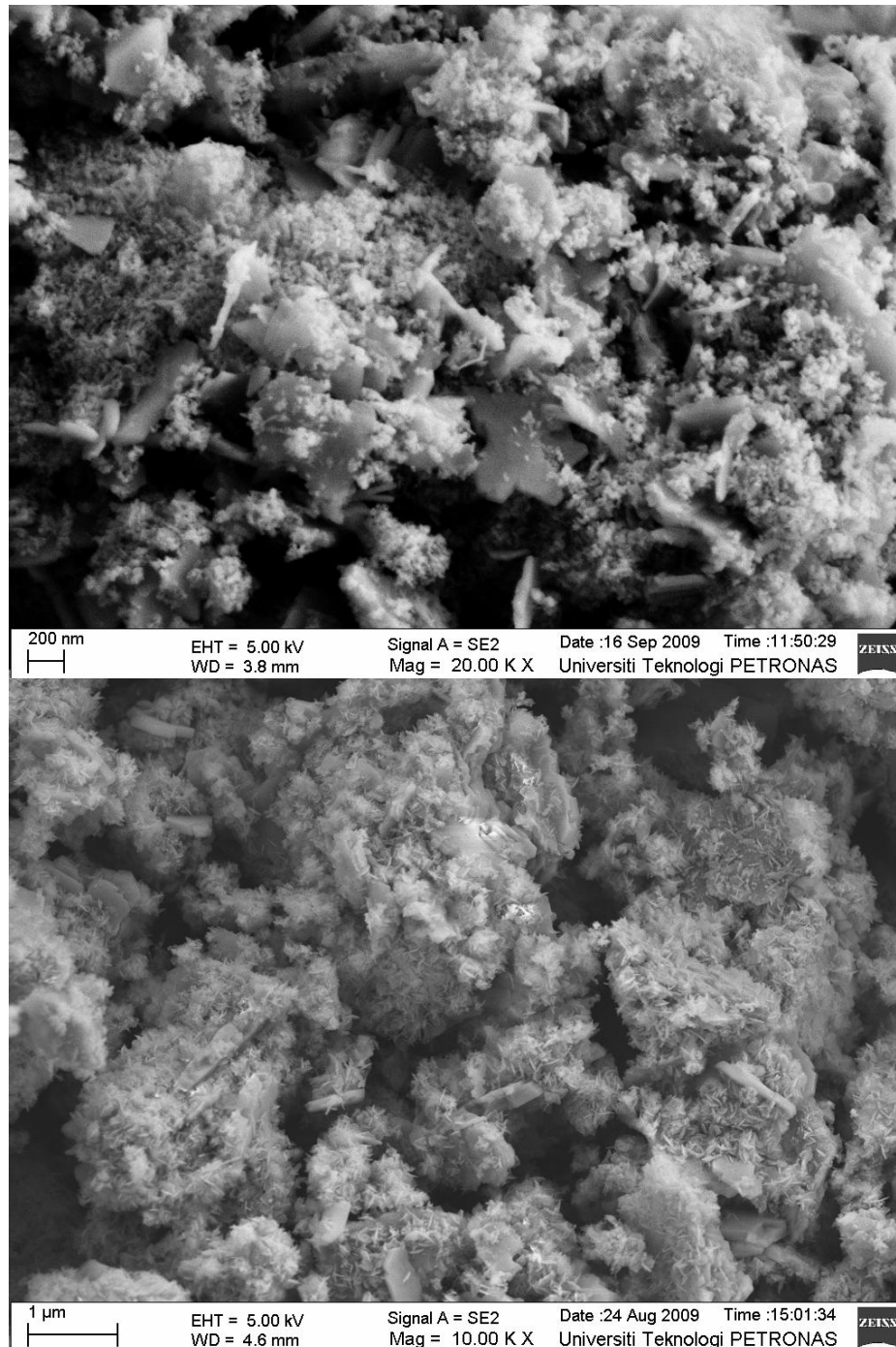


Figure 4.20a and b: (a) (TOP) Commercial pre-catalyst.

(b) (BOTTOM) Spent Industrial sample

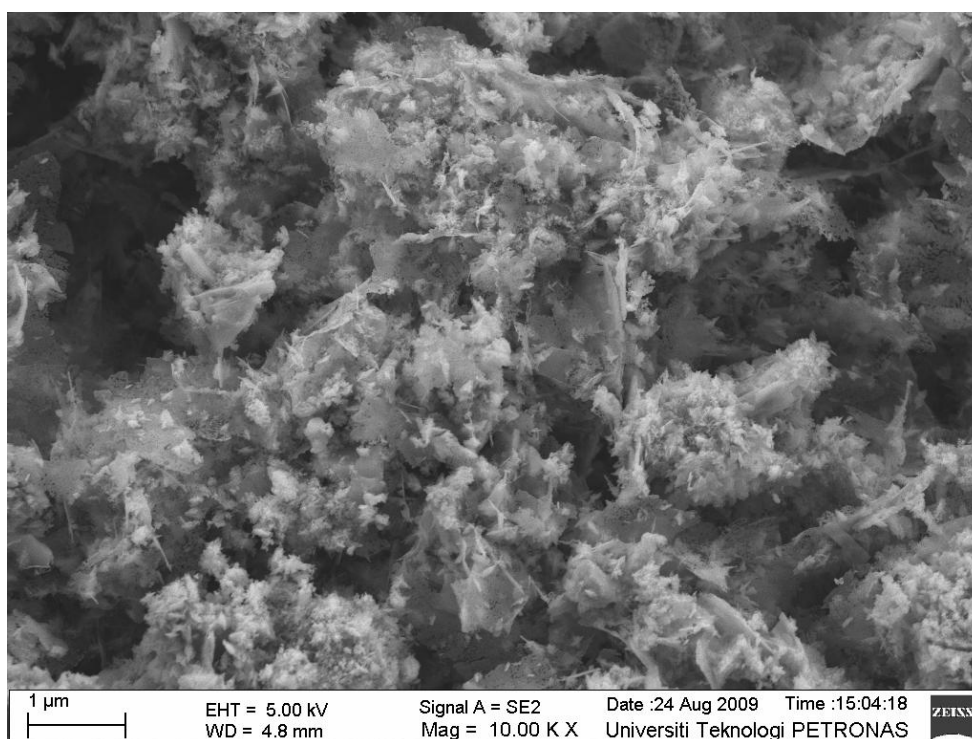
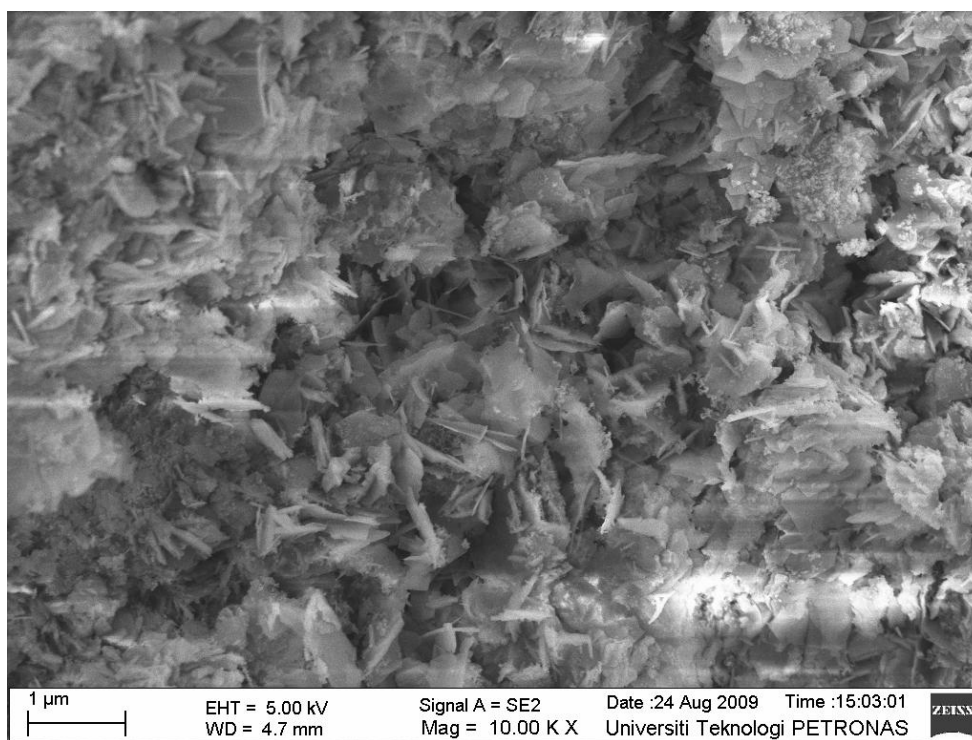


Figure 4.21a and b: (a) (TOP) In-house made Cu/ZnO/Al₂O₃ pre-catalyst
(b) (BOTTOM) In-house made Cu/ZnO/Al₂O₃ catalyst.

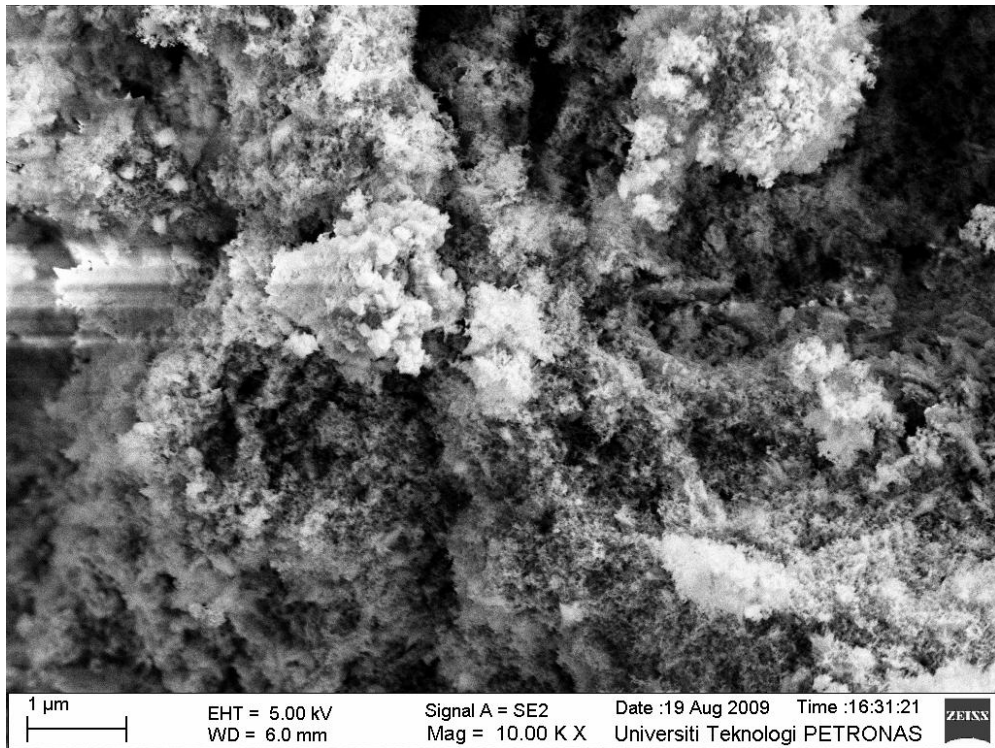
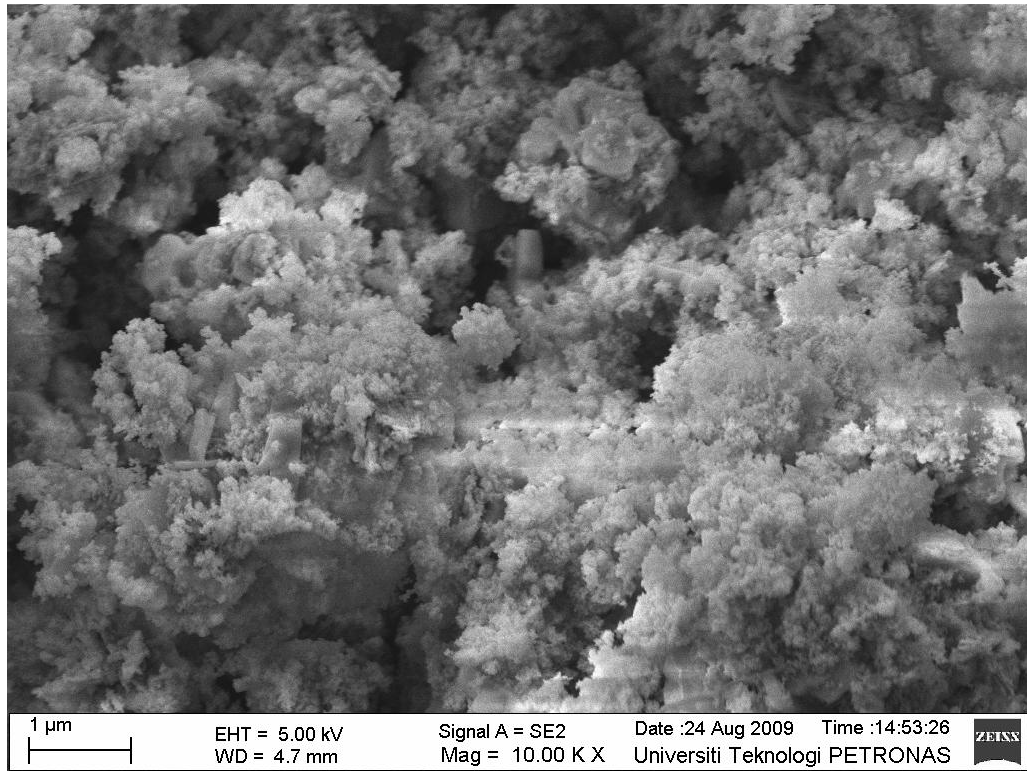


Figure 4.22a and b: (a) (TOP) 1% CNT supported pre-catalyst.
(b) (BOTTOM) 1% CNT supported catalyst.

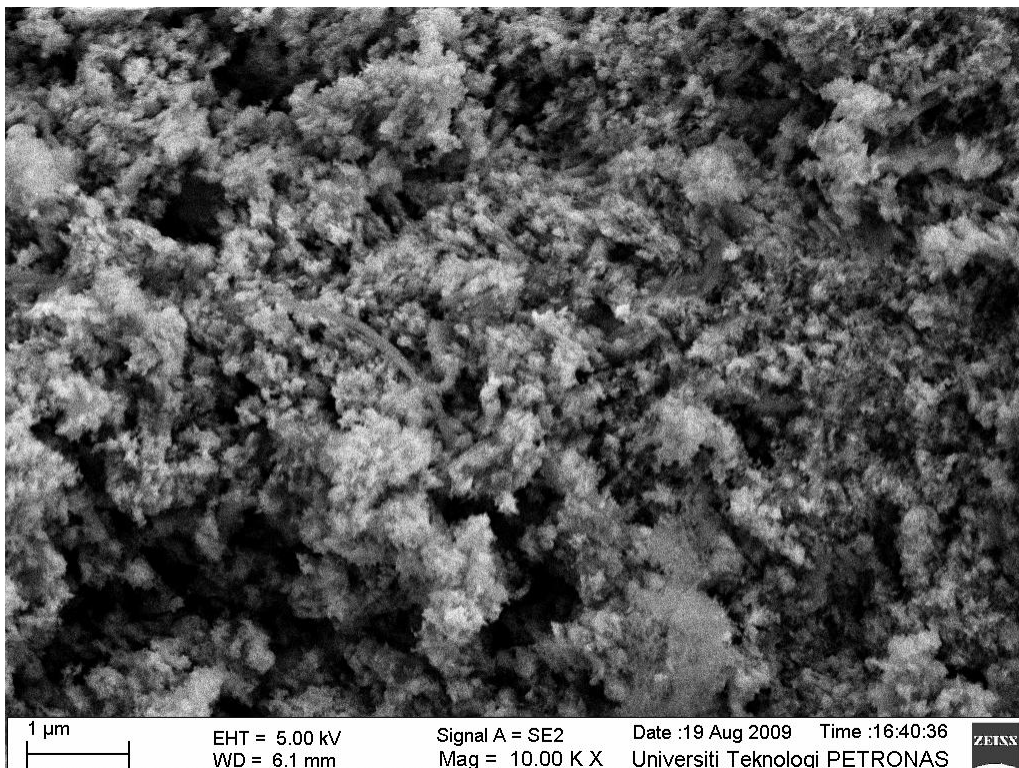
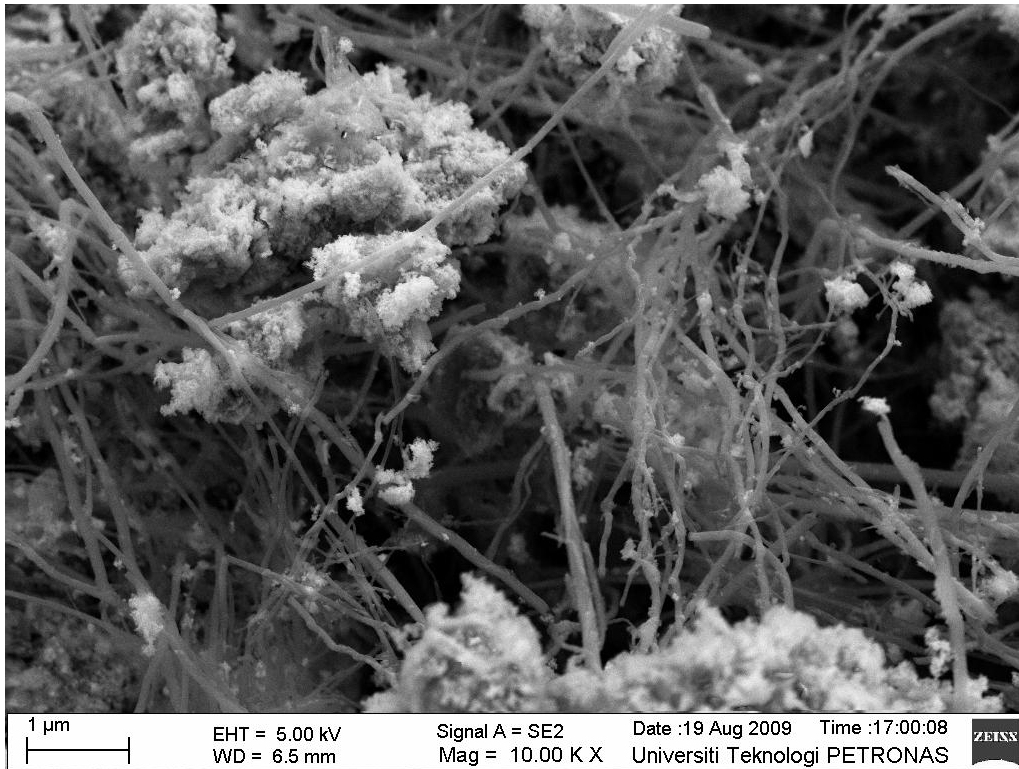


Figure 4.23a and b: (a) (TOP) 2% CNT supported pre-catalyst.
(b) (BOTTOM) 2% CNT supported catalyst.

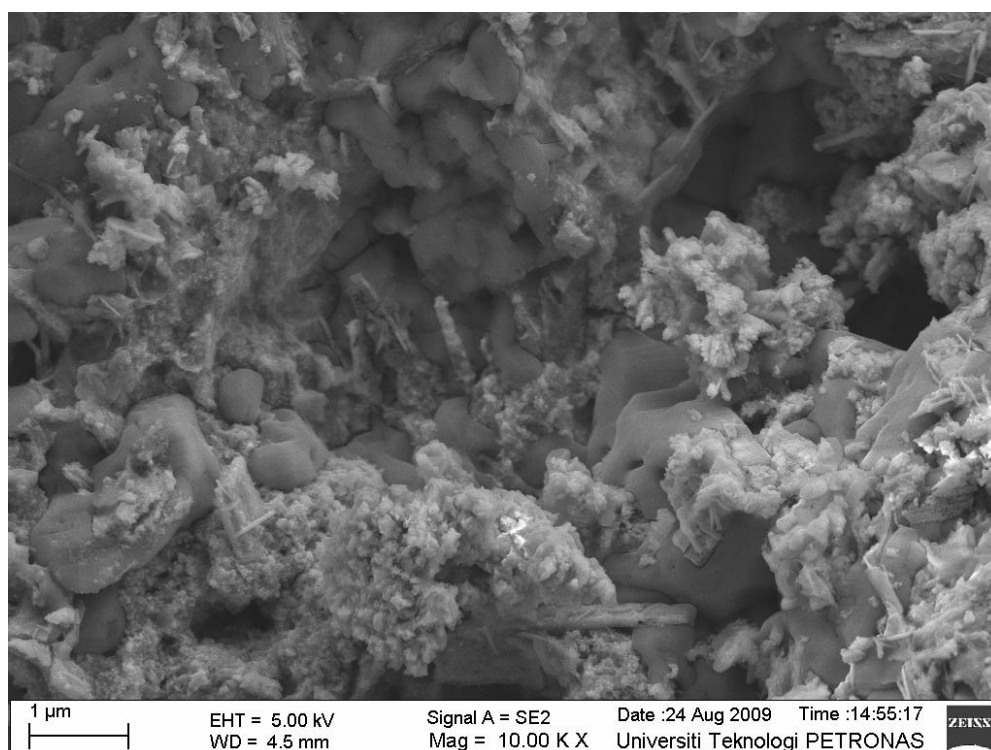
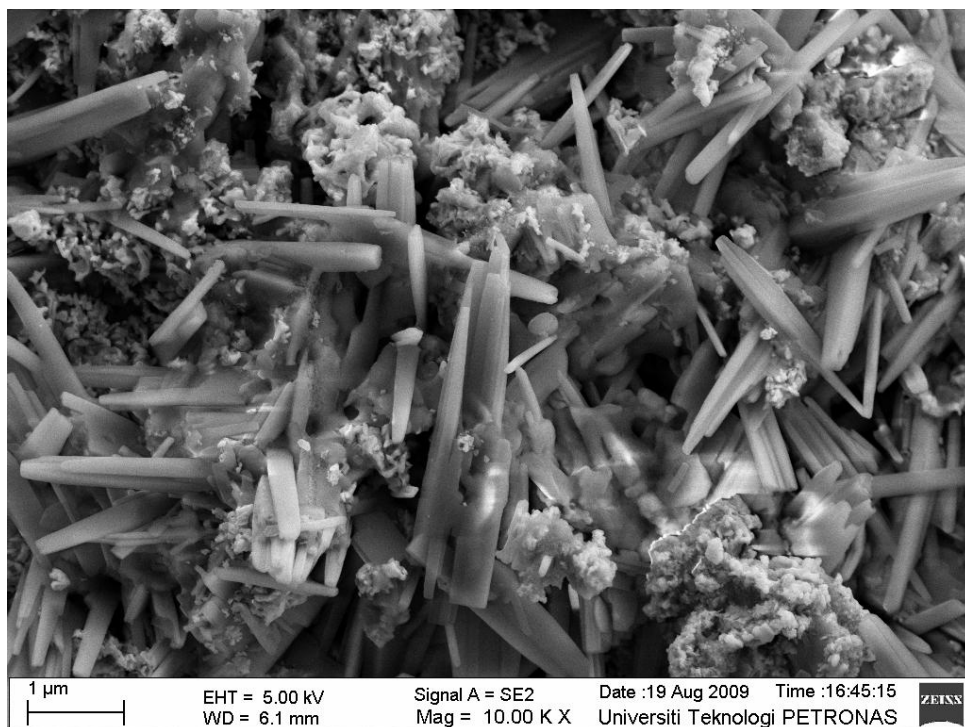


Figure 4.24a and b: (a) (TOP) 3% CNT supported pre-catalyst.
(b) (BOTTOM) 3% CNT supported catalyst.

APPENDIX C

Reactor Standard Operating Procedure

I. Catalysts Sample Loading Into Reactor

1. Open glass door panel to expose the reactor
2. Use Allen key to loosen tubular reactor shell from its support
3. Remove the Inner shell from the Outer shell and lock the filter to the base of the Inner shell tube
4. Insert Alumina balls into Inner shell until $\frac{1}{2}$ of tube length is full
5. Insert $\frac{1}{2}$ cm thick layer of Quartz wool and then insert 1g of catalysts sample
6. Insert another $\frac{1}{2}$ cm thick layer of Quartz wool and then insert alumina balls until catalysts is firmly placed in the middle of the reactor tube.
7. Insert Inner shell into the Outer shell and Screw the Reactor tube back to its support
8. Clamp heater arms on both side and shut the glass door panel tight
9. CAUTION: Since the thermocouple is located on the bottom of the reactor, beware not to accidentally drop the reactor while removing reactor from its support.

II. Reactor Initiation

1. Turn the main switch 'ON' located on the control panel
2. Ensure that all gas lines are tightly connected to the reactor inlet.
3. Perform a Pressure Leak test by flowing Nitrogen gas at 3 bars into the pressure monitoring the drop for 15 minutes. If there is rapid Pressure drop in the reactor, perform leak test along the lines to detect leak site. If there is one, STOP all operation and repair the leaking pipeline.

4. If there is no Pressure drop, purge Nitrogen gas from the Pressure relief valve
5. To start reduction process, set the desired Temperature at the Temperature controller located on the control panel
6. Open the Needle valve located beside the reactor manually as well as the check valve switch located on the control panel for desired gas flow line.
7. Open gas flow from cylinder and set regulator to desired Pressure in the reactor
8. Monitor the Pressure gauge on the reactor to obtain the desired Reactor Pressure
9. Switch the heater on from the control panel to begin heating process
10. Reduction conditions are : 1bar, sample specific Temperatures (see Section 4.1.5) and additional 1 hour of heating after reaching set point
11. After reduction, Inert (Nitrogen) gas is flowed at 10 bars for 1 hour to cool sample to 250°C (change Temperature controller set point to 250°C) and remove excess reduction gas (5% H₂ in N₂). Flow line should be changed from reduction to inert gas line.
12. Reaction is then commenced at 250°C , 30 bars. Line is changed to reactant gas line.
13. Outlet gas line is maneuvered either to GC for analysis or effluent vacuum.

III. System Shutdown

1. Close gas flows from cylinder
2. Heater is turned off by control panel switch
3. Release gas to vacuum effluent line by switching ON the pressure relief valve.
4. Ensure there is no pressure reading from regulator
5. Switch off the valves' and heater switches on control panel
6. Close all needle valves beside the reactor
7. Turn off main switch on control panel
8. Allow reactor to cool down overnight before commencing the next sample loading

APPENDIX D

The Kinetic Model of Methanol Synthesis over Cu/ZnO/Al₂O₃ Supported by CNT.

1. The generalized model of the active sites on the surface of Cu/ZnO/Al₂O₃ catalyst.

The deeper understanding of the nature of active sites on the surface of ZnO is required as ZnO is a key component of the Cu/ZnO/Al₂O₃ catalyst. Its role in the methanol synthesis in presence of Cu is still the subject of wide speculations [138, 145, 156-157]. Recent models of methanol synthesis on the ternary catalysts consider ZnO to be more than only a support oxide. A combined study using TEM, XRD, EXAFS and catalytic activity measurements revealed the sensitivity of methanol synthesis pattern to a structure on zinc oxide [111]. It was found using different ZnO samples featuring a range of crystallite sizes and specific surface areas that catalytic activity increase is not linearly depend on the BET surface area. In the case of very small ZnO crystallites, the samples were less active than expected based on their large BET surface area. Instead, samples with large crystallites and well-developed crystal faces tended to be quite active despite their rather limited surface area. Therefore, there are factors other than just the dispersion and surface area that are controlling the catalytic activity. For instance, by comparison the data of Bowker et al. [114,115] with their own results Wilmer et al. [111] came to a conclusion, that the polar surfaces of the ZnO crystallites were more active than the non-polar ones.

“Perfect "crystal surfaces of oxides usually show little catalytic activity if any. So one can conclude that the reactivity should be attributed to a small amount of active sites [117, 118], possibly resulting from a local distortions of the crystal surface structure. Several types of such active sites referred to as “defects" were

experimentally characterized. These are dislocations, interstitial atoms or different types of vacancies [116, 119]. In the case of ZnO, the most commonly observed defects are oxygen vacancies and interstitial zinc atoms [119,120], as well as Zn-O dimer vacancies (i. e. a missing Zn-O unit) [121]. Vacancy formation is one of the possible mechanisms for a stabilization of polar crystal surfaces [122, 123]. To counterbalance the large surface dipole moment, the oxygen-terminated ZnO (00011) surface, for example, can either form surface hydroxyl groups or oxygen vacancies (in both cases the dipole moment is directed outward of the surface). It was shown in a quantum chemical study that the composition of surrounding gas phase determines, which of the two processes is thermodynamically more favorable. Under the conditions of methanol synthesis, both processes were proposed likely to occur [123].

It was proposed [135-137] that the interface area between copper and partially reduced ZnO is an important formation that promotes high catalytic activity. The CuZnO_x species ($0 < x < 1$) are believed to act as highly active sites for methanol synthesis. The commonly observed and characterized surface and bulk defects in ZnO are shown at Figures 4.55 and 4.57

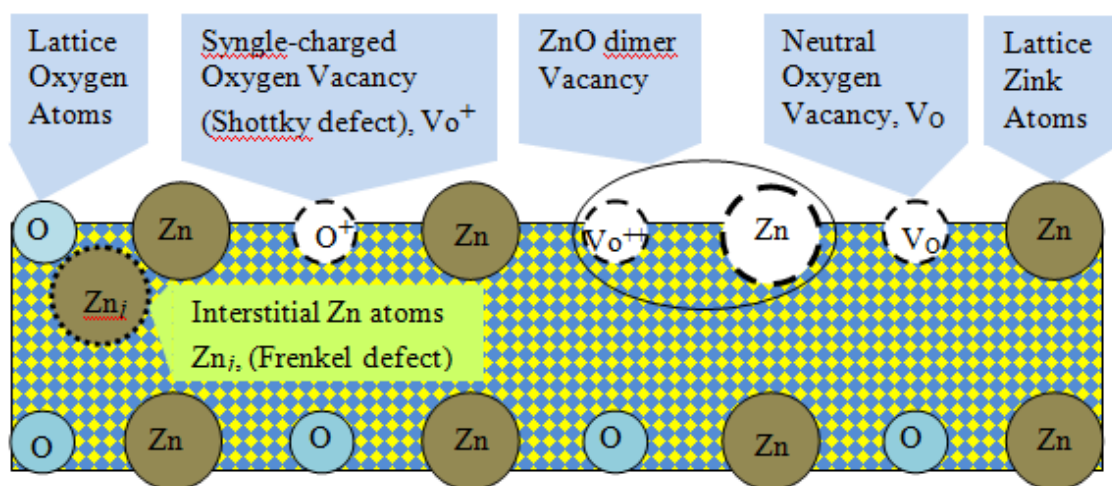


Figure 4.55 The most common active sites (defects) on the surface of ZnO

2. The role of oxygen vacancies in the ZnO based catalyst of methanol synthesis

The roles of oxygen vacancies in methanol synthesis over ZnO based catalysts were explored in model study with highly oxygen-deficient ZnO samples obtained from thermolysis of an organometallic ZnO precursor [157]. The relative amounts of oxygen vacancies in the samples were determined by EPR spectroscopy and by reactive frontal chromatography (N₂O-RFC) [159]. The steady state catalytic activity was measured in absence and presence of CO₂. In a CO₂-free synthesis gas, higher oxygen vacancy content caused a better catalytic performance. In presence of CO₂, the steady state catalytic activity was remarkably lower.

The results provide strong evidence for the role of oxygen vacancies in ZnO as active sites for hydrogenation of CO to methanol in absence of CO₂. The presence of CO₂, instead, causes the oxygen vacancies to be filled up either by abstracted oxygen atoms or by strongly adsorbed species.

The presence of two active components, Cu and ZnO, in the industrial copper catalyst Cu/ZnO/Al₂O₃ leads to a more complicated situation. Presently, it is commonly believed that Al₂O₃ acts only as structural promoter to induce high dispersion of Cu and improving mechanical strength of ZnO. In the early days of the use of Cu/ZnO catalysts, it was believed that ZnO was the major source for the catalytic activity. Copper was believed to be present as Cu⁺, incorporated or dissolved in the ZnO lattice [116, 124-127]. The role of Cu⁺ was debated. While Klier et al. [124-127] considered the role of Cu⁺ to assist the binding and activation of carbon monoxide, Kung [116] proposed that the presence of Cu in the ZnO lattice increased the amount of vacancies on the ZnO surface, thus creating a higher amount of active sites. Presently, metallic Cu is considered to be the main or even the only source of the catalytic activity [113, 128-131]. Several researchers proposed a partial coverage of the Cu surface with oxygen in the working catalyst [130, 131]. However, experiments using CO pulse experiments demonstrated that no significant oxygen coverage is present on the surface of Cu under methanol synthesis conditions [132]. Though copper seems to be the major source of the catalytic activity, the Cu/ZnO catalysts showed rather better performance than Cu/Al₂O₃ ones [133, 134]. This

suggests that some special surface formation is created as a result of interaction between Cu crystals and ZnO. Using a large amount of different co-precipitated samples, it was shown that catalysts of the type Cu/Al₂O₃ and Cu/ZnO/Al₂O₃ clearly represent two different catalyst classes. With the same specific copper surface area, ternary catalysts were rather more active than the corresponding ZnO free binary systems [133]. Varying the Zn/Cu ratio in Cu/ZnO/Cr₂O₃ catalysts, Klier et al. [124-127] found, that the activity did not depend linearly on the content of either component. Instead, two maxima in activity were observed, corresponding to Zn/Cu = 7/3 or 3/6 (Fig 4.56)

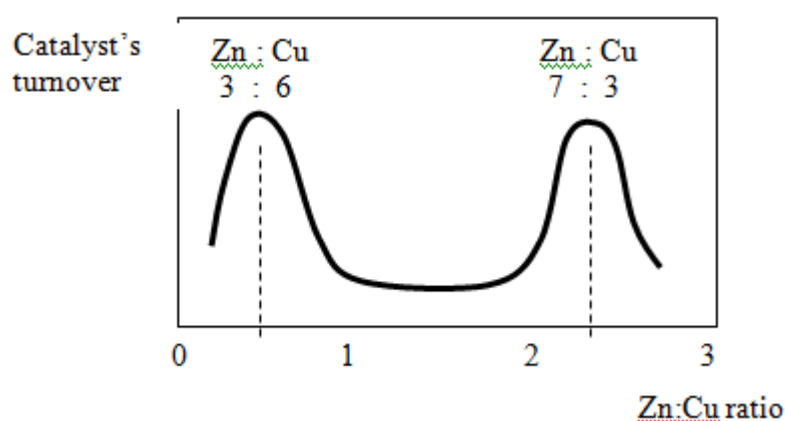


Figure 4.56 The effect of Zn:Cu ratio on activity of the Cu/ZnO/Cr₂O₃ catalyst.

It was proposed that an increased catalytic activity of Cu/ZnO catalysts compared to Cu on other supports might be explained with strong metal-support interactions between Cu and ZnO [135-138]. Under strongly reducing conditions of synthesis gas a wetting behavior of the Cu particles was observed that is due to strong metal-support interactions the Cu particles flattened and spread out over the surface of ZnO [139, 140], which led to a change in the area of exposed faces of the Cu crystals as well as the size of Cu-ZnO interface. It was proposed that Cu particles on Cu/ZnO/Al₂O₃ when they were pretreated with synthesis gas, CO/H₂, exposed mainly their most reactive Cu(111) face [141, 142].

On the contrary, after a pretreatment with CO/He, other surfaces were suggested to dominate [53], probably Cu(110) and Cu(211) [142]. Under severe reducing conditions surface alloy formation was proposed to occur [140] due to the migration of partially reduced ZnO_x species ($0 \leq x \leq 1$) on the Cu surface [135, 143]. Under highly reducing conditions even the formation of surface brass might occur $CuZnO_x$ with $x=0$ [144].

The morphological changes occurring as consequence of the SMSI effect have been suggested to influence the catalytic activity [139, 140]. This might have different reasons. The wetting behavior of the Cu particles increases the Cu surface area. Based on the models of Chinchin [130] et al. or the data from Kurtz et al. [133] a higher catalytic activity is then expected. Furthermore, recent models of methanol synthesis ascribe the Cu-ZnO interface a major role for the high catalytic activity in providing highly active sites [138, 143, 145, 146]. The single crystal studies of clean and Zn-deposited Cu(111) surfaces in comparison with studies of real catalysts performed by Nakamura [138, 143, 146-151] revealed that a Zn-deposited Cu(111) surface is an appropriate model for a Cu/ZnO catalyst. In these studies, the importance of a Cu-Zn or a Cu-O-Zn site for methanol synthesis from CO_2 or CO, respectively, was clearly indicated. A main difference between the purely oxidic ZnO/Cr_2O_3 catalyst and the ternary $Cu/ZnO/Al_2O_3$ system is also the preferred carbon source for the formation of methanol.

The copper-containing system, in contrast to purely oxidic catalysts like ZnO/Cr_2O_3 , deactivates in CO/H_2 . In this case CO_2 is not only necessary to retain catalytic activity. Using isotope labeled reactants, it was shown that CO_2 is the preferred carbon source for methanol formation on these catalyst systems [112, 113]. Reaction rates of methanol formation from CO_2 are about 100 times larger than methanol formation starting from CO [128]. For Cu(100), a comprehensive kinetic model of methanol synthesis, including the water gas shift reaction, has been developed by Askgaard et al. [160]. Generally, formate species on Cu [152,153] or Cu-Zn [138,146] were reported to be key intermediates in methanol synthesis. Their further hydrogenation was proposed to be the rate-determining step in the mechanism of methanol formation [154, 155].

In present study we ascribe the catalytic activity of the ternary Cu/ZnO/Al₂O₃ system to the area immediately adjacent to the Cu-ZnO interface.

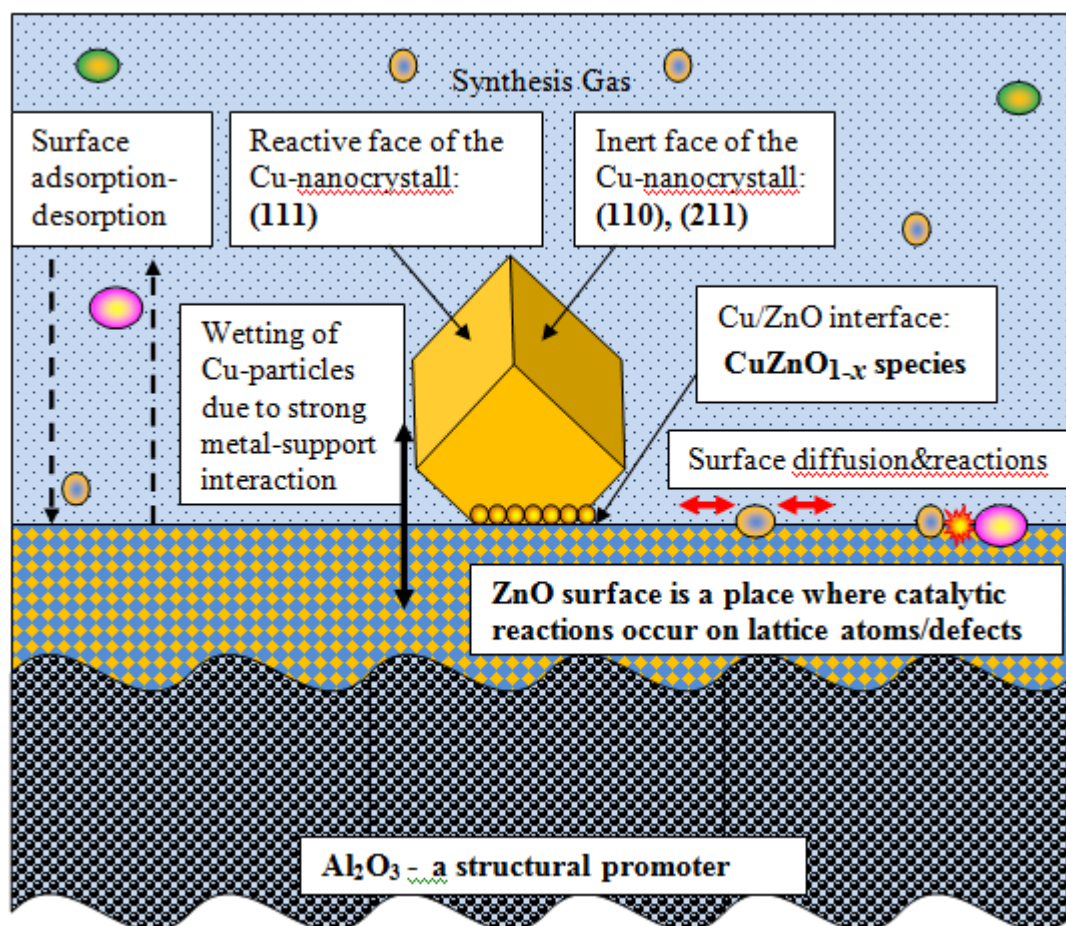


Figure 4.57 The contemporary concept of active sites on surface of Cu/ZnO/Al₂O₃ catalyst

3. The kinetic model for the methanol synthesis over Cu/ZnO/Al₂O₃ catalyst supported by CNT

To rationalize the experimental findings on the process kinetics obtained in this study the mechanism of methanol synthesis depicted at Fig4.55 was elaborated from the analysis of the literature data. Next features were taken into consideration to outline a kinetic model:

- Gas phase molecules adsorb, transform and desorb with respective rate constants
- Mechanism of surface reactions is influenced by the nature and dynamics of the surface active sites (defects) on ZnO particles and Cu nanocrystals, a missing Zn-O unit [121]
- Key active sites on ZnO are oxygen vacancies and interstitial zinc atoms as well as Zn-O dimer vacancies
- Energetically heterogeneous surface

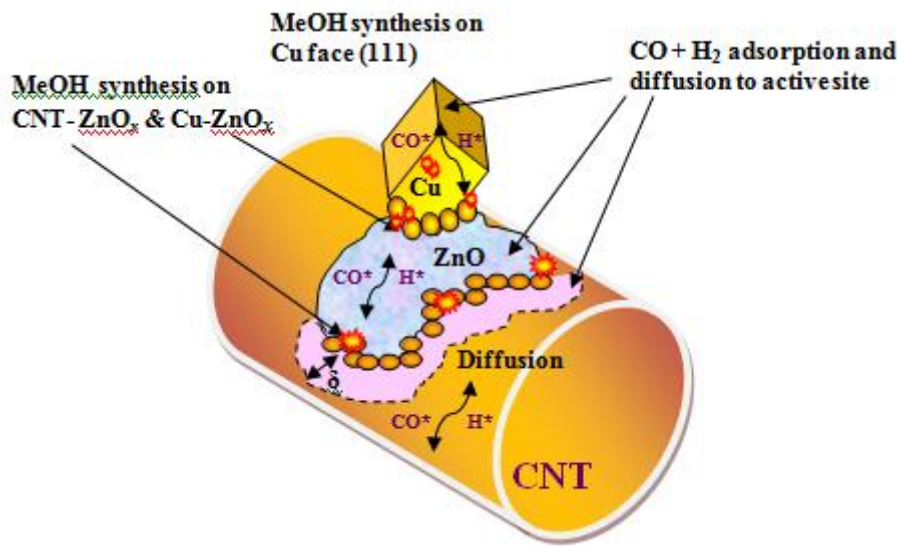


Figure 4.58 The physical model for the methanol synthesis over Cu/ZnO/Al₂O₃ catalyst supported by CNT

Above analysis of recent findings in the mechanisms of methanol synthesis over Cu/ZnO/Al₂O₃ catalyst allows considering the overall rate of methanol synthesis reaction, R_{Σ} , as to be proportional a sum of the rates of intermediate steps of the reaction

$$R_{\Sigma} \sim [R_{adsZnO} + R_{adsCNT} + R_{adsCu}] + \{ [R_{difCu} + R_{difZnO} + R_{difCNT}] + R_{Cu(111)} + R_{intCuZnOx} + R_{intCNTZnOx} \} + R_{desZnO} + R_{desCNT} + R_{desCu}$$